

# Numerical Simulation of Turbulent Natural Convection on Enclosures

by

Mohammed Abdul Razzaq Khan

A Thesis Presented to the

FACULTY OF THE COLLEGE OF GRADUATE STUDIES  
KING FAHD UNIVERSITY OF PETROLEUM & MINERALS  
DHAHRAN, SAUDI ARABIA

In Partial Fulfillment of the  
Requirements for the Degree of

**MASTER OF SCIENCE**

In

**MECHANICAL ENGINEERING**

June, 1996

## INFORMATION TO USERS

This manuscript has been reproduced from the microfilm master. UMI films the text directly from the original or copy submitted. Thus, some thesis and dissertation copies are in typewriter face, while others may be from any type of computer printer.

**The quality of this reproduction is dependent upon the quality of the copy submitted.** Broken or indistinct print, colored or poor quality illustrations and photographs, print bleedthrough, substandard margins, and improper alignment can adversely affect reproduction.

In the unlikely event that the author did not send UMI a complete manuscript and there are missing pages, these will be noted. Also, if unauthorized copyright material had to be removed, a note will indicate the deletion.

Oversize materials (e.g., maps, drawings, charts) are reproduced by sectioning the original, beginning at the upper left-hand corner and continuing from left to right in equal sections with small overlaps. Each original is also photographed in one exposure and is included in reduced form at the back of the book.

Photographs included in the original manuscript have been reproduced xerographically in this copy. Higher quality 6" x 9" black and white photographic prints are available for any photographs or illustrations appearing in this copy for an additional charge. Contact UMI directly to order.

# UMI

A Bell & Howell Information Company  
300 North Zeeb Road, Ann Arbor MI 48106-1346 USA  
313/761-4700 800/521-0600





**NUMERICAL SIMULATION OF TURBULENT  
NATURAL CONVECTION IN ENCLOSURES**

BY  
**MOHAMMED ABDUL RAZZAQ KHAN**

A Thesis Presented to the  
FACULTY OF THE COLLEGE OF GRADUATE STUDIES  
**KING FAHD UNIVERSITY OF PETROLEUM & MINERALS**  
DHAHRAN, SAUDI ARABIA

In Partial Fulfillment of the  
Requirements for the Degree of

**MASTER OF SCIENCE**  
In  
**MECHANICAL ENGINEERING**

**JUNE 1996**

**UMI Number: 1382794**

---

**UMI Microform 1382794**  
**Copyright 1997, by UMI Company. All rights reserved.**

**This microform edition is protected against unauthorized  
copying under Title 17, United States Code.**

---

**UMI**  
**300 North Zeeb Road**  
**Ann Arbor, MI 48103**

**KING FAHD UNIVERSITY OF PETROLEUM AND MINERALS  
DHAHRAN, SAUDI ARABIA**

**COLLEGE OF GRADUATE STUDIES**

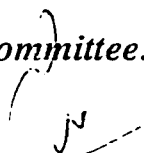
*This thesis, written by*

**Mohammed Abdul Razzaq Khan**

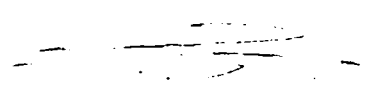
*under the direction of his Thesis Advisor, and approved by his Thesis committee, has been presented to and accepted by the Dean, College of Graduate Studies, in partial fulfillment of the requirements for the degree of*

**MASTER OF SCIENCE  
IN  
MECHANICAL ENGINEERING**

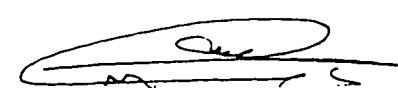
*Thesis Committee:*

  
\_\_\_\_\_  
Dr. Syed A. M. Said (Chairman)

*Med Habib*  
\_\_\_\_\_  
Dr. Mohamed A. Habib (Co-Chairman)

  
\_\_\_\_\_  
Dr. Mohammed O. Budair  
Department Chairman

*Hassan Badr*  
\_\_\_\_\_  
Dr. Hassan M. Badr (Member)

  
\_\_\_\_\_  
Dr. Abdulla M. Al-Shehri  
Dean, College of Graduate Studies

Date: 9-12-96



Dedicated to

My

*Father,*

*Mother,*

*Brothers and Sisters*

## Acknowledgement

In the name of Allah, Most Gracious, Most Merciful. Read in the name of thy Lord and Cherisher, Who created. Created man from a ( *leach-like* ) clot. Read and thy Lord is Most Bountiful. He taught ( *the use of* ) the pen. Taught man that which he knew not. Nay, but man doth transgress all bounds. In that he looketh upon himself as self-sufficient. Verily, to thy Lord is the return ( *of all* ).

(The Holy Quran, Surah 96)

Praise be to ALLAH for giving me the courage and patience to carry out this work. I am happy to have had a chance to glorify His name in the sincerest way through this small accomplishment and ask Him to accept my efforts. May He guide us and the whole humanity to the right path (*Aameen*).

Peace and mercy be upon His Holy Prophet.

Acknowledgement is due to King Fahd University of Petroleum and Minerals for support of this research.



My deep appreciation goes to my major thesis advisor Dr. Syed A. M. Said for his constant help, guidance and the countless hours of attention he devoted throughout the course of the work. His priceless suggestions made this work interesting and learning for me. He was always kind, understanding and sympathetic to me. Working with him was indeed a wonderful and learning experience which i thoroughly enjoyed.

Thanks are also due to my thesis committee members Dr. M. A. Habib and Dr. H. M. Badr for their interest, cooperation, advice and constructive criticism.

I am also indebted to the department chairman, Dr. M. O. Budair and other faculty members for their support.

Lastly, but not the least, thanks are due to my family members for their patience, understanding and encouragement throughout my academic career, and also to my fellow graduate students, and all my friends from whom i learned a lot.

# Contents

Acknowledgements	ii
List of Tables	viii
List of Figures	ix
Abstract(English)	xv
Abstract(Arabic)	xvi
Nomenclature	xix
<b>1 Introduction</b>	<b>1</b>
1.1 Background . . . . .	1
1.2 External Natural convection . . . . .	2
1.3 Internal Natural Convection . . . . .	3
1.3.1 Natural Convection in Enclosures . . . . .	5

<b>2 Literature Survey</b>	<b>7</b>
2.1 Natural Convection in Vertical Enclosures . . . . .	7
2.2 Natural Convection in Inclined Enclosures . . . . .	13
2.3 Natural Convection in Inclined and Partitioned Enclosures . . . . .	15
2.4 Scope of the work . . . . .	17
<b>3 Mathematical Formulation</b>	<b>20</b>
3.1 Problem Considered . . . . .	22
3.2 The Effect of Extremely Small Scale of Turbulence . . . . .	25
3.3 The Mean Flow Equations . . . . .	26
3.4 The Problem of Closure . . . . .	27
3.5 Turbulence Modelling . . . . .	28
3.5.1 First Order Models . . . . .	30
3.5.2 Turbulence Models Used in the Present Study . . . . .	39
3.6 Boundary Conditions . . . . .	45
<b>4 Numerical Solution of the Governing Equations</b>	<b>46</b>
4.1 Methods of Deriving the Discretization Equations . . . . .	47
4.1.1 Taylors-series Formulation . . . . .	47
4.1.2 Variational Formulation . . . . .	49
4.1.3 Method of Weighted Residual . . . . .	49
4.1.4 Control Volume Formulation . . . . .	50

4.2	The Discretization Procedure used in the Present Study . . . . .	51
4.3	Grid Generation . . . . .	57
4.4	Calculation Procedure . . . . .	59
4.4.1	Solution Algorithm . . . . .	61
<b>5</b>	<b>Results and Discussions</b>	<b>64</b>
5.1	Validation of the Numerical Code . . . . .	65
5.1.1	Laminar Flow . . . . .	65
5.1.2	Turbulent Flow . . . . .	68
5.2	Comparison of the Two Turbulence Models . . . . .	70
5.3	Grid Independence Test . . . . .	74
5.4	Natural Convection in Enclosures without partition . . . . .	74
5.4.1	Effect of Angle of Inclination in Laminar Flow . . . . .	74
5.4.2	Effect of Angle of Inclination in Turbulent Flow . . . . .	85
5.5	Natural Convection in Partitioned Enclosure . . . . .	92
5.5.1	Effect of number of Partitions . . . . .	92
5.5.2	Effect of Rayleigh number . . . . .	103
5.5.3	Effect of Aspect ratio . . . . .	111
5.5.4	Effect of Angle of Inclination . . . . .	118
<b>6</b>	<b>Conclusions and Recommendations</b>	<b>120</b>
6.1	Conclusions . . . . .	120

6.2 Recommendations . . . . .	122
<b>Bibliography</b>	<b>123</b>
<b>Vita</b>	<b>130</b>

# List of Tables

3.1	Constants for $k - \varepsilon$ model . . . . .	40
3.2	Constants for $k - \varepsilon$ model . . . . .	44

# List of Figures

1.1	Representative velocity and temperature distribution in natural convection boundary layer flow on a heated vertical plate . . . . .	4
3.1	A Rectangular Enclosure . . . . .	23
4.1	Three consecutive grid points used for Taylor-series expansion . . . . .	48
4.2	A finite control volume . . . . .	52
4.3	magnified view of bottom portion of the Computational Grid in an Enclosure with a single partition . . . . .	58
5.1	Effect of Angle of inclination on the Average Nusselt no. for laminar Natural convection in an enclosure without partition: $Ra = 1 \times 10^6$ , $A=1.0$ , $Pr = 0.71$ . . . . .	67
5.2	Effect of Angle of inclination on the Average Nusselt no. for Turbulent Natural convection in an enclosure without partition: $Ra = 1 \times 10^{10}$ , $A=1.0$ , $Pr = 0.71$ , using standard k-e model . . . . .	69

5.3	Temperature distribution at the mid-height of the enclosure for $Ra = 8 \times 10^{10}$ , $A=10:1$ , $\Phi = 90^0$ . . . . .	72
5.4	Vertical Velocity distribution at the mid-height of the enclosure for $Ra = 8 \times 10^{10}$ , $A=10:1$ , $\Phi = 90^0$ . . . . .	73
5.5	Vertical Velocity at the mid-height of the enclosure for different mesh sizes . . . . .	75
5.6	Isotherms for Laminar Natural Convection in an Enclosure without partition; $Ra = 1 \times 10^6$ , $A=1.0$ , $P_r = 0.71$ , $\Phi = 135^0$ . . . . .	77
5.7	Isotherms for Laminar Natural Convection in an Enclosure without partition; $Ra = 1 \times 10^6$ , $A=1.0$ , $P_r = 0.71$ , $\Phi = 90^0$ . . . . .	78
5.8	Isotherms for Laminar Natural Convection in an Enclosure without partition; $Ra = 1 \times 10^6$ , $A=1.0$ , $P_r = 0.71$ , $\Phi = 60^0$ . . . . .	79
5.9	Isotherms for Laminar Natural Convection in an Enclosure without partition; $Ra = 1 \times 10^6$ , $A=1.0$ , $P_r = 0.71$ , $\Phi = 40^0$ . . . . .	80
5.10	Streamlines for Laminar Natural Convection in an Enclosure without partition; $Ra = 1 \times 10^6$ , $A=1.0$ , $P_r = 0.71$ , $\Phi = 135^0$ . . . . .	81
5.11	Streamlines for Laminar Natural Convection in an Enclosure without partition; $Ra = 1 \times 10^6$ , $A=1.0$ , $P_r = 0.71$ , $\Phi = 90^0$ . . . . .	82
5.12	Streamlines for Laminar Natural Convection in an Enclosure without partition; $Ra = 1 \times 10^6$ , $A=1.0$ , $P_r = 0.71$ , $\Phi = 60^0$ . . . . .	83



5.13	Streamlines for Laminar Natural Convection in an Enclosure without partition; $Ra = 1 \times 10^6$ , $A=1.0$ , $P_r = 0.71$ , $\Phi = 40^\circ$ . . . . .	84
5.14	Isotherms for Turbulent Natural Convection in an Enclosure without partition; $Ra = 1 \times 10^{10}$ , $A=1.0$ , $P_r = 0.71$ , $\Phi = 90^\circ$ . . . . .	86
5.15	Isotherms for Turbulent Natural Convection in an Enclosure without partition; $Ra = 1 \times 10^{10}$ , $A=1.0$ , $P_r = 0.71$ , $\Phi = 60^\circ$ . . . . .	87
5.16	Isotherms for Turbulent Natural Convection in an Enclosure without partition; $Ra = 1 \times 10^{10}$ , $A=1.0$ , $P_r = 0.71$ , $\Phi = 30^\circ$ . . . . .	88
5.17	Streamlines for Turbulent Natural Convection in an Enclosure without partition; $Ra = 1 \times 10^{10}$ , $A=1.0$ , $P_r = 0.71$ , $\Phi = 90^\circ$ . . . . .	89
5.18	Streamlines for Turbulent Natural Convection in an Enclosure without partition; $Ra = 1 \times 10^{10}$ , $A=1.0$ , $P_r = 0.71$ , $\Phi = 60^\circ$ . . . . .	90
5.19	Streamlines for Turbulent Natural Convection in an Enclosure without partition; $Ra = 1 \times 10^{10}$ , $A=1.0$ , $P_r = 0.71$ , $\Phi = 30^\circ$ . . . . .	91
5.20	Effect of number of partitions on the Efficiency of the partition for Turbulent Natural convection in an enclosure with partition; $Ra = 8 \times 10^{10}$ , $A=10.0$ , $\Phi = 90^\circ$ . . . . .	95
5.21	Isotherms for turbulent natural convection in an enclosure without Partition; $Ra = 8 \times 10^{10}$ , $A=10.0$ , $\Phi = 90^\circ$ . . . . .	96

5.22 Isotherms for turbulent natural convection in a single partition enclosure with $Ra = 8 \times 10^{10}$ , $A=10.0$ , $N=1.0$ , $K_r = 1.0$ , $\Phi = 90^0$ , $t=0.1$ . . . . .	97
5.23 Isotherms for turbulent natural convection in a multiple partitioned enclosure with $Ra = 8.0 \times 10^{10}$ , $A=10.0$ , $N=4.0$ , $K_r = 1.0$ , $t=0.1$ , $\Phi = 90^0$ . . . . .	98
5.24 Streamlines for turbulent natural convection in an enclosure without Partition; $Ra = 8 \times 10^{10}$ , $A=10.0$ , $\Phi = 90^0$ . . . . .	99
5.25 Streamlines for turbulent natural convection in a single partition enclosure with $Ra = 8.0 \times 10^{10}$ , $A=10.0$ , $N=1.0$ , $K_r = 1.0$ , $t=0.1$ , $\Phi = 90^0$ : (a) Magnified view of the bottom (b) Magnified view of the top . . . . .	100
5.26 Streamlines for turbulent natural convection in a multiple partitioned enclosure with $Ra = 8.0 \times 10^{10}$ , $A=10.0$ , $N=4.0$ , $K_r = 1.0$ , $t=0.1$ , $\Phi = 90^0$ . . . . .	101
5.27 Dimensionless Temperature at the mid-height of the enclosure at different number of partitions. . . . .	102
5.28 Isotherms for Turbulent Natural convection in an enclosure with partition; $Ra = 1 \times 10^9$ , $A=10.0$ , $N=1$ , $K_r = 1.0$ , $t=0.1$ , $\Phi = 90^0$ . . . . .	105
5.29 Isotherms for Turbulent Natural convection in an enclosure with partition; $Ra = 1 \times 10^{13}$ , $A=10.0$ , $N=1$ , $K_r = 1.0$ , $t=0.1$ , $\Phi = 90^0$ . . . . .	106

- 5.30 Streamlines for Turbulent Natural convection in an enclosure with partition;  $Ra = 1 \times 10^9$ ,  $A=10.0$ ,  $N=1$ ,  $K_r = 1.0$ ,  $t=0.1$ ,  $\Phi = 90^\circ$ :  
 (a) Magnified view of the bottom (b) Magnified view of the top . . . 107
- 5.31 Streamlines for Turbulent Natural convection in an enclosure with partition;  $Ra = 1 \times 10^{13}$ ,  $A=10.0$ ,  $N=1$ ,  $K_r = 1.0$ ,  $t=0.1$ ,  $\Phi = 90^\circ$ :  
 (a) Magnified view of the bottom (b) Magnified view of the top . . . 108
- 5.32 velocity vectors for Turbulent Natural convection in an enclosure with partition;  $Ra = 1 \times 10^{13}$ ,  $A=10.0$ ,  $N=1$ ,  $K_r = 1.0$ ,  $t=0.1$ ,  $\Phi = 90^\circ$ :  
 (a) Magnified view of the bottom (b) Magnified view of the top . . . 109
- 5.33 Effect of Rayleigh number on the Average Nusselt no. for Turbulent Natural convection in an enclosure with partition;  $\Phi = 90^\circ$ ,  $A=10$ ,  $N=1$ ,  $t=0.1$ ,  $K_r = 1.0$ ,  $P_r = 0.71$  . . . . . 110
- 5.34 Effect of Aspect ratio on the Average Nusselt no. for Turbulent Natural convection in an enclosure with and without partition;  $Ra = 8.0 \times 10^{10}$ ,  $K_r = 1.0$ ,  $t=0.1$ ,  $\Phi = 90^\circ$  . . . . . 113
- 5.35 Isotherms for turbulent natural convection in a single partition enclosure with  $Ra = 8.0 \times 10^{10}$ ,  $A=2.0$ ,  $N=1.0$ ,  $K_r = 1.0$ ,  $t=0.1$ ,  $\Phi = 90^\circ$  . 114
- 5.36 Isotherms for turbulent natural convection in a single partition enclosure with  $Ra = 8.0 \times 10^{10}$ ,  $A=15.0$ ,  $N=1.0$ ,  $K_r = 1.0$ ,  $t=0.1$ ,  $\Phi = 90^\circ$  115
- 5.37 Streamlines for turbulent natural convection in a single partition enclosure with  $Ra = 8.0 \times 10^{10}$ ,  $A=2.0$ ,  $N=1.0$ ,  $K_r = 1.0$ ,  $t=0.1$ ,  $\Phi = 90^\circ$  116

- 5.38 Streamlines for turbulent natural convection in a single partition enclosure with  $Ra = 8.0 \times 10^{10}$ ,  $A=15.0$ ,  $N=1.0$ ,  $K_r = 1.0$ ,  $t=0.1$ ,  $\Phi = 90^\circ$  117
- 5.39 Effect of Angle of inclination on the Average Nusselt no. for Turbulent Natural convection in an enclosure with a partition;  $Ra = 8.0 \times 10^{10}$ ,  $A=10$ ,  $N=1$ ,  $K_r = 1.0$  . . . . . 119

## THESIS ABSTRACT

**Name:** MOHAMMED ABDUL RAZZAQ KHAN

**Title:** NUMERICAL SIMULATION OF  
TURBULENT NATURAL CONVECTION  
IN ENCLOSURES

**Major Field:** MECHANICAL ENGINEERING

**Date of Degree:** JUNE 1996

*This study represents the numerical solutions of the buoyancy driven turbulent flows in an inclined two dimensional rectangular enclosure in which one of the vertical walls is heated and the other is cooled. Low Reynolds number extension of the two equation  $k - \varepsilon$  model is used to model the turbulent flow. The effect of various parameters such as the number of partitions, the angle of inclination and the Rayleigh number on the flow field and the average Nusselt number have been investigated and presented.*

*The results indicate that the insertion of a single partition having a finite thickness and thermal conductivity reduces significantly the average Nusselt number. The rate of reduction decreases as more partitions are added. The results also indicate that there is an optimum angle of inclination at which the maximum average Nusselt number occurs and that the average Nusselt number increases as the Rayleigh number increases.*

*Keywords: Natural Convection, Rectangular Enclosure, Two-dimensional Flow, Turbulent Flow, Buoyant Flow, Partition,  $k - \varepsilon$  model.*

Master of Science Degree  
King Fahd University of Petroleum and Minerals  
Dhahran, Kingdom of Saudi Arabia.  
June 1996

## خلاصة الرسالة

الاسم :	محمد عبد الرزاق خان
عنوان الرسالة :	الكشف الرقمي عن الحمل الحراري الاضطرابي الطبيعي في المحتويات المستطيلة
التخصص :	هندسة ميكانيكية
تاريخ الشهادة :	يونيه ١٩٩٦م

تعرض الدراسة حلوًا رقميًا للتدفقات القوية المدفوعة بالتدفق الاضطرابي في منحوى مستطيلي مائل ثنائي الأبعاد تكون فيه واحدة من الجدران الرأسية ساخنة والأخرى باردة. وقد استعمل رقم رينولز المنخفض في النموذج  $k-\epsilon$  محاكاة التدفق. وتمت أيضًا دراسة أثر التغيرات الأخرى مثل عدد الوحدات الفاصلة ودرجة الميل ورقم رالي في مجال التدفق وكذلك متوسط رقم نسلت.

وتشير النتائج إلى أن إدخال وحدة فاصلة واحدة بسمك محدد موصلية حرارية تخفض إلى حد كبير من متوسط رقم نسلت. وأن معدل الانخفاض يتناقص مع إدخال وحدات فاصلة إضافية. وتبين النتائج أيضًا إلى أن هناك زاوية ميلان يحدث فيها الحد الأقصى لمتوسط رقم نسلت وأن رقم نسلت يزيد مع زيادة رقم رالي.

درجة الماجستير في العلوم

جامعة الملك فهد للبترول والمعادن

الظهران - المملكة العربية السعودية

يونيو ١٩٩٦م

## Nomenclature

$A$	Aspect ratio of enclosure ( $= H/L$ )
$C_p$	Specific heat
$g$	Acceleration due to gravity
$H$	Height of the enclosure
$K_f$	Thermal conductivity of the fluid
$K_s$	Thermal conductivity of the solid partition
$K_r$	Conductivity ratio ( $K_s/K_f$ )
$k$	Kinetic energy of turbulence
$L$	Distance between the two isothermal walls
$N$	Number of partitions
$Nu_y$	Local Nusselt number along the vertical wall
$\overline{Nu}$	Average Nusselt number
$P$	Pressure
$Pr$	Laminar Prandtl number ( $\mu C_p/K_f$ )
$Ra$	Rayleigh number ( $g\beta(T_h - T_c)H^3/\alpha\nu$ )
$Re_t$	Turbulence Reynolds number ( $k^2/\varepsilon \times 1/\nu$ )
$S_\theta$	Source term in the energy equation
$t$	Dimensionless thickness of the partition ( $x_2 - x_1/L$ )
$T$	Temperature

$u, v$	Velocities in the x,y directions, respectively
$x, y$	Horizontal and vertical co-ordinate directions
$y^+$	Dimensionless wall distance
$y_p$	Y-coordinate at grid node p

## Symbols

$\alpha$	Thermal diffusivity ( $K_f/\rho C_p$ )
$\beta$	Coefficient of thermal expansion
$\Delta T$	Temperature difference between the two walls
$\varepsilon$	Rate of dissipation of kinetic energy
$\mu$	Laminar viscosity
$\mu_t$	Turbulent viscosity
$\nu$	Laminar kinematic viscosity
$\Theta$	Fluctuating temperature
$\theta$	mean temperature
$\Phi$	Angle of inclination
$\phi$	General field variable represented in the transport equations
$\psi$	Stream function ( $\int u dy + \int v dx$ )

## Subscripts

$i, j$	Direction x, y or z
--------	---------------------



*max*      Maximum value

*min*      Minimum value

## Superscripts

'          Fluctuating quantity

–          Mean quantity

# Chapter 1

## Introduction

### 1.1 Background

Buoyancy forces arise as a result of variation of density in a fluid subject to gravity, and produce a wide range of phenomena of importance in fluid mechanics and heat transfer. Natural convection is one of these phenomena. Natural convection heat transfer occurs whenever a body is placed in a fluid at higher or lower temperature than that of the body. This difference in temperature causes change in the density of the fluid near the heated or cooled body. The lighter fluid moves up and the heavier fluid moves down resulting in natural motion of the fluid. Hence the process in which fluid flow arises due to the effect of density difference in a body force field such as gravitational field, is termed as natural convection. The fluid velocities in natural convection currents, especially those generated by the gravity, are generally

low, but the characteristics of the flow in the vicinity of the heat transfer surface are similar to those in forced convection. A boundary layer forms near the surface and the fluid velocity at the interface is zero. Natural convection flow may be laminar or turbulent, depending on the characteristic length, the fluid properties, the body force and the temperature difference between the surface and the fluid [1].

Generally there are two basic modes of flow generated by buoyancy. The first referred as conventional convection, occurs when the density gradient is normal to the gravity vector and the second mode known as unstable convection (also referred to as Rayleigh Benard convection), occurs when the density gradient is parallel to the gravity vector. Natural convection problems are classified as either external natural convection (eg. vertical plate) or internal natural convection (eg. enclosures).

## 1.2 External Natural convection

Natural convection flow arising due to a body placed in an extensive quiescent isothermal medium is termed as external natural convection flow. Flow through vertical surfaces, inclined surfaces, curved surfaces such as cylinders and spheres are some examples of the external natural convection.

Consider, as an example, the natural convection heat transfer from a heated vertical surface placed in an extensive medium at a uniform temperature. If the plate surface temperature is greater than the ambient temperature, the fluid adjacent to

the vertical surface gets heated, becomes lighter and rises. Heavier fluid from the neighboring areas rushes in to take the place of the rising fluid, similarly the flow for a cooled surface is downwards. The fluid next to the surface is stationary due to the no-slip condition and the fluid far from the vertical surface is stagnant because of the extensive quiescent medium. Therefore the flow exists in a layer adjacent to the surface with zero velocities on either side as shown in figure 1.1. A boundary layer exists and the region outside the boundary layer is unaffected by the flow [2].

External natural convection has wide range of application both in nature and in technology. Heat transfer processes in natural environment such as the buoyant flow arising from heat rejection to the atmosphere, circulation arising in atmosphere are few examples of external natural convection. In order to avoid overheating when the usual mode of heat transfer fails, natural convection is considered in the design of electronic devices and systems in power generation. Natural convection is also responsible for heat losses from pipes carrying steam or other heated fluids and from the coil of a refrigerating unit to the surrounding air.

### **1.3 Internal Natural Convection**

Natural convection flow arising in enclosed areas is termed as internal natural convection. The internal flow problems are generally more complex than the external ones. In the latter, the region outside the boundary layer is taken as unaffected by

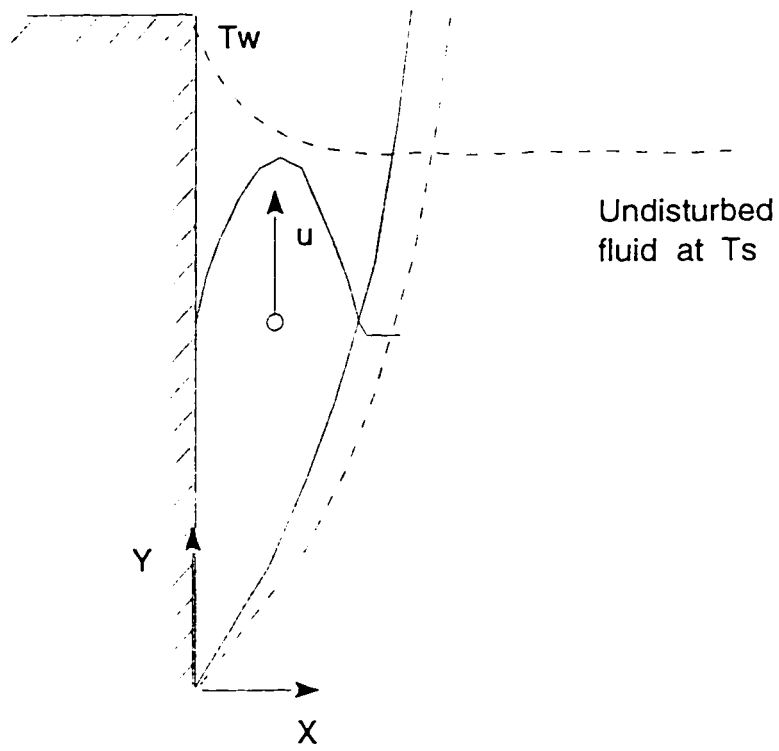


Figure 1.1: Representative velocity and temperature distribution in natural convection boundary layer flow on a heated vertical plate

the flow where as in internal flows, boundary layer form near the walls but the region exterior to them is enclosed by the boundary layers and form a core region. The core is partially or fully encircled by the boundary layers. The two are obviously coupled in most cases and it is this coupling that introduces a considerable amount of complexity in the analysis of internal flows [3].

A problem considered very extensively, as an example of internal natural convection flows, is that of flow between parallel plane walls, horizontal and vertical. The two walls are taken at different temperatures and the flow is studied as a function of the temperature difference and the distance between the walls. The case of horizontal layer of fluid heating from below have been studied by several investigators. Other problems of interest and which have been considered in some detail are the flow in rectangular enclosures, in closed end tubes and in horizontal circular cylinders. The two cases of flow, between infinite vertical and horizontal plates, are special circumstances of flow in a rectangular enclosure.

### **1.3.1 Natural Convection in Enclosures**

Natural convection in enclosures is a topic of contemporary importance. because enclosures filled with fluid are central components in a long list of engineering and geographical systems. The flow and heat transfer induced, for example in the inner air space of a double-pane window system differs fundamentally from the external natural convection. Natural convection in enclosure is the result of the complex

interaction between the finite size fluid system in thermal communication with all the walls. The complexity of this internal interaction is responsible for the diversity of flows that can exist inside enclosures [3].

The phenomenon of natural convection in an enclosure is varied as the geometry and orientation of the enclosure. Judging from the number of potential engineering applications, the enclosure phenomena can loosely be organized into two large classes

1. Enclosure heated from the side
2. Enclosure heated from below

The first class is representative of applications such as solar collectors, double wall insulations and air circulation through rooms in a building. The second class refers to the functioning of thermal insulation oriented horizontally. eg. Heat transfer through a flat roof attic space.

The present study primarily focuses on enclosures heated from the side. The reason for this choice is because of its applications in thermal insulation engineering, solar technology and energy management in architectural design.

# Chapter 2

## Literature Survey

The study of natural convection flows in an enclosure has received considerable attention during the past three decades. A review article by Ostrach [4] represents an excellent summary of the past research activities. The important variables in the problem are the temperature difference between the two vertical surfaces,  $\Delta T$ , the horizontal distance between them,  $L$ , and their height,  $H$ . Different flow regions have been found to occur under various conditions on the basis of experimental information.

### 2.1 Natural Convection in Vertical Enclosures

The heat transfer in rectangular cavities, with isothermal vertical walls and either perfectly conducting or perfectly insulating horizontal surfaces, was studied by



Batchelor [5]. Different flow regimes which arise depending on  $Ra$  and  $H/L$ , were examined. For small values of Rayleigh number  $Ra$ , heat transfer was found to be predominantly by conduction. Batchelor mentioned the fact that for air gap thickness of less than 1 cm, convection was negligible and that as  $L$  increases from 1 to 2.5 cms, the heat transfer rate decreases, being essentially constant beyond about 2.5 cm.

Eckert and Carlson [6] carried out detailed experimental study on the flow and heat transfer in rectangular enclosures. The aspect ratio was varied from 2.1 to 46.7 and the Rayleigh number from 200 to  $2 \times 10^5$ . It was concluded that at low values of  $Ra$ , conduction is the dominant mechanism. The temperature distribution from the hot wall to the cold wall was found to be linear indicating the predominance of conduction heat transfer. The lower and upper ends of the flow region showed a little disturbance in the field indicating significant effect of convection at these ends. At higher values of  $Ra$ , boundary layers on the two vertical walls were observed and the temperature variation was seen to be largely in these boundary regions, the central region being isothermal in the horizontal direction. Three flow regimes i.e conduction regime, transition regime and the boundary layer regime were indicated in their study. Turbulent fluctuations were also observed as the  $Ra$  was increased.

Another work of considerable significance, on the physical mechanism related to flow between vertical walls, is that by Elder [7]. The aspect ratio was varied from 1-60 and the Rayleigh number to the order of  $10^8$ . For low values of  $Ra$ ,  $Ra < 10^3$ ,

a weak, steady, unicellular circulation was observed, with fluid rising near the hot wall and descending near the cold wall. This then is the conduction regime. At higher  $Ra$ , in range  $10^3 < Ra < 10^5$ , large temperature gradients were observed near the walls, with a uniform temperature gradient in the interior region. As  $Ra$  increases, more inflexion points appear and the flow gradually becomes localized near the walls, the central region being at a much lower velocity. With a further increase in  $Ra$  i.e  $3 \times 10^5$  the unicellular motion is disturbed and secondary flow arises. The transition of the flow from laminar to turbulent flow was studied by Elder [8]. Disturbances, in the form of waves, propagated up the hot surface and down the cold one. Turbulence was found to arise around  $Ra = 10^9$ .

Schmidt et.al [9] observed two flow regions in rectangular enclosures with aspect ratio 2 and  $Ra = 6 \times 10^8$ , a primary flow moved up the hot wall and down the cold wall, and the secondary flow region was observed at the upper part of hot wall and at the lower part of cold wall. Experimental results of turbulent natural convection in rectangular enclosure by Giel et.al [10] shows the properties of laminar, transition, turbulent, relaminarization and the quiescent region. Formation of recirculating vortices along the 70 percent of each wall was also observed.

Analytical and experimental determination of heat transfer through vertical plane layers was studied by Emery and chu [11]. The governing equations were solved by applying the boundary layer assumptions and then integrating the equation yielded results which differed by no more than 12 percent from the measured

data. Numerical computation were performed for free convection under isothermal wall and constant heat flux boundary conditions by MacGregor and Emery [12]. It was concluded that the net heat transfer is a strong function of the cell aspect ratio and for Prandtl numbers less than one, a significant separate Prandtl number effect exists.

Nobuhiro Seki et.al [13] studied the behavior of heat transfer in a rectangular cavity with isothermal vertical walls. Heat transfer coefficients are measured for  $Pr$  of 3 - 40.000 and aspect ratio from 5 - 47.5 and their correlations were presented for laminar, transition and turbulent regions. An important conclusion was made regarding the height of the vertical wall as a representative length in Rayleigh number and Nusselt number. The visual observations performed by using various heights of the cavity with constant width under the same temperature of the vertical walls indicate that turbulent flow is generated at the upper part of the heated wall as the height of the cavity was increased. It was concluded that height of the cavity plays a significant role in the heat transfer, therefore height of the cavity is a better representative length than the width of the cavity.

In recent years a large number of numerical investigations have been carried out in parallel with experiments. Markatos and Pericleous [14] carried out a number of numerical computations utilizing the control volume upwind scheme for laminar and turbulent natural convection in square cavities. The Rayleigh number was varied from  $10^3 - 10^6$  for laminar region and from  $10^7 - 10^{16}$  for turbulent regime using

the standard  $k - \varepsilon$  model of turbulence. Their results were found to be in good agreement with the benchmark solutions of G.De Val Davis [15].

Ozoe et. al. [16] studied the heat transfer characteristics of a three dimensional natural convection flow in cubical enclosure using a two equation model for turbulence with Rayleigh number ranging between  $10^6 - 10^7$ . They concluded that spiral vortex exist near the side walls and the maximum value of the time-averaged eddy diffusivity was 2.6 times the molecular kinematic viscosity. Their computational scheme was also applicable to different boundary conditions, different aspect ratios and for different enclosure inclinations.

A large number of papers have been published in turbulent natural convection in vertical enclosures ( inclination angle  $\theta = 90^0$  ) utilizing various numerical schemes and different turbulence models. Ince and Launder [17] studied turbulent flows in rectangular enclosures utilizing Jones-Launder low Reynolds number  $k - \varepsilon$  model and found that the model leads to satisfactory agreement with the reported experimental data. It was concluded that the original form of low Reynolds number  $k - \varepsilon$  model did not succeed in predicting correct flow rate and heat transfer. However the modification made in the low Reynolds number  $k - \varepsilon$  model showed good agreement with the experiments.

Henkes et.al. [18] utilized three different turbulent models i.e. standard  $k - \varepsilon$  model, Jones-Launder low Reynolds number model and Chien's low Reynolds number model, to investigate the heat transfer characteristics of turbulent natural convec-

tion flow in square cavity. It has been concluded that the average wall heat transfer coefficient obtained using standard  $k-\varepsilon$  model is quite high, while the ones obtained using low Reynolds models of Jones-Launder and Chien are in a reasonable agreement compared to the corresponding experimental values. It was also concluded that using higher Prandtl number fluids (water) results in significant differences between the models.

Hanjalic and Vasic [19] utilized algebraic flux model for the prediction of turbulent natural convection in rectangular enclosure. It was concluded that for a simple class of problems like side heating and cooling, results obtained using different models of turbulence are reasonably close to each other. But in case of tall cavities and for cavities with simultaneous heating from sides and from bottom the prescribed algebraic flux model could serve better results.

Hiendel et.al. [20] used fixed coefficient (FC) and variable coefficient (VC) low Reynolds number models to predict the average nusselt number for turbulent natural convection within a differentially heated enclosure. They concluded that average nusselt numbers are predicted more accurately using variable coefficient model compared to using the fixed coefficient model.

Henkes and Hoogendoorn [21] derived the scaling of the turbulent natural convection for Rayleigh number upto  $10^{20}$  using three different  $k-\varepsilon$  models of turbulence. The scaling found were almost independent of the  $k-\varepsilon$  model used.

A detailed numerical study of the various models of turbulence has been studied

by Betts and Dfa'Alla [22]. Predictions from a range of low Reynolds number  $k - \varepsilon$  of turbulence have been compared with the experimental data. Out of the ten models tested, only those of Jones-Launder, Launder-Sharma, Hassid-Poreh and Wolfshtein's models predicted results that were reasonably comparable with the experimental data. It was also concluded that the use of wall laws based on forced flows, where shear stress is constant near the wall, is obviously wrong in natural convection.

Sun and Emery [23] investigated heat transfer characteristics in a two dimensional square cavity with a conducting vertical baffle. The velocity and temperature profiles indicated that effect of inserting baffle on the overall heat transfer is within limits except when the height of the baffle is more than 0.5 and if the location is near the heated walls.

## 2.2 Natural Convection in Inclined Enclosures

The knowledge of heat transfer characteristics of natural convection flow across inclined fluid layers is often of interest. Such fluid layers occurs, for example, between the absorber and cover plates of a solar collector, insulation of buildings and in window glazing. An active research in this problem led to numerous analytical and experimental studies, but the numerical studies are rather sparse.

Arnold et.al [24] investigated the effect of angle of inclination on the heat transfer

across rectangular regions of several aspect ratios in the laminar range i.e Rayleigh number between  $10^3 - 10^6$ . The angle of inclination was varied from 0 deg (heated from above) to 180 deg (heated from below) with aspect ratio of one, three, six and twelve. It was concluded that the scaling law could not be applied for the cases with  $\theta > 90$  deg as the flow becomes more complex.

Extensive experiments involving high aspect ratio enclosures heated from below are reported by Hollands et.al [25]. The Rayleigh number range covered is from  $10^3 - 10^5$  and the angle of inclination is from  $0 < \theta < 70$  deg (heated from below). A correlation was developed which gives Nusselt number as a function of  $Ra \times \cos \theta$  and  $\theta$ .

Another significant contribution on the study of inclined rectangular enclosure was given by ElSherbiny et.al [26]. Measurements are reported for high aspect ratios between 5-110 and Ra ranging from  $10^2 - 2 \times 10^7$ . It was concluded that the average Nusselt number depends on Ra, aspect ratio and the angle of inclination. Correlations has been provided for inclined and vertical layers.

Badr and Siddiqui [27] investigated the effect of angle of inclination on the coupling effect between natural convection inside a rectangular enclosure and forced convection outside the enclosure. It was concluded that the coupling effect resulted in a reduction in the heat transfer rate. The angles of inclination was varied between  $40^\circ$  and  $90^\circ$ .

Results concerning turbulent natural convection in inclined enclosures have so

far been very limited. Kuyper et.al. [28] studied numerically both the laminar and turbulent natural convection in inclined enclosure utilizing the standard  $k - \varepsilon$  model to account for turbulence. They reported that the nusselt number shows strong dependence on the orientation of the cavity and power law dependence on the Rayleigh number of the flow.

Ben Yedder and Bilgen [29] studied turbulent natural convection in enclosure bounded by a massive wall and concluded that maximum heat transfer occurs for an inclination angle of 80 -90 degrees and also stated that the heat transfer is an increasing function of the Rayleigh number and of the wall conductivity.

## **2.3 Natural Convection in Inclined and Partitioned Enclosures**

One of the least studied, yet most frequently encountered cases, is the one of an inclined enclosure in which partitions are inserted in order to reduce the heat transfer rate. Most of the studies in a partitioned enclosure have been concerned with vertical air filled enclosures.

Tong and Gerner [30] studied numerically the effect of partition position on the heat transfer rate. He compared the results of the bisected air-filled enclosure (partitioned enclosure) with that of an enclosure fully filled with a porous insulation and concluded that bisecting the enclosure with a partition is an effective method



of reducing heat transfer. Maximum reduction in heat transfer occurs when the partition is placed midway between the vertical walls.

Anderson and Bejan [31] studied enclosures with a single partition analytically based on the Oseen linearization method. The study was in the boundary layer regime and the effect of the conductance through the partition was supposed to be negligible. They confirmed their results experimentally using an enclosure with a double partition. The experimental results were correlated to obtain a relation of heat transfer between the two isothermal walls. It was proportional to  $(1 + N)^{0.61}$  where  $N$  is the number of partitions.

Nishimura et.al. [32] developed a boundary layer solution for natural convection in enclosures with a partition and the solution validity is confirmed by experiments. It has been concluded that the heat transfer rate is independent of the position of the partition if the boundary-layer thickness is less than the half width of each cell constructed by the partition.

Nishimura et.al. [33] studied the effect of multiple partitions on heat transfer rates in horizontal enclosures. It was also found from the engineering standpoint that the horizontal and vertical enclosures are equivalent in the thermal insulation capability of partitions under the same conditions, in spite of different flow pattern.

Kangni et.al [34] studied laminar natural convection and conduction in enclosures having multiple partitions. Effect of Rayleigh number, aspect ratio, thickness of the partition and the conductivity ratio (solid to fluid conductivity) has been studied for

air as the fluid medium. It was concluded that at high Ra the heat transfer decreases with increasing  $N$ , increasing partition thickness and increasing conductivity ratio  $K_r$ .

Mamou et.al. [35] studied extensively the effect of different parameters like Rayleigh number, angle of inclination, solid to fluid conductivity ratio, thickness of fluid layer, thickness of solid partitions, and number of partitions on the overall nusselt number for laminar natural convection in inclined enclosures. Stream function and temperature field is obtained analytically and compared with the numerical calculations. Good agreement was found between the parallel flow approximation and the numerical simulation when the conductivity ratio ' $K_r$ ' was not too large.

Analytical and Numerical study of natural convection in inclined enclosures was also performed by Vasseur et.al. [36]. The governing equations of the fluid layers are solved analytically in the limit of thin layered system with constant flux boundary conditions. This study was limited to Rayleigh numbers upto  $10^7$  i.e. laminar regime.

## 2.4 Scope of the work

From the literature review relevant to the present study, it is evident that along with the experimental and analytical work, there is a great emphasis on the numerical computation. This is on one hand because of the cost effectiveness and wider

availability of high speed computers and on the other hand due to the fact that a numerical solution provide more detailed information about the flow and temperature field as compared to the experimental observation. In the experimental work, number of points at which measurements are taken is very limited because it requires heavy instrumentation. The literature review clearly shows that even those cases which have already been solved experimentally, are being solved numerically so as to establish validation of newly developed numerical schemes and computer codes.

As can be seen from the literature review that the fluid flow and heat transfer calculations for natural convection in inclined partitioned enclosures is limited to laminar flow i.e  $Ra < 10^7$ . No such calculations exist in the literature for natural convection in inclined partitioned rectangular enclosures in the turbulent regime.

Consequently in the present study, the numerical simulation of turbulent natural convection in inclined and partitioned rectangular enclosure is being accomplished. Partitions in the enclosure is introduced to reduce the heat transfer which reflects the insulation capability of partitions. Such information is very essential and beneficial to the design of double glazed windows and in the energy conservation in architectural design of buildings. Effect of number of partition, aspect ratio, angle of inclination and Rayleigh number will be discussed. For all the cases studied, the average Nusselt number is determined.

To accomplish this task, we use the control volume method. In this method, the

equations are discretized into algebraic equations by performing the integration of the governing non-linear partial differential equations across a finite control volume. These equations are then solved using Semi Implicit Method for Pressure-Linked Equation (SIMPLE) algorithm which is an iterative method. A well developed finite-volume code (PHOENICS) is being used to accomplish this simulation. PHOENICS stands for Parabolic, Hyperbolic or Elliptic Numerical Integration Code.

## Chapter 3

# Mathematical Formulation

In Natural convection, as in other convective processes, a consideration of fluid flow is necessary in the study of the energy and mass transfer mechanisms. A study of convection further necessitates a consideration of the coupling between the fluid flow and the mechanism underlying conduction. This is due to the fact that the heat transported due to the moving fluid element would eventually be transferred to its neighboring elements through conduction. In natural convection processes, unlike forced convection, the flow itself arises due to the temperature difference in the body-force field. Therefore the heat transfer and the fluid flow processes are inseparably linked together and one may not be determined independent of the other.

The physical situation involving fluid flow, mass transfer and heat transfer are governed by the conservation principles of mass, momentum and energy. These

principles have been derived in the form of partial differential equation. These equations have the general form of a transport equation as described below

$$\rho \frac{\partial \phi}{\partial t} + \frac{\partial}{\partial x_i} (\rho u_i \phi) = \frac{\partial}{\partial x_i} \left[ \frac{\mu}{Pr} \frac{\partial \phi}{\partial x_i} \right] + S \quad (3.1)$$

Here  $\phi$  is any field variable and  $u$  is the velocity vector. This equation describes the transport of scalar or vector quantity which takes place because of convection and diffusion processes.

The first term in the general transport equation is called the transient term. It represents the accumulation of variable  $\phi$  in the control volume. The second term is called convection term. This represents the transport of property  $\phi$  due to mass flow in the control volume. The third term is called diffusion. This represents the flow of property  $\phi$  due to its gradient in the flow field. The fourth term is called source term. This represents the rate of generation of the transport variable  $\phi$  within the control volume.

The equations renders a great convenience from the point of view of solution methodology. A computer program which seeks to solve this equation is actually able to simulate transport of any variable by merely changing the Prandtl number

and the source term. For example if  $P_r=1$  and  $S = -\frac{\partial p}{\partial x_i} + \rho g_i$ , the above equation describes the momentum equation. If  $P_r = \frac{\mu C_p}{k}$  and  $S=0$  the above equation describes energy equation without internal heat generation.

### 3.1 Problem Considered

The problem considered is depicted schematically in figure 3.1 and refers to the two dimensional flow in a rectangular enclosure with height 'H'. and the distance between the isothermal walls as 'L'. The upper and lower walls are kept insulated while the two vertical walls are heated and cooled uniformly. The enclosure is inclined at an angle  $\Phi$  measured from the heated side (i.e.  $\Phi=90$  deg corresponds to vertical enclosure). A solid partition of thickness ' $t$ '. ( $\frac{x_2-x_1}{L}$ ) and conductivity of  $k_s$  is placed at a distance  $x_1$  from the origin. Two flow regions exist which are separated by a solid partition.

The particular form of the general transport equation which governs the process of natural convection in an enclosure is being presented below. It is composed of a continuity, two momentum and an energy equation. The considered flow is assumed to be steady state, two dimensional with negligible viscous dissipation. As the velocities involved in natural convection processes are very low we neglect the effect of viscous dissipation. The fluid is an ideal gas with  $\mu$ ,  $C_p$  and  $k$  as constant.

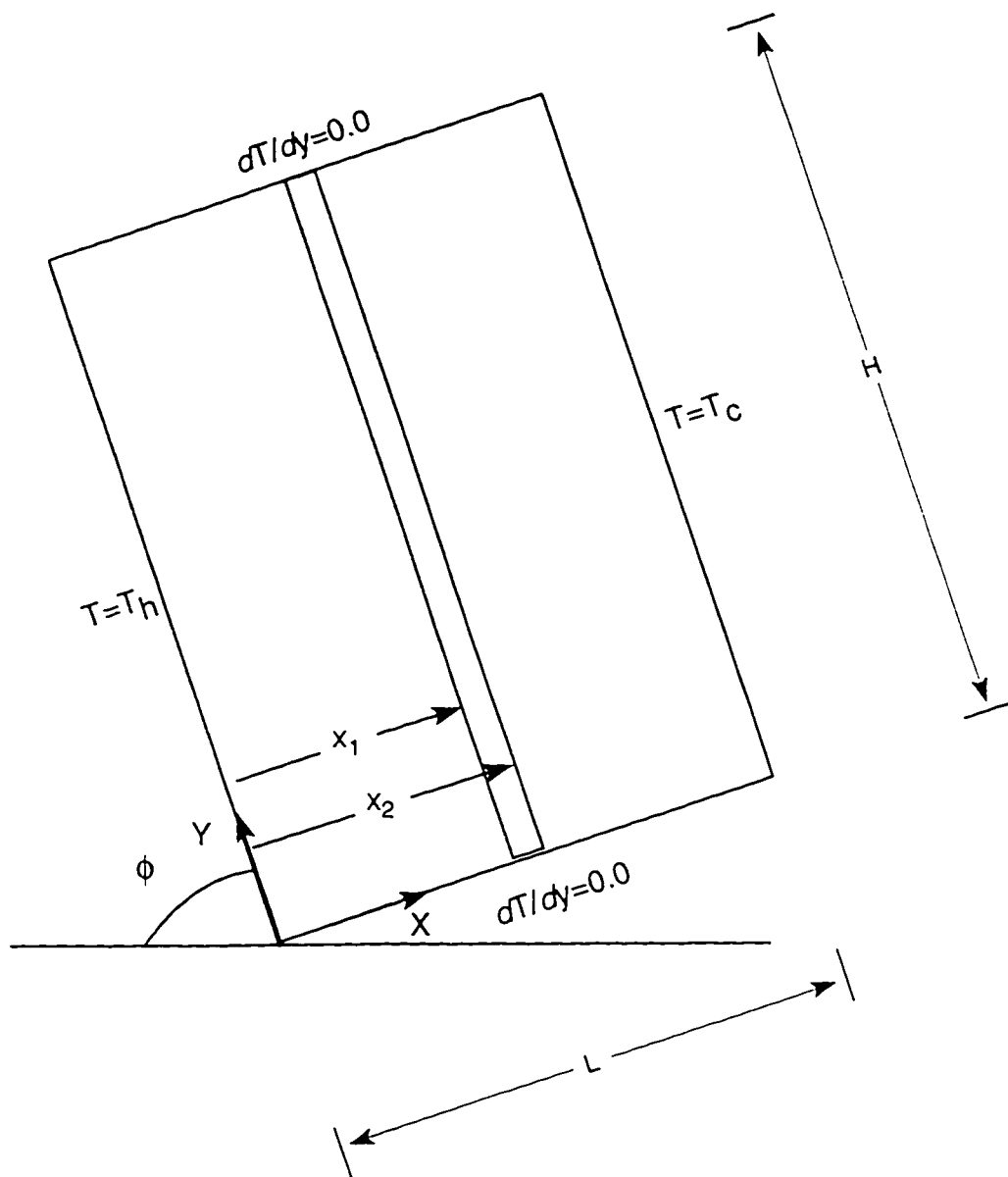


Figure 3.1: A Rectangular Enclosure



Mass Conservation: Continuity equation;

$$\frac{\partial}{\partial x_i}(\rho u_i) = 0 \quad (3.2)$$

Momentum Conservation: Navier-Stokes equation

$$\frac{\partial}{\partial x_i}(\rho u_i u_j) = -\frac{\partial p}{\partial x_j} + S_{x_j} + \frac{\partial}{\partial x_i} \left[ \mu \left[ \frac{\partial u_j}{\partial x_i} + \frac{\partial u_i}{\partial x_j} \right] \right] \quad (3.3)$$

Energy Conservation: Energy Equation

$$\frac{\partial}{\partial x_i}(\rho u_i T) = S_\theta + \frac{\partial}{\partial x_i} \left[ \frac{\mu}{Pr} \frac{\partial T}{\partial x_i} \right] \quad (3.4)$$

where  $u_j$  is the velocity component in the coordinate directions  $x_j$ ,  $p$  is the local pressure,  $\rho$  is the fluid density,  $S_{x_j}$  is the source (body force) term in the co-ordinate direction  $x_j$  i.e  $S_{x_1} = S_x = -g\beta(T_h - T_c) \cos(\Phi)$  and  $S_{x_2} = S_y = -g\beta(T_h - T_c) \sin(\Phi)$ , and  $S_\theta$  is the source term in the energy equation which is taken as zero.

## 3.2 The Effect of Extremely Small Scale of Turbulence

Many Natural convection flows of interest, in nature and in technology, are turbulent. Turbulence is a term which denotes a motion in which an irregular fluctuation is superimposed on the main flow. The velocity, pressure and temperature at a given point do not remain constant with time, but vary irregularly at a relatively high frequency. There is a considerable amount of mixing, with the fluid packets moving around irregularly, giving rise to the observed fluctuations. The scale of these fluctuations is several orders of magnitude smaller than the flow domain size. The consequence is that a grid typically of the order of 1000 points is required in each flow direction. It means that the total number of grid points will be of the order of  $10^9$  to fill the three dimensional space. To add to this, the flow being unsteady requires extremely small time steps.

The computational facilities available at present are far beyond those required for an analysis of this kind. In fact many researchers express the idea that we may never be able to simulate turbulent flows using direct numerical simulation (i.e. using full Navier Stokes Equations without any modelling assumptions about structure of turbulence). At the same time, it should be clear that Engineers in any case are not interested in these small scale fluctuations. The scale of motion which is of practical significance to them is much higher than that of these fluctuations.

both temporally and spatially.

### 3.3 The Mean Flow Equations

Above discussion leads us in a logical way to the statistical approach to obtain the time averaged behavior of the flow properties.

The time averaged values of the velocity components are denoted as  $\bar{u}$ ,  $\bar{v}$ ,  $\bar{w}$  and the disturbance or fluctuating quantities are represented as  $u'$ ,  $v'$ ,  $w'$ . The instantaneous value of velocity, pressure and temperature is given as  $u = \bar{u} + u'$ ,  $v = \bar{v} + v'$ ,  $w = \bar{w} + w'$ ,  $p = \bar{p} + p'$ ,  $T = \bar{\theta} + \Theta$

The time averages are found by integrating the local instantaneous value, of the particular quantity at a given point, over a sufficiently long interval of time. The interval is large as compared to the time period of the fluctuations, but sufficiently smaller than the time level of interest. The time average flow properties are much smoother in the spatial as well as temporal domains. The consequences are that to capture the flow, a grid with the enormous number of nodes is no more required. In fact, if the mean flow behavior is not changing with time, then, no time marching is required. With time averaged equations, we require a grid having size of the same order as required by a laminar flow for the same system, and, fortunately this time mean behavior is the one of interest to an engineer. The time averaged equations are described as [37]

Mass conservation: (Continuity Equation)

$$\frac{\partial}{\partial x_i}(\rho \bar{u}_i) = 0 \quad (3.5)$$

Momentum Conservation: (Momentum equation)

$$\frac{\partial}{\partial x_i}(\rho \bar{u}_i \bar{u}_j) = -\frac{\partial \bar{p}}{\partial x_j} + S_{xj} + \frac{\partial}{\partial x_i} \left[ \mu \left( \frac{\partial \bar{u}_j}{\partial x_i} + \frac{\partial \bar{u}_i}{\partial x_j} \right) - (\rho \overline{u'_i u'_j}) \right] \quad (3.6)$$

Energy Conservation: (Energy equation)

$$\frac{\partial}{\partial x_i}(\rho \bar{u}_i \theta) = S_\theta + \frac{\partial}{\partial x_i} \left[ \frac{\mu}{Pr} \left( \frac{\partial \theta}{\partial x_i} \right) - (\rho \overline{u'_i \Theta}) \right] \quad (3.7)$$

The above equations are formally identical with the governing equations for laminar flow, if velocities, pressures and Temperature are replaced by their time averages except for some additional terms, which depend on the turbulent fluctuations of the flow. These terms have appeared as a consequence of the averaging process.

### 3.4 The Problem of Closure

The above equations, although time averaged, are still exact since no assumptions have been introduced in deriving them, but they no longer form a closed set. The

averaging procedure introduces unknown correlations among the fluctuating velocities. These terms have the behavior of additional stresses on the fluid elements and are called turbulent or Reynolds stresses ( $\overline{\rho u'_i u'_j}$ ) and turbulent fluxes ( $\overline{\rho u'_i \Theta}$ ). In most cases, these are much larger than their laminar counterpart.

The real difficulty in these equations is that the relationship between the mean and turbulent components is not known. The determination of these correlations is the main problem in calculating the turbulent flow properties. Exact transport equations can be described for these turbulent stresses, but they contain correlations of the next higher order. Their closure is, therefore, not possible in an exact way [38]. Hence, turbulent flows can not be simulated in an exact way using time-averaged equations. We need to make some modelling assumptions about these correlations so as to close our mathematical model. Different modelling assumptions have been proposed for these correlations. These modelling assumptions are called turbulence models. These turbulence models approximate these correlations in terms of mean flow quantities and some empirical constants.

### 3.5 Turbulence Modelling

In order to predict turbulent flows by numerical solutions to the Reynolds equations, it becomes necessary to make closing assumptions about the apparent turbulent stress and heat flux quantities, turbulent modelling is thus needed to calculate the

turbulent flows.

If modelling assumptions are introduced for the Reynolds stresses and Turbulent fluxes appearing in the time mean equations then turbulence model is known as 'First Order Turbulence Model' [38].

If, however, exact transport equations are introduced for these apparent stresses and fluxes, then they will contain turbulent correlations of the next higher order. If modelling assumptions are introduced for these correlations, then model is known as 'Second Order Turbulence Model' [38]. With appropriate modelling assumptions and empirical constants these models are much more general and become widely applicable as compared to first order models.

Similarly, higher turbulence models can still be developed which, with appropriate modelling assumptions and empirical inputs, are expected to work better than lower order models.

However, there is a serious problem in this regard. The advantage of higher order models are offset by the fact that number of differential equations comprising the turbulence model increases with the order of turbulence model. The consequences are two fold. Firstly, there is a great increase in the computational effort to solve the problem. Secondly, and far more serious, is that they require a greater number of empirical inputs and modelling assumptions and, thus, demand great effort to determine the suitable ones. In fact, with poor modelling assumptions and empirical information they can work even poorer than first order models.

For these reasons, to our knowledge, models having an order higher than second order have not been used yet. Great majority of problems is solved using first order models which have so far been reasonably developed and provide satisfactory solution for many problems.

### 3.5.1 First Order Models

#### Boussinesq Approximation

Perhaps the first move towards a model of turbulence can be attributed to Boussinesq. All first order models are based on his approximation. He suggested that the effective turbulent shear stress, arising from the cross correlations of fluctuating velocities, could be replaced by the product of the mean velocity gradient and a quantity termed as the 'turbulent viscosity' [39].

Boussinesq approximation:

$$\tau_{ij} = \overline{\rho u'_i u'_j} = -\mu_t \left[ \frac{\partial \bar{u}_j}{\partial x_i} + \frac{\partial \bar{u}_i}{\partial x_j} \right] + 2/3 \rho k \delta_{ij} \quad (3.8)$$

$$\overline{\rho u'_i \Theta} = -\frac{\mu_t}{\sigma_\theta} \frac{\partial \bar{\theta}}{\partial x_i} \quad (3.9)$$

Where  $\mu_t$  is the turbulent eddy viscosity and  $\sigma_\theta$  is the turbulent Prandtl number which is taken as a constant. With this approximation being introduced, the time averaged equations take the form.

Mass conservation: (Continuity Equation)

$$\frac{\partial}{\partial x_i}(\rho \bar{u}_i) = 0 \quad (3.10)$$

Momentum Conservation: (Momentum equation)

$$\frac{\partial}{\partial x_i}(\rho \bar{u}_i \bar{u}_j) = -\frac{\partial \bar{p}}{\partial x_j} + S_{x_j} + \frac{\partial}{\partial x_i} \left[ (\mu + \mu_t) \left( \frac{\partial \bar{u}_j}{\partial x_i} + \frac{\partial \bar{u}_i}{\partial x_j} \right) \right] \quad (3.11)$$

Energy Conservation: (Energy equation)

$$\frac{\partial}{\partial x_i}(\rho \bar{u}_i \theta) = S_\theta + \frac{\partial}{\partial x_i} \left[ \left( \frac{\mu}{Pr_\tau} + \frac{\mu_t}{\sigma_\theta} \right) \frac{\partial \theta}{\partial x_i} \right] \quad (3.12)$$

Here the last term in the Boussinesq approximation has been included in the pressure term, since it represents the normal stress.

Now there remains the task of determining  $\mu_t$ . Many equations have been proposed to determine it. Some of them will be described briefly.



### Basic Concept in determining $\mu_t$

All the models which seek to determine  $\mu_t$  utilize a fundamental concept. They assume an analogy between molecular motion and turbulent motion. The turbulent eddies are thought of as lumps of fluids which like molecules collide and exchange momentum. The kinematic viscosity is proportional to the average velocity of molecules and mean free path between them. Likewise the eddy viscosity is considered proportional to a velocity characterizing the fluctuating motion and a typical length of this motion which Prandtl called the mixing length [39].

$$\mu_t \propto \bar{v} L_m \quad (3.13)$$

The analogy is not complete and objections have been raised by researchers, but still the eddy viscosity has been found to work well in practice, especially for two dimensional boundary layer type flows.

Depending on the number of differential equations comprising the models, first order models can be divided into following types.

1. Zero equation models
2. One equation models
3. Two equation models

We will describe one example of each with particular emphasis on two equation  $k - \epsilon$  model, since this is the model which has been selected for the purpose of this study.

### Zero equation models

These models do not involve transport equations for turbulence quantities, but instead employ the eddy viscosity concept and specify the eddy viscosity either directly from experiments, through empirical formulae, or by relating it to the mean velocity distribution. The most popular model of this kind is the Prandtl mixing length model. In this model, Prandtl postulated that the velocity of turbulence,  $\bar{v}$  is equal to the mean velocity gradient times the mixing length.

$$\bar{v} = L_m \left[ \frac{\partial u}{\partial y} \right] \quad (3.14)$$

With this relation, the eddy viscosity can now be expressed as

$$\mu_t = \rho L_m^2 \left[ \frac{\partial u}{\partial y} \right] \quad (3.15)$$

Where  $L_m$  is the mixing length which is specified by simple empirical formulae.

In confined geometries i.e. Enclosure, turbulence is produced mainly near the walls and is transported by convection. This model neglects the convective and diffusive transport and hence predicts unrealistically low values in recirculating flows. It has many advantages and disadvantages.

The advantages are :

1. It is simple and requires no additional differential equation.
2. With good choices of mixing length distribution, the realistic predictions are possible.
3. Enough experience has accumulated.

The disadvantages are :

1. There is no successful experience of predicting recirculating flows.
2. It implies zero effective viscosity and thermal conductivity at zero velocity gradient.
3. It takes no account of process of convection and diffusion.

## One equation Models

The state of turbulence at a point is influenced by the state of turbulence at other points in the flow. It means that it is not very suitable to determine the velocity scale of turbulence merely by the local flow properties, as is the case with the mixing length model. Rather, a transport equation should be used in determining the velocity scale so that the net effect of neighboring points due to convection and diffusion can be accounted for. The same is true for the case of length scale of turbulence, whose magnitude varies in the flow.

One equation transport models provide a differential transport equation for one of the two properties; the velocity scale of turbulence. Still the length scale is determined from empirical data.

A well known one equation model is proposed by Prandtl and is called 'K model'. In this model, the velocity scale is taken to be the square root of turbulence kinetic energy. A differential equation is derived from Navier Stokes equations and the unknown terms appearing in the equations are modelled using appropriate assumptions. The modelled form of this approach is given by

$$\rho \bar{u}_i \frac{\partial k}{\partial x_i} = \frac{\partial}{\partial x_i} \left[ \left( \mu + \frac{\mu_t}{\sigma_k} \right) \frac{\partial k}{\partial x_i} \right] + P_k + G_k - \rho \varepsilon \quad (3.16)$$

Where  $P_k$  is the production term given by the relation.

$$P_k = \mu_t \left[ \frac{\partial \bar{u}_j}{\partial x_i} + \frac{\partial \bar{u}_i}{\partial x_j} \right] \frac{\partial u_i}{\partial x_j} \quad (3.17)$$

$G_k$  is the buoyancy production/Destruction term which is given as

$$G_k = g_i \beta \frac{\mu_t}{\sigma_t} \left[ \frac{\partial \theta}{\partial x_i} \right] \quad (3.18)$$

and  $\varepsilon$  is the dissipation term. Here,

$$k = \Sigma u_i'^2 \quad (3.19)$$

and

$$\mu_t = \rho k L \quad (3.20)$$

This type of model has not gained popularity, because there is no transport equation for the length scale and empirical determination of length scale is difficult.

Hence, the advantage of a transport equation for velocity scale is offset.

To obtain the level of generality, especially seeking for recirculating flows we must search the model in which transport effects on the turbulence length scale are also accounted for.

### Two equation models

The simplest models for calculating the turbulent complex flows are two equation models employing an additional transport equation for the length scale. Among them the  $k-\varepsilon$  model has been tested most widely and has been shown to predict with the same empirical input, many different flows, including shear layer flows, confined recirculating and complex three dimensional flows with an accuracy sufficient for practical purposes [39]. This model has all the desirable attributes required of turbulence models, i.e. width of applicability, accuracy, economy of computation and simplicity. Because of these distinguishing features we are employing this model in the present study.

In this model the differential equation for velocity scale is the same as for the "K model". The length scale is determined indirectly, i.e. a differential transport equation is derived for the dissipation of turbulence kinetic energy from Navier Stokes equations. This equation implicitly possesses the length scale. Modelling assumptions are made for the unknown terms appearing in this equation. The complete model is as described below.

The Turbulent kinetic energy is given by : ( k- Equation )

$$\rho \bar{u}_i \frac{\partial k}{\partial x_i} = \frac{\partial}{\partial x_i} \left[ \left( \mu + \frac{\mu_t}{\sigma_k} \right) \frac{\partial k}{\partial x_i} \right] + P_k + G_k - \rho \varepsilon \quad (3.21)$$

The isotropic dissipation rate of the turbulent kinetic energy is given by : (  $\varepsilon$  Equation )

$$\rho \bar{u}_i \frac{\partial \varepsilon}{\partial x_i} = \frac{\partial}{\partial x_i} \left[ \left( \mu + \frac{\mu_t}{\sigma_\varepsilon} \right) \frac{\partial \varepsilon}{\partial x_i} \right] + \frac{\varepsilon \rho}{k} (C_{\varepsilon 1} f_1 (P_k + C_{\varepsilon 3} G_k) - C_{\varepsilon 2} f_2 \varepsilon) + E' \quad (3.22)$$

where  $\mu_t$  is called turbulent viscosity and is given by:

$$\mu_t = \text{turbulent viscosity, } C_\mu f_\mu \rho \frac{k^2}{\varepsilon}$$

The last term in equation (3.21),  $\rho \varepsilon$  is the destruction rate and  $P_k$  is the rate of generation of turbulent kinetic energy and  $G_k$  is the buoyancy production term which are given in equations (3.17) (3.18).

The advantages of Two equation  $k - \varepsilon$  model are :

1. Two equation models account for the transport not only of the turbulence velocity scale but also of the length scale.

2. Its predictive capabilities for shear layer flows and confined recirculating flows are well established.

### 3.5.2 Turbulence Models Used in the Present Study

#### Standard $k - \varepsilon$ Model with Wall Functions

In case of standard  $k - \varepsilon$ , the viscous sublayer is bridged by employing empirical formulae called wall functions to provide near wall boundary conditions for the mean flow and turbulence transport equations. These formulae therefore connect the wall conditions (i.e wall shear stress) to the dependent variable at the near wall grid node. The grid node is presumed to lie outside the viscous sublayer in fully turbulent fluid. The advantages of this approach are that it escapes the need to extend the computation right down to the wall and it avoids the need to account for viscous effects in the turbulence model.

From a large amount of experimental data, it has been determined that at a point P near a wall which is at a distance  $y_p$  from the wall, the flow velocity  $\overline{u}_p$  is given by

$$\overline{u}_p = \frac{u^*}{\kappa} \ln(Ey_p^+) \quad (3.23)$$



$C_\mu$	$C_{\epsilon 1}$	$C_{\epsilon 2}$	$C_{\epsilon 3}$	$\sigma_t$	$\sigma_k$	$\sigma_\epsilon$	$f_\mu$	$f_1$	$f_2$	D	$E'$
0.09	1.44	1.92	1.0	1.0	1.0	1.3	1.0	1.0	1.0	0.0	0.0

Table 3.1: Constants for  $k - \epsilon$  model

Here  $u^*$  is called the friction velocity, and  $y_p^+$  represents the dimensionless distance from P to the wall and;

$$u^* = \sqrt{\frac{\tau_w}{\rho}} \quad (3.24)$$

$$y_p^+ = \frac{\rho y_p u^*}{\mu} \quad (3.25)$$

Here  $\kappa$  is the Von karman constant and its value is 0.435 [39].  $\tau_w$  is the shear stress at the wall. E is a roughness parameter and its value is taken to be 9 for smooth walls. The constants in the  $k$  and  $\epsilon$  equations are given in Table (3.1).[38]

It should be noted that this law is applicable when  $y_p^+$  has a value greater than 11.63 . If the distance is less than this value, then point P is in the laminar sublayer so there will be no need of any empirical information for the velocity at point P and Navier Stokes equations can be solved for velocity with the eddy viscosity being set to zero.

We now suppose that the turbulent sublayer is in local equilibrium which means that the rate of production of turbulent kinetic energy is equal to its dissipation rate. Hence the differential equation for  $k$  reduces to

$$\frac{\mu_t}{\rho} \left( \frac{\partial u}{\partial y} \right)^2 = \epsilon \quad (3.26)$$

Using the fact that shear stress at point P in the turbulent layer is approximately equal to the wall shear stress, we obtain

$$\epsilon = \frac{\mu_t}{\rho} \left( \frac{\partial u}{\partial y} \right) \cdot \frac{\partial u}{\partial y} = \frac{\tau_w}{\rho} \left( \frac{\partial u}{\partial y} \right) \quad (3.27)$$

$$\epsilon = u^{*2} \left( \frac{\partial u}{\partial y} \right) \quad \left[ \text{since } u^* = \sqrt{\frac{\tau_w}{\rho}} \right] \quad (3.28)$$

Now from Prandtl Kolmogorov law

$$\nu_t = c_\mu \frac{k^2}{\epsilon} \quad (3.29)$$

$$k = \sqrt{\frac{\nu_t \epsilon}{c_\mu}} \quad (3.30)$$

Substituting value of  $\epsilon$  from equation (3.28) in the above equation yields

$$k = \sqrt{\frac{1}{c_\mu}} \sqrt{\frac{\mu_t}{\rho} \cdot u^{*2} \cdot \left(\frac{\partial u}{\partial y}\right)} \quad (3.31)$$

$$k = \sqrt{\frac{1}{c_\mu}} \sqrt{\frac{\tau_w}{\rho} u^{*2}} \quad [\text{since } \mu_t \frac{\partial u}{\partial y} = \tau_w] \quad (3.32)$$

Hence:

$$k = \sqrt{\frac{u^{*4}}{c_\mu}} \quad [\text{since } \frac{\tau_w}{\rho} = u^{*2}] \quad (3.33)$$

This expression is used as the boundary condition for k. Now, Differentiating equation (3.23) with respect to y

$$\frac{\partial u}{\partial y} = \frac{u^*}{k} \frac{1}{E y_p^+} \frac{E \rho u^*}{\mu} \quad (3.34)$$

Substituting in equation (3.26)

$$\epsilon = u^{*2} \frac{u^{*2} \rho}{k \mu y_p^+} \quad (3.35)$$

$$\epsilon = \frac{u^{*4}}{k y_p u^*} \quad [\text{since from equation (3.25) } \frac{y_p^+ \mu}{\rho} = y_p u^*] \quad (3.36)$$

Therefore;

$$\epsilon = \frac{u^{*3}}{ky_p} \quad (3.37)$$

This expression is used as the boundary condition for  $\epsilon$ .

To obtain  $u^*$  appearing in  $k$  and  $\epsilon$  boundary condition expressions we combine (3.23) and (3.25) to obtain

$$|\overline{u_p}| = \frac{u^*}{\kappa} \ln\left(\frac{E\rho y_p u^*}{\mu}\right) \quad (3.38)$$

$\overline{u_p}$  is known from the solution of momentum equation. It should be noted that  $k$  and  $\epsilon$  have not been specified at the wall in contrast to other variables. It is for the reason that the flow immediately adjacent to the wall is laminar and the concept of eddy viscosity does not apply there. therefore, the  $k$  and  $\epsilon$  values are not required there.

### **Low Reynolds number extension of the two equation $k - \epsilon$ model**

In this approach wall damping and viscous effects are incorporated by making several of the model coefficients functions of a local turbulence Reynolds number. This model requires that the equation be integrated right down to the wall. For this

$C_\mu$	$C_{\varepsilon 1}$	$C_{\varepsilon 2}$	$C_{\varepsilon 3}$	$\sigma_t$	$\sigma_k$	$\sigma_\varepsilon$	$D$	$E'$
0.09	1.44	1.92	1.0	1.0	1.0	1.3	0.0	0.0

Table 3.2: Constants for  $k - \varepsilon$  model

we should have a very fine grid distribution near the walls. We have used Lam-Bremhost low Reynolds number extension of the two equation  $k - \varepsilon$  model. All the constants in the  $k - \varepsilon$  equations are same as the Standard  $k - \varepsilon$  model with wall functions, except  $f_\mu$ ,  $f_1$  and  $f_2$ . These model co-efficients are given as

$$f_\mu = \left[1. - e^{0.0165 \times Re_\varepsilon}\right]^2 \left[1 + \left(\frac{20.5}{Re_t}\right)\right] \quad (3.39)$$

$$f_1 = 1. + \left(\frac{0.05}{f_\mu}\right)^3 \quad (3.40)$$

$$f_2 = 1. - \left[e^{-(Re_t^2)}\right] \quad (3.41)$$

where  $Re_x = \frac{\sqrt{k} \times y_n}{\nu}$ ,  $y_n$  = normal distance to the nearest wall and  $Re_t = \frac{k^2}{\varepsilon} \times \frac{1}{\nu}$

Boundary conditions are  $k = 0$ ;  $\frac{\partial \varepsilon}{\partial y} = 0$  at the wall. The constants are given in table (3.2).

### 3.6 Boundary Conditions

To solve the governing equations comprising the mathematical model, boundary conditions are needed at each part of the domain boundary. The problem has been solved in x-y plane. At

$$x = 0 \quad u = 0, \quad v = 0, \quad T = T_h$$

$$x = L \quad u = 0, \quad v = 0, \quad T = T_c$$

$$y = 0 \quad u = 0, \quad v = 0, \quad \frac{\partial T}{\partial y} = 0.0$$

$$y = H \quad u = 0, \quad v = 0, \quad \frac{\partial T}{\partial y} = 0.0$$

The Energy equation across the solid partition takes the form

$$\frac{\partial^2 T}{\partial x^2} + \frac{\partial^2 T}{\partial y^2} = 0.0 \quad (3.42)$$

The boundary conditions at the interface where the partition is introduced are

$$\text{At } x = x_1 \quad u = v = 0, \quad K_f \frac{\partial T}{\partial x} \Big|_{x_1^-} = K_s \frac{\partial T}{\partial x} \Big|_{x_1^+}$$

$$\text{At } x = x_2 \quad u = v = 0, \quad K_s \frac{\partial T}{\partial x} \Big|_{x_2^-} = K_f \frac{\partial T}{\partial x} \Big|_{x_2^+}$$

## Chapter 4

# Numerical Solution of the Governing Equations

Numerical methods are developed to determine the numerical solution to the set of differential equations. These methods involve two basic steps which include discretization of the differential equation into an algebraic equation and then solving these algebraic equations by direct or iterative methods.

Numerical methods differ from each other in the method of approximation introduced for the discretization of the differential equations. The second step i.e. solution to the resulting algebraic equations is general for all the numerical methods.

## 4.1 Methods of Deriving the Discretization Equations

For a given differential equation, the required discretization equation can be derived in many ways. The common methods are described briefly and the method which is employed by PHOENICS will be presented in detail.

### 4.1.1 Taylors-series Formulation

The usual procedure for deriving finite-difference equations consists of approximating the derivatives in the differential equation via a truncated Taylor series. Let us consider the grid point shown in figure(4.1). For grid point 2, located midway between grid points 1 and 3 such that  $\Delta x = x_2 - x_1 = x_3 - x_2$ , the Taylors series expansion around 2 gives

$$\phi_1 = \phi_2 - \Delta x \left( \frac{d\phi}{dx} \right)_2 + \frac{1}{2}(\Delta x)^2 \left( \frac{d^2\phi}{dx^2} \right)_2 - \dots \quad (4.1)$$

and

$$\phi_3 = \phi_2 + \Delta x \left( \frac{d\phi}{dx} \right)_2 + \frac{1}{2}(\Delta x)^2 \left( \frac{d^2\phi}{dx^2} \right)_2 + \dots \quad (4.2)$$

Truncating the series just after the third term, and adding and subtracting the two equations, we obtain



$$\left(\frac{d\phi}{dx}\right)_2 = \frac{\phi_3 - \phi_1}{2\Delta x} \quad (4.3)$$

and

$$\left(\frac{d^2\phi}{dx^2}\right)_2 = \frac{\phi_1 + \phi_3 - 2\phi_2}{(\Delta x)^2} \quad (4.4)$$

The substitution of such expressions into the differential equation leads to the finite-difference equation.

The Taylors-series formulation is relatively straightforward but allows less flexibility and provides little insight into the physical meaning of the terms.

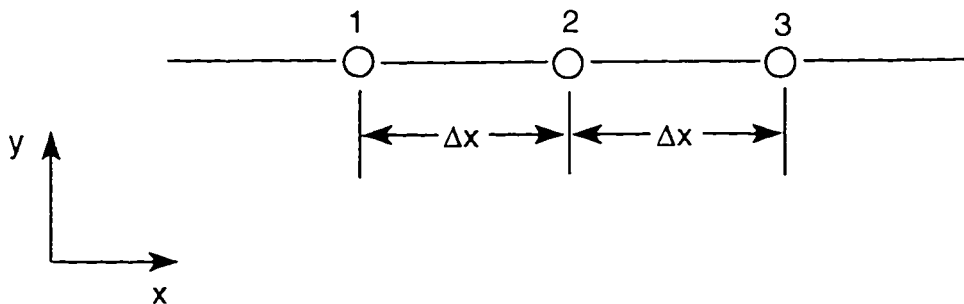


Figure 4.1: Three consecutive grid points used for Taylor-series expansion

### 4.1.2 Variational Formulation

This method is based on the method of calculus of variations. Calculus of variation shows that certain differential equations is equivalent to minimizing a related quantity called the functional. This equivalence is known as the variational principle. If the functional is minimized with respect to the grid point values of the dependent variable, the resulting condition give the required discretization equations. The variational formulation is very commonly employed in finite element methods for stress analysis.

The main drawback of this formulation is its limited applicability, since a variational principle does not exist for all differential equations of interest.

### 4.1.3 Method of Weighted Residual

In this method the differential equation is represented as  $L(\bar{\phi}) = 0$ . We have to consider an approximate solution of  $\bar{\phi}$  that contains a number of undetermined parameters like

$$\bar{\phi} = a_0 + a_1x + a_2x^2 + \dots + a_mx^m, \quad (4.5)$$

the  $a$ 's being the parameters. The substitution of  $\bar{\phi}$  into the differential equation leaves a residual  $R$ , defined as

$$R = L(\bar{\phi}). \quad (4.6)$$

In order to make this residual small we have to suppose

$$\int WRdx = 0, \quad (4.7)$$

where  $W$  is a weighting function and the integration is performed over the domain of interest. By choosing a number of weighting functions we can generate as many equations as are required for evaluating the parameters. These algebraic equations containing the parameters as the unknown are solved to obtain the approximate solution to the differential equation.

#### 4.1.4 Control Volume Formulation

In this method, the calculation domain is divided into a number of non-overlapping control volumes such that there is one control volume surrounding each grid point. The differential equation is integrated over the control volume. Piecewise profiles expressing the variation of variable  $\phi$  are used to evaluate the required integrals. The result is the discretization equation containing the values of  $\phi$  for a group of grid points. The discretization equation obtained in this manner expresses the conservation principle for the finite control volume just as the differential equation expresses it for the infinitesimal control volume.

The most attractive feature of the control volume formulation is that the resulting solution would imply that the integral conservation of quantities such as mass, momentum, and energy is exactly satisfied over any group of control volumes and, of course, over the whole calculation domain. This characteristic exists for any number of grid points. Thus, even the coarse grid would produce an exact integral balance [40].

## 4.2 The Discretization Procedure used in the Present Study

As described earlier, partial differential equations are to be discretized into algebraic equations by using appropriate approximation to obtain a numerical solution to the problem. The procedure followed is the Finite Volume Method. It will be described in general cartesian coordinates for the general transport equation.

In vector notation, the general transport equation for steady state situation is given by

$$\nabla \cdot (\rho \mathbf{U} \phi) = \nabla \cdot (\Gamma_{\phi} \nabla \phi) + S \quad (4.8)$$

This equation is integrated over the finite control volume around node P shown in figure 4.2. The integration is given as:

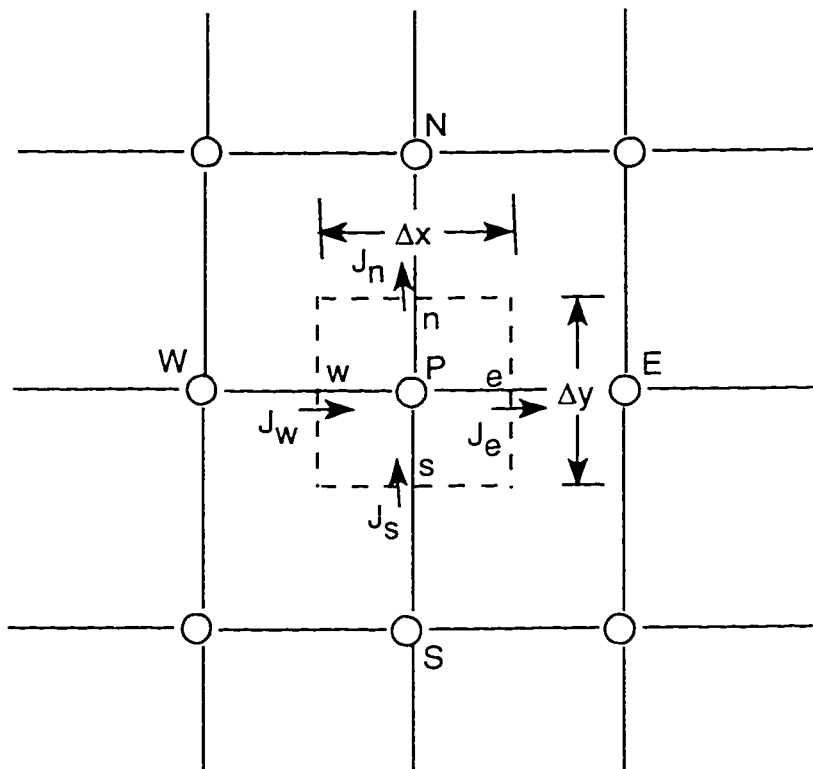


Figure 4.2: A finite control volume

$$\int_s^n \int_w^e [\nabla \cdot (\rho \mathbf{U} \phi)] dy dx = \int_s^n \int_w^e \nabla \cdot (\Gamma_\phi \nabla \phi) dy dx + \int_s^n \int_w^e S dy dx \quad (4.9)$$

Performing the integration results in

$$[(\rho u_y \phi - \Gamma_\phi \frac{\partial \phi}{\partial y}) \Delta x]_s^n + [(\rho u_x \phi - \Gamma_\phi \frac{\partial \phi}{\partial x}) \Delta y]_w^e = \bar{S}_\phi \Delta x \Delta y \quad (4.10)$$

Where  $\bar{S}_\phi$  is the average value of S over the finite control volume and  $u_x, u_y$  are the components of velocity vector U in the cartesian coordinate directions  $x$  and  $y$  respectively.

The total flux across any face of the finite control volume is represented by J. Focussing the attention on the east face, the total flux across this face will be given as:

$$J_e = [\rho u_x \phi_e - (\Gamma_\phi \frac{\partial \phi}{\partial x})_e] \Delta y \quad (4.11)$$

As can be seen from equation 4.11, the total flux is composed of a convective flux  $(\rho u_x \phi_e)$  and a diffusive flux  $((\Gamma_\phi \frac{\partial \phi}{\partial x})_e)$  which are represented by  $C_e$  and  $D_e$  respectively and written as:

$$C_e = \rho u_r \phi_e \Delta y \quad (4.12)$$

$$D_e = (\Gamma_{\phi_e} \frac{\partial \phi}{\partial x})_e \quad (4.13)$$

The source term is appropriately linearized and written as:

$$S_\phi = S_0 + S_p \phi_p \quad (4.14)$$

Substituting equations (4.11) to (4.14) into equation (4.10), equation (4.10) can be written as:

$$J_e - J_w + J_n - J_s = (S_0 + S_p \phi_p) \Delta y \Delta x \quad (4.15)$$

Furthermore, profile assumptions have to be made about the variation of  $\phi$  within the finite control volume. For the diffusion flux a linear profile can be assumed. This results in the central discretization given as:

$$D_e = (\Gamma_{\phi_e} \frac{\partial \phi}{\partial x})_e = \Gamma_{\phi_e} \frac{(\phi_E - \phi_P)}{\Delta x_{PE}} \quad (4.16)$$

Central discretization is usually not appropriate for the convective flux and may result in non-physical oscillations in the solution. To make the discretization compatible with physical reality a hybrid scheme is used. Depending on the Cell Peclet number it uses either an upwind or central discretization for the convective flux  $C_e$ . Cell Peclet number is defined as

$$P_e = \frac{\rho u_x \Delta x_{PE}}{\Gamma_{\phi_e}} \quad (4.17)$$

Using Hybrid Scheme [40]

$$C_e = \rho u_x \frac{(\phi_E + \phi_P)}{2} \Delta x, \quad \text{if } -2 \leq P_e \leq 2 \quad (4.18)$$

$$C_e = \rho u_x \phi_E \Delta x, \quad \text{if } P_e > 2 \quad (4.19)$$

$$C_e = \rho u_x \phi_P \Delta x, \quad \text{if } P_e < -2 \quad (4.20)$$

Similar expressions are obtained at other faces of the finite control volume. Substituting these expressions in equation 4.15 we get

$$(A_P - S_P)\phi_P = A_n\phi_n + A_s\phi_s + A_e\phi_e + A_w\phi_w + S_0 \quad (4.21)$$



where

$$A_e = \frac{\Gamma_{\phi_e}}{\Delta x_{PE}} - \rho u_x)_e \quad (4.22)$$

$$A_w = \frac{\Gamma_{\phi_w}}{\Delta x_{WP}} - \rho u_x)_w \quad (4.23)$$

$$A_n = \frac{\Gamma_{\phi_n}}{\Delta y_{PN}} - \rho u_y)_n \quad (4.24)$$

$$A_s = \frac{\Gamma_{\phi_s}}{\Delta y_{SP}} - \rho u_y)_s \quad (4.25)$$

$$A_P = A_e + A_w + A_n + A_s \quad (4.26)$$

Here  $u_x)_e$  represents  $u_x$  velocity at the east cell face. In this connection it should be clear that this velocity is not an interpolated one, but rather it is indeed calculated at cell faces in contrast to other variables whose values are calculated at the center of the cells, therefore, at faces the values can be obtained through interpolation. This arrangement is highly beneficial to avoid a non-physical oscillatory solution for the pressure field and to increase the accuracy.

### 4.3 Grid Generation

For numerical simulation of natural convection flow in a rectangular enclosure a non-uniform grid arrangement is used and is shown in Figure(4.3).

The grid for the present study was generated using symmetric power law distribution with an effort to minimize the non-smoothness of the grid, but at the same time having grid clustering at regions of larger gradients to obtain an economic and accurate solution.

The iterative method is sensitive to the smoothness of the mesh generated. For non-smooth meshes, heavy underrelaxation is required to prevent divergence of the solution. This large underrelaxation reduces the convergence rate with the consequence of increased computational effort ([41]).

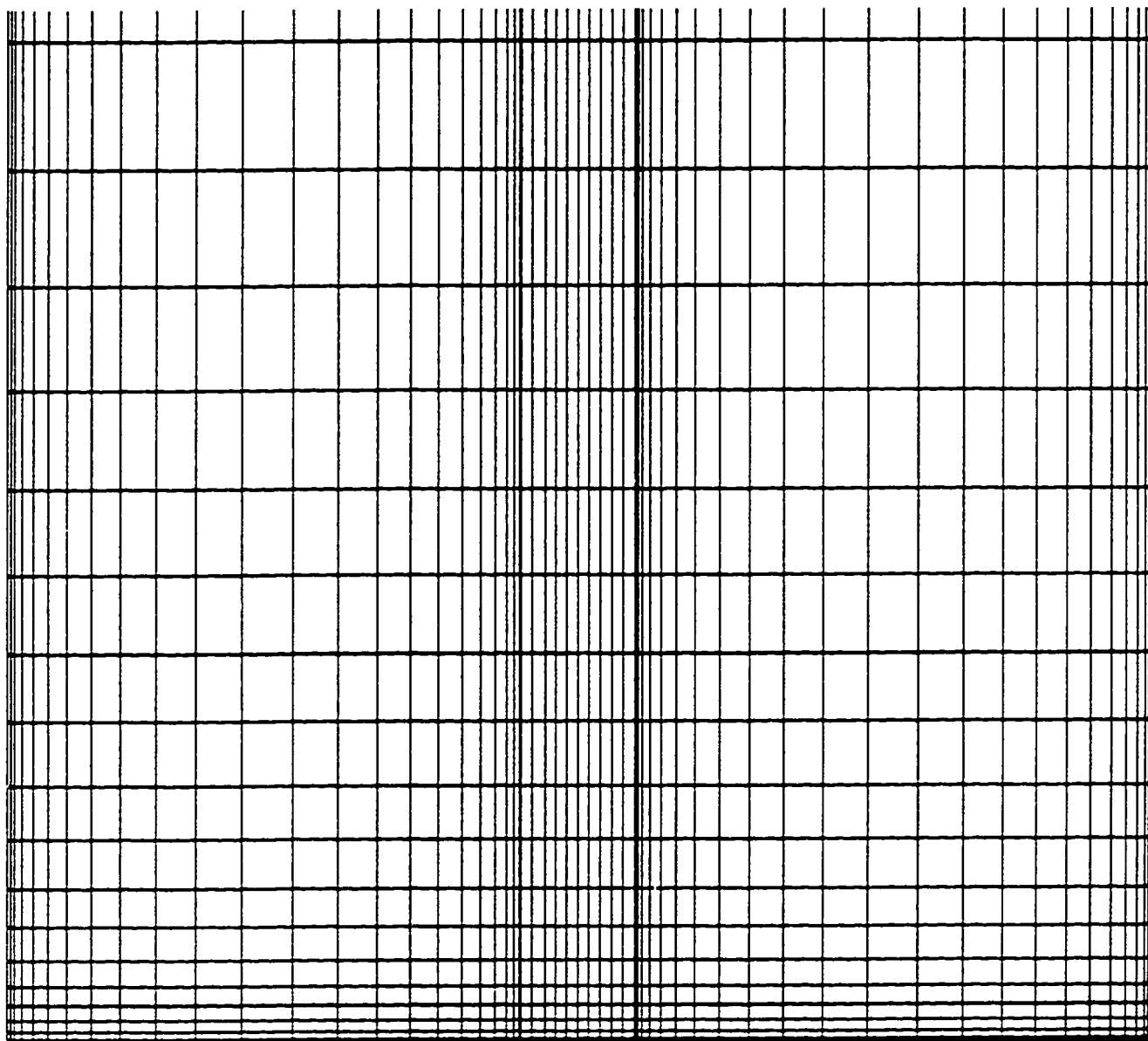


Figure 4.3: magnified view of bottom portion of the Computational Grid in an Enclosure with a single partition

## 4.4 Calculation Procedure

For the general variable  $\phi$  the solution to the discretized algebraic equations can be obtained using either direct or iterative methods. Direct method needs the algebraic equations to be linear. If, however, the equations are nonlinear then an iterative method is necessary. Some of the algebraic equation solvers which PHOENICS ([42]-[43]) possesses are

1. Gauss Siedal Method
2. Whole field solution method
3. Tri Diagonal Matrix Algorithm
4. Multigrid Method

Gauss Siedal method requires the least number of calculations, over the solution domain, per iteration. However, it requires a large number of iterations for convergence, since the boundary information enters the solution domain one node forward every iteration. Whole field is very efficient for linear algebraic equations for a moderate size matrix. It shifts the boundary information inside the flow system immediately, since it solves the equations simultaneously. However if the grid size is large, then matrix size becomes very large, and requires a very large computer memory and enormous computational power [39]. If the algebraic equations are

nonlinear, then whole field method has to work iteratively since the coefficients of the discretized equations, being tentative, are to be updated at the end of every sweep using the new values of  $\phi$ , until the convergence is met. Hence, for nonlinear algebraic equations, even for a moderate size of matrix, this method may require a much larger total computational effort as per required by the Gauss Siedal Method.

A method which has the benefits of both, but disadvantages of none is the Tri Diagonal Matrix Algorithm. In this method, algebraic equations for a row of nodes are solved simultaneously. A very efficient algorithm which is called Thomas Algorithm is available to solve the tridiagonal matrix, thus, formed. Hence, the boundary point information is carried in a single iteration for that row. The solution procedure proceeds to the next column and repeats itself. Therefore, this method works like whole field method in the row wise direction and like Gauss Siedal method in the column wise direction. The number of total computational effort needed is only little greater than Gauss Siedal Method. This is due to the usage of Thomas Algorithm. Most of the time, we used this method for the solution of our problem. However, equation for pressure correction was solved using the whole field method, since a simultaneous satisfaction of the continuity in the whole domain increases the convergence rate. Usually several hundred sweeps are required to obtain a converged solution.

It should be noted that multigrid method is an advanced iterative method and has very high convergence rate. For problems requiring enormous computational effort, it is very attractive. However, for moderate size problems like ours, the more traditional methods suffice. These days it is in the development stage, and a good account of this method can be found in [40].

#### 4.4.1 Solution Algorithm

If the pressure field is given, the solution to the momentum equations can be obtained by employing the method described above. However, unless the correct pressure is employed, the resulting velocity field obtained from the solution of the momentum equations will not satisfy the continuity equation. However, no explicit equation for the pressure is given. This is particularly true for an incompressible flow. In this regard several methods are available. PHOENICS uses the SIMPLE procedure. This method has been described in detail in the literature [40] and it is basically an iterative process.

Let a tentatively calculated velocity field based on a guessed pressure field  $p^*$  is denoted by  $u_x^*$ ,  $u_y^*$  and let the correct pressure  $p$  be obtained from

$$p = p^* + p' \quad (4.27)$$

The corresponding correction in velocities  $u'_x$ ,  $u'_y$  can be introduced in a similar manner

$$u_x = u_x^* + u'_x \quad (4.28)$$

$$u_y = u_y^* + u'_y \quad (4.29)$$

Making certain assumptions, the velocity correction formula for east face of the mesh element, for example, is given by

$$u_x = u_x^* + \frac{\Delta y}{A_e}(p'_P - p'_E) \quad (4.30)$$

Now, discretizing the continuity equation and using the velocity correction formulas, one can obtain an equation for pressure correction

$$(A_P - S_P)p_P = A_n p'_n + A_s p'_s + A_e p'_e + A_w p'_w + S_0 \quad (4.31)$$

Thus we have obtained an equation for pressure correction or in turn for pressure. The important steps to compute the flow properties are as follows.

1. Guess the pressure field  $p^*$ .
2. Solve the momentum equations to obtain  $u_x^*$  and  $u_y^*$ .
3. Solve the pressure correction equation.
4. Calculate  $p$  by adding  $p'$  to  $p^*$ .
5. Calculate “ $u$ ” and “ $v$ ” from eq.(4.30).
6. Solve equations for other variables  $\phi$  (e.g. Energy equation, turbulence kinetic energy and its dissipation), if they have a coupling with momentum equations.
7. Treat the corrected pressure as a new guessed pressure  $p^*$ . Return to step 2 and repeat the whole procedure until a converged solution is obtained.



# Chapter 5

## Results and Discussions

The heat transfer and fluid flow characteristics of natural convection in an enclosure are studied for both laminar and turbulent regimes. A non uniform grid with high refinement near the walls is used to increase the accuracy of the computational results.

Comparisons with experiments have been performed for both laminar and turbulent flow in inclined enclosures in order to validate the numerical procedure. Grid independence tests were performed for various grid sizes such as  $30 \times 60$ ,  $40 \times 80$ ,  $60 \times 100$  and  $80 \times 120$ . For the parametric study in a partitioned enclosure the Rayleigh number was varied from  $10^9$  to  $10^{13}$ , angle of inclination from  $30^\circ$  to  $90^\circ$ , aspect ratio ranges from 2 to 15 and the number of partitions from 0 to 4.

## 5.1 Validation of the Numerical Code

To validate the numerical procedure, the computational results of few selected cases were compared with the experimental results of Hamady et. al. [44] and Giel et. al [10] and the numerical results of Kuyper et. al. [28]. The selected cases were

- Laminar flow in square enclosure with  $Ra = 10^6$ ,  $A=1.0$ ,  $Pr = 0.71$  and angle of inclination varied from  $20^\circ - 140^\circ$  [44], and
- Turbulent flow in a square enclosure with  $Ra = 10^{10}$ ,  $A=1.0$ ,  $Pr = 0.71$ , and angle of inclination varied from  $30^\circ - 90^\circ$  using standard  $k - \varepsilon$  model to account for turbulence [28].
- Turbulent flow in a rectangular enclosure with  $Ra = 8 \times 10^{10}$ ,  $A=10.0$ ,  $Pr = 0.71$ , and angle of inclination at  $90^\circ$  using standard  $k - \varepsilon$  model and the low Reynolds extension of the  $k - \varepsilon$  model [10].

### 5.1.1 Laminar Flow

Two dimensional laminar natural convection in a square enclosure have been studied at different angles of inclination ranging from  $20^\circ - 140^\circ$ . In these computations  $60 \times 60$  grid points were used. Figure 5.1 shows the average Nusselt number distribution at different angles of inclination. In this figure the numerical results of Kuyper et. al. [28] and the experimental results of Hamady et. al. [44] are compared with

the results of the present study. As can be seen the results of the present study show a very good agreement with the experimental results of Hamady et. al. [44] in comparison with the numerical results of Kuyper et. al. [28]. The difference with the experimental results is due to the conduction through the connecting walls in their experiments. As can be seen from Figure 5.1, a decrease in the angle of inclination from  $180^{\circ}$  causes an increase in the average Nusselt number which is due to the increase in the driving potential for natural convection. A decrease in the angle of inclination below  $90^{\circ}$  will reduce the gravity component along the heated wall, although the average Nusselt number continues to increase until a maximum value is reached at an angle of  $75^{\circ}$ . Beyond this angle a decrease in angle of inclination will result in a decrease in the average Nusselt number until a local min. is obtained at an angle of  $30^{\circ}$ . This reduction in  $\overline{Nu}$  is due to the interaction of the two cells forming a counter clockwise rotating closed cell in the center of the cavity as seen in Figure 5.13. Because of the good mixing obtained in the core region temperature gradients are small as seen in Figure 5.9. Further reduction in the angle of inclination to  $20^{\circ}$  shows an upward trend in the average Nusselt number. The experimental results of Hamady et. al. [44] show an increase in the average Nusselt number as the angle of inclination is further reduced towards  $0^{\circ}$ . This increase in the  $\overline{Nu}$  is due to the transition of the unicellular flow structure to a highly unstable flow. Because of the unstable and probably three dimensional nature of flow at angles close to  $0^{\circ}$ , the present numerical results were obtained upto an angle of inclination of  $20^{\circ}$  only.

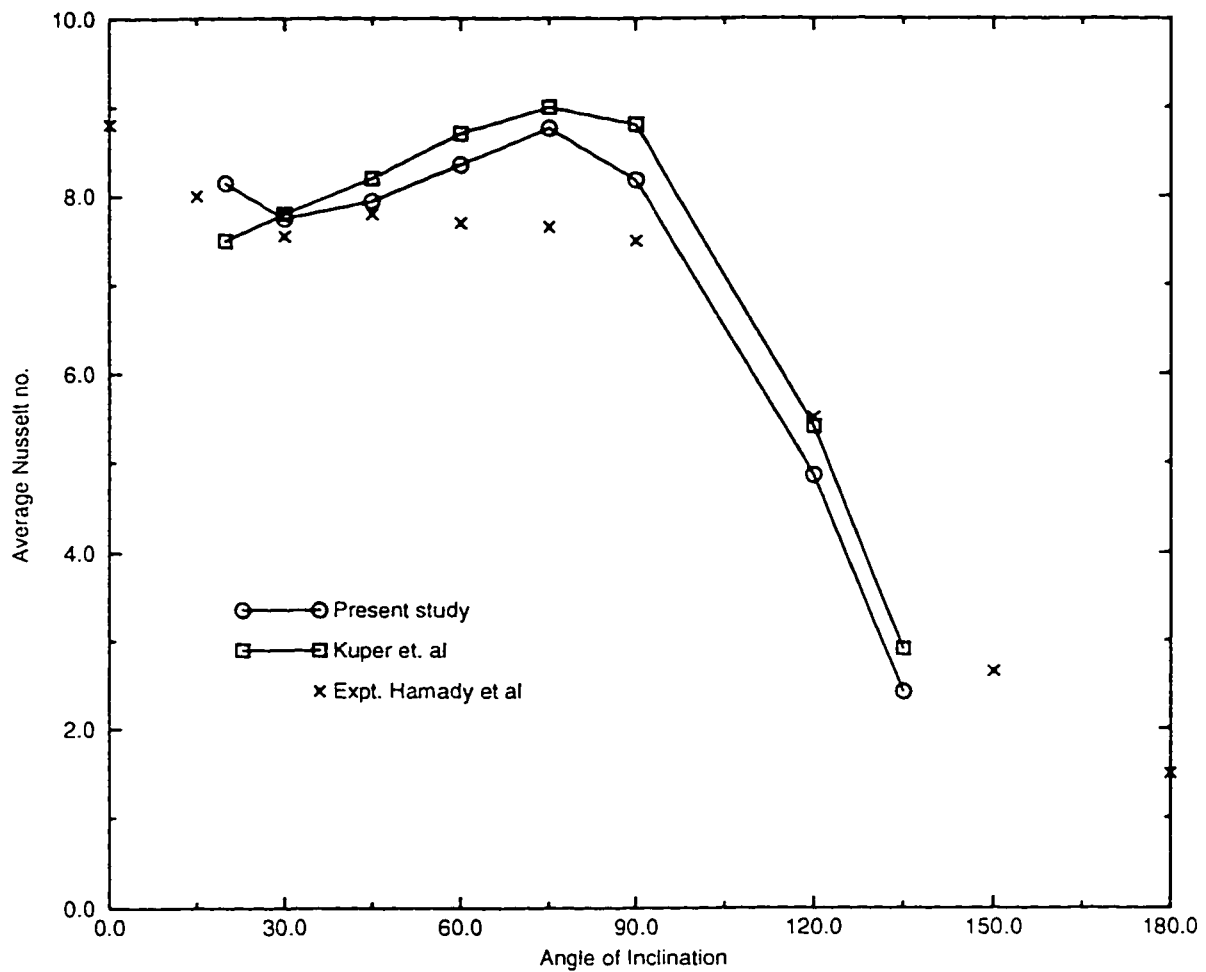


Figure 5.1: Effect of Angle of inclination on the Average Nusselt no. for laminar Natural convection in an enclosure without partition;  $Ra = 1 \times 10^6$ ,  $A=1.0$ ,  $Pr = 0.71$

### 5.1.2 Turbulent Flow

Turbulent natural convection in a square enclosure have been studied at  $Ra = 10^{10}$  and  $Pr = 0.71$  for different angles of inclination ranging from  $30^\circ - 90^\circ$ . These computations are performed using standard  $k - \varepsilon$  model with wall functions. Figure 5.2 shows the calculated average Nusselt number as a function of the angle of inclination. The results of the present study have been compared with the results of Kuyper et. al. [28]. At an angle of inclination of 90 degrees the present study results show a very good agreement with the results reported in the literature [28] and also for other angle of inclinations the present results agrees within 3% to the reported results.

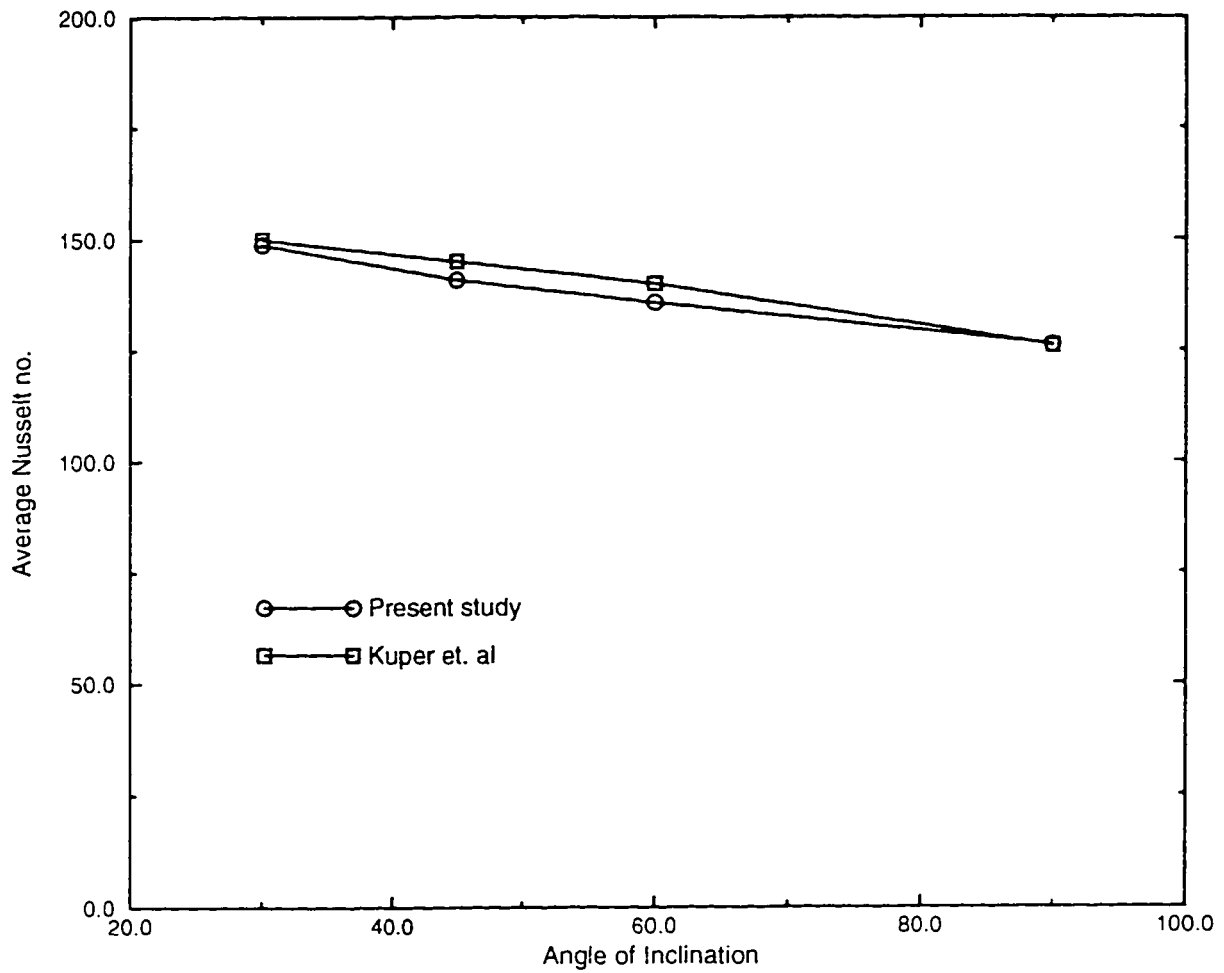


Figure 5.2: Effect of Angle of inclination on the Average Nusselt no. for Turbulent Natural convection in an enclosure without partition;  $Ra = 1 \times 10^{10}$ ,  $A=1.0$ ,  $Pr = 0.71$ , using standard k-e model

## 5.2 Comparison of the Two Turbulence Models

At high Rayleigh numbers ( $Ra > 10^9$ ) the flow becomes turbulent with thin boundary layers along the heated walls of the enclosure. The velocity and temperature gradients within this thin boundary layer, are very large and require the use of many computational grid points. In most turbulence calculations the velocity, temperature and other dependent variables in this part of the boundary layer are approximated by logarithmic wall functions. However it is reported in the literature [17, 18, 22] that using the standard  $k - \varepsilon$  model with the wall functions does not give accurate solution. Hence the  $k - \varepsilon$  model was modified and named as low Reynolds number  $k - \varepsilon$  model [17, 18, 22]. In the present study both models were used to model turbulent natural convection in rectangular enclosure and the results are compared with the experimental results of Giel et. al [10] in order to choose the one that will exhibit good agreement. Figures 5.3 and 5.4 show the comparison of the temperature and vertical velocity distributions at the mid-height of the enclosure at  $Ra = 8 \times 10^{10}$  and  $A=10$ . As can be seen from the figures that the low Reynolds number  $k - \varepsilon$  model results exhibit a very good agreement with the experimental results as compared to the standard  $k - \varepsilon$  model results. This is due to the fact that the standard  $k - \varepsilon$  model uses logarithmic wall functions which were originally derived for forced convection viscous sublayer and hence does not predict well the natural convection behavior, while the low Reynolds number  $k - \varepsilon$  model equations

can be integrated right up to the wall. Based on the above findings, it has been decided to use the low Reynolds number  $k-\varepsilon$  model to account for turbulence when performing further computations.



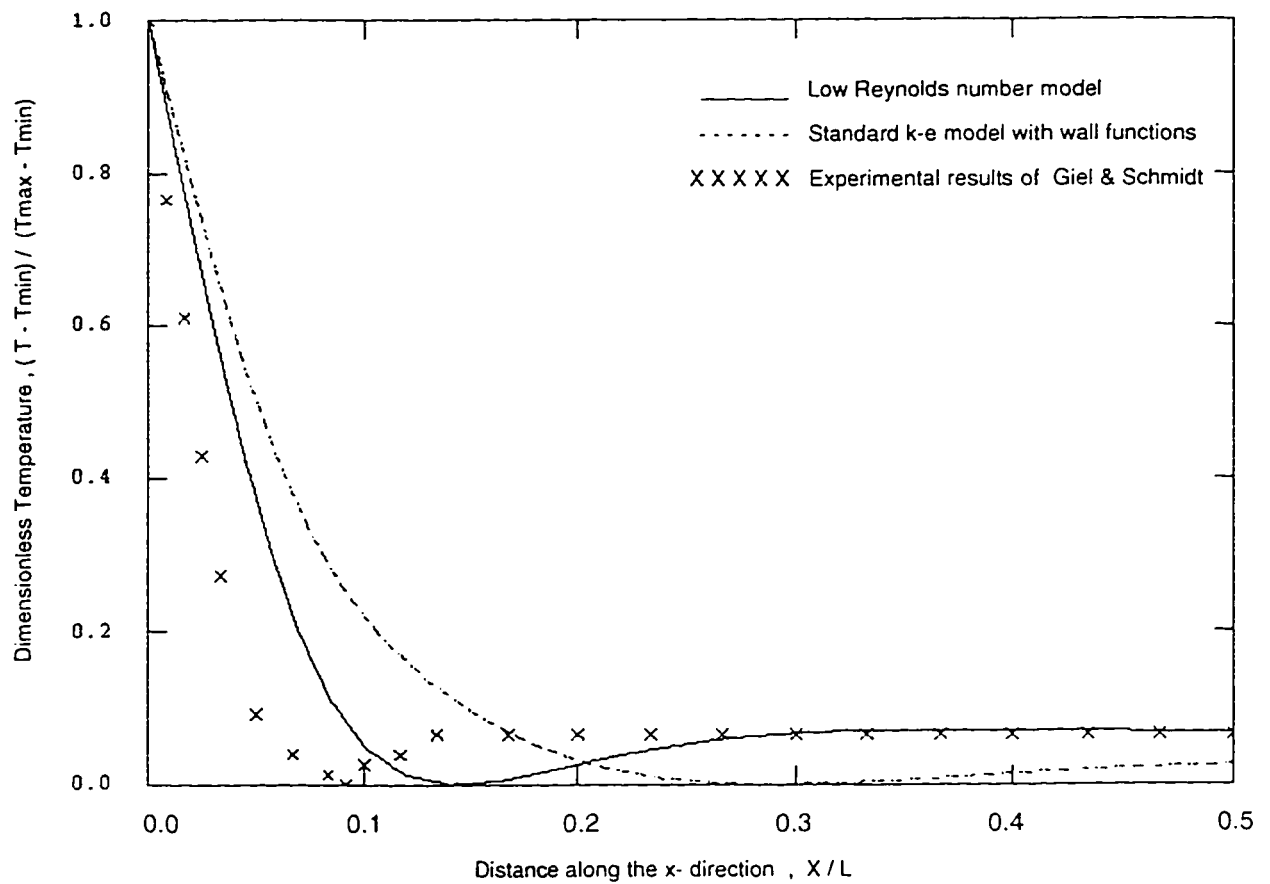


Figure 5.3: Temperature distribution at the mid-height of the enclosure for  $Ra = 8 \times 10^{10}$ ,  $A=10:1$ ,  $\Phi = 90^\circ$

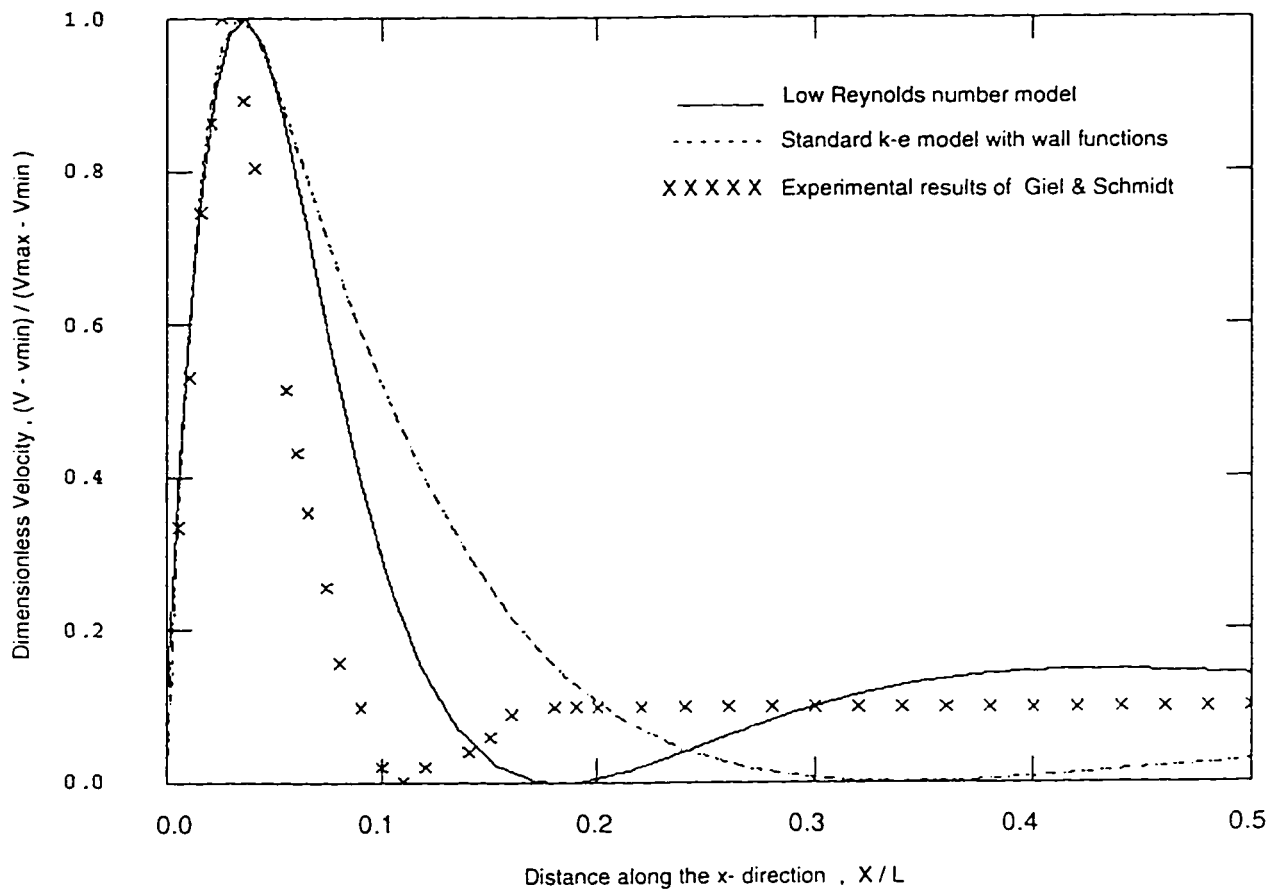


Figure 5.4: Vertical Velocity distribution at the mid-height of the enclosure for  $Ra = 8 \times 10^{10}$ ,  $A=10:1$ ,  $\Phi = 90^\circ$

### 5.3 Grid Independence Test

A grid independence test was carried out to make sure that the grid size does not effect the computational results. Computations were carried out using four different grid sizes:  $30 \times 60$ ,  $40 \times 80$ ,  $60 \times 100$  and  $80 \times 120$  grid points. Figure 5.5 shows the vertical velocity profile at the mid-height of the enclosure obtained using these different grid sizes. As can be seen the difference in results obtained using  $60 \times 100$  and  $80 \times 120$  grid size is very small. Therefore in this study a grid size of  $60 \times 100$  is used in order to utilize the computation time efficiently without compromising on the accuracy of the computation.

### 5.4 Natural Convection in Enclosures without partition

#### 5.4.1 Effect of Angle of Inclination in Laminar Flow

Figures 5.6 to 5.13 show the isotherms and streamlines for different angles of inclination. The flow field and temperature distributions for the case where the cavity is heated from the top ( $\phi = 180^\circ$ ) confirm to situation that can be fully determined by conduction heat transfer. As soon as the cavity is rotated the fluid is set in motion. The isotherms shown in the Figure 5.6 ( $\phi = 135^\circ$ ) indicate that the temperature gradient in the core region gets larger. Diffusion is still the dominating

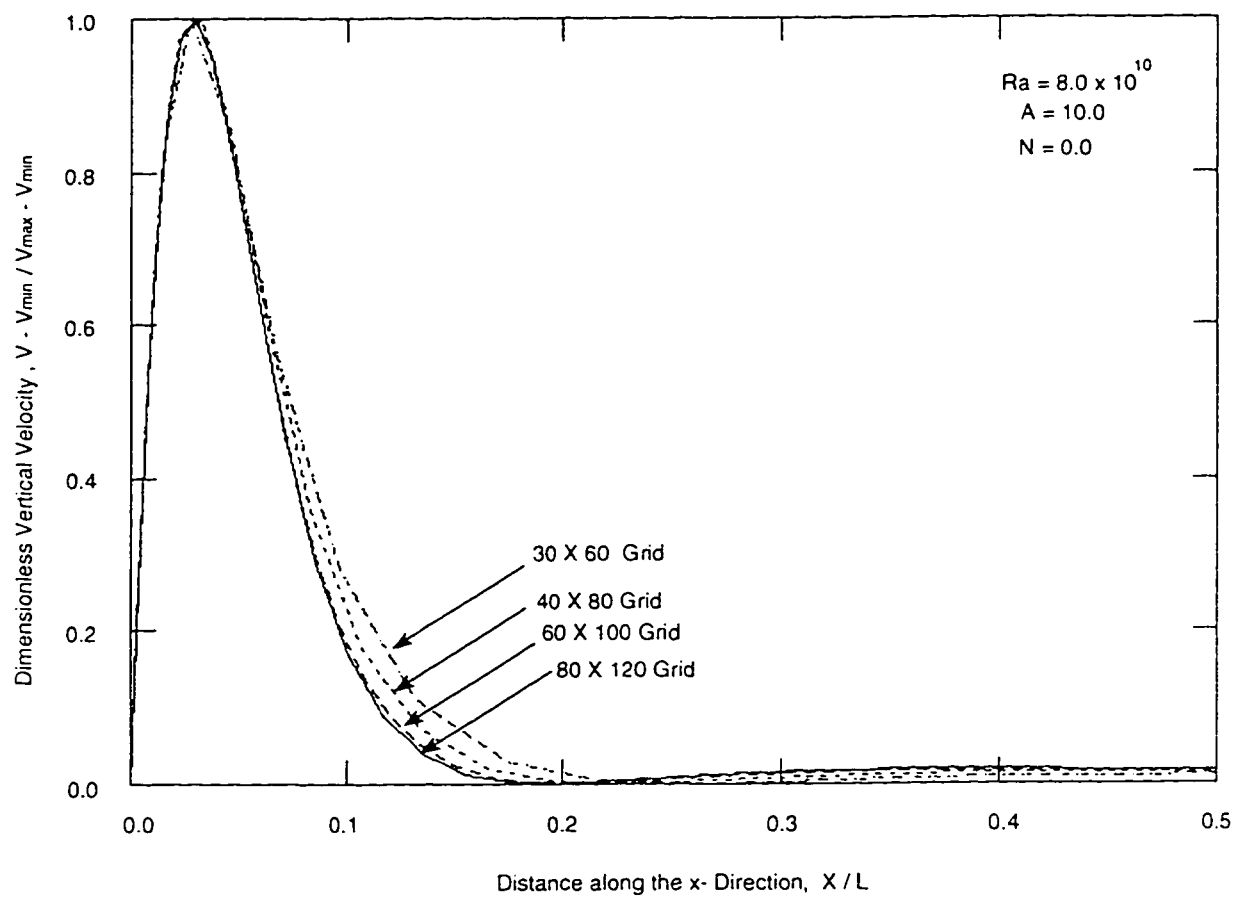


Figure 5.5: Vertical Velocity at the mid-height of the enclosure for different mesh sizes

process in the enclosure since the hot fluid is positioned in the upper corner and the cold fluid in the lower corner. Figure 5.7 shows that the essential part of the flow is the thermal boundary layer structure along the hot and cold surfaces. The figure shows a zero temperature gradient along the x-direction in the core region and higher gradients near the walls. The thickness of the thermal boundary layer increases with the height along the hot wall while it decreases along the cold wall. Figure 5.8 shows that the stratified temperature is broken up as the flow in the core region pushes the flow along the adiabatic walls to the side. Figure 5.9 shows that the counterclockwise rotation of the cell in the core region is accelerated, bending the isotherms in the core region such that they are no longer orthogonal to the gravitational field. This distortion of the temperature field is due to the increase in the speed of the counter clockwise rotating cell.

The streamlines in Figure 5.10 show that the fluid leaving the heated and cooled walls is being decelerated back to the wall due to the effect of gravity forming a stretched cell along both walls. The velocity along the hot and cold walls increases with rotation. As can be seen from Figure 5.11 that a small portion of the fluid is entering the boundary layer upstream again, forming a narrow cell. These cells get stretched along the adiabatic walls as the angle is reduced to  $\phi = 60^\circ$  as shown in Figure 5.12. As the angle of inclination is further reduced to  $\phi = 40^\circ$  the two cells begin to interact forming a counterclockwise rotating closed cell in the core region of the enclosure as shown in Figure 5.13.

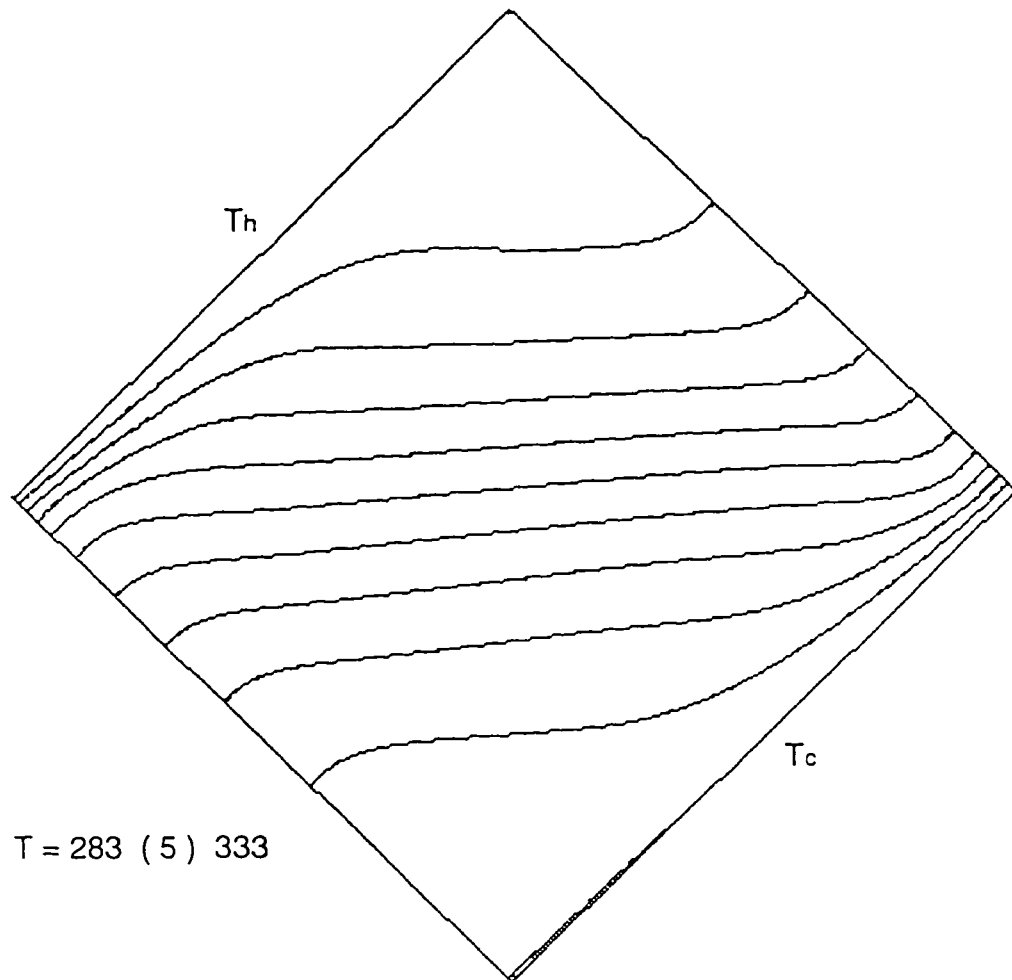


Figure 5.6: Isotherms for Laminar Natural Convection in an Enclosure without partition:  $Ra = 1 \times 10^6$ ,  $A=1.0$ ,  $P_r = 0.71$ ,  $\Phi = 135^\circ$

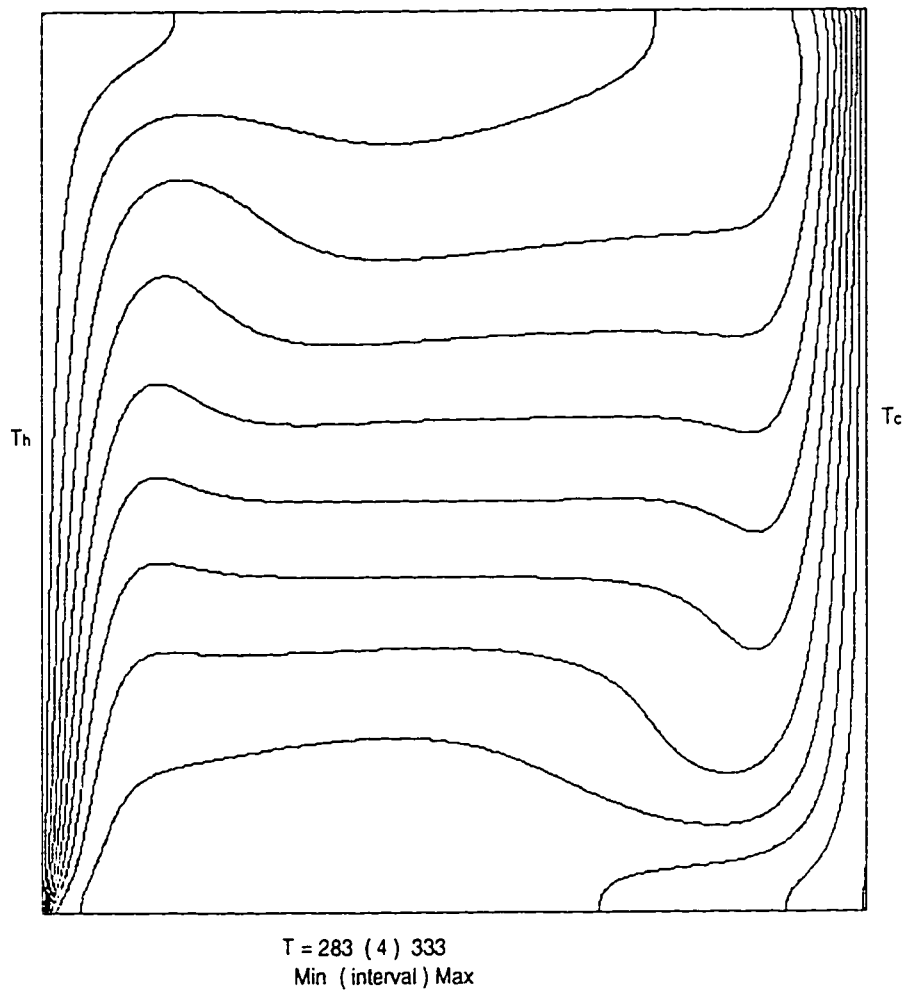


Figure 5.7: Isotherms for Laminar Natural Convection in an Enclosure without partition:  $Ra = 1 \times 10^6$ ,  $A=1.0$ ,  $Pr = 0.71$ ,  $\Phi = 90^\circ$

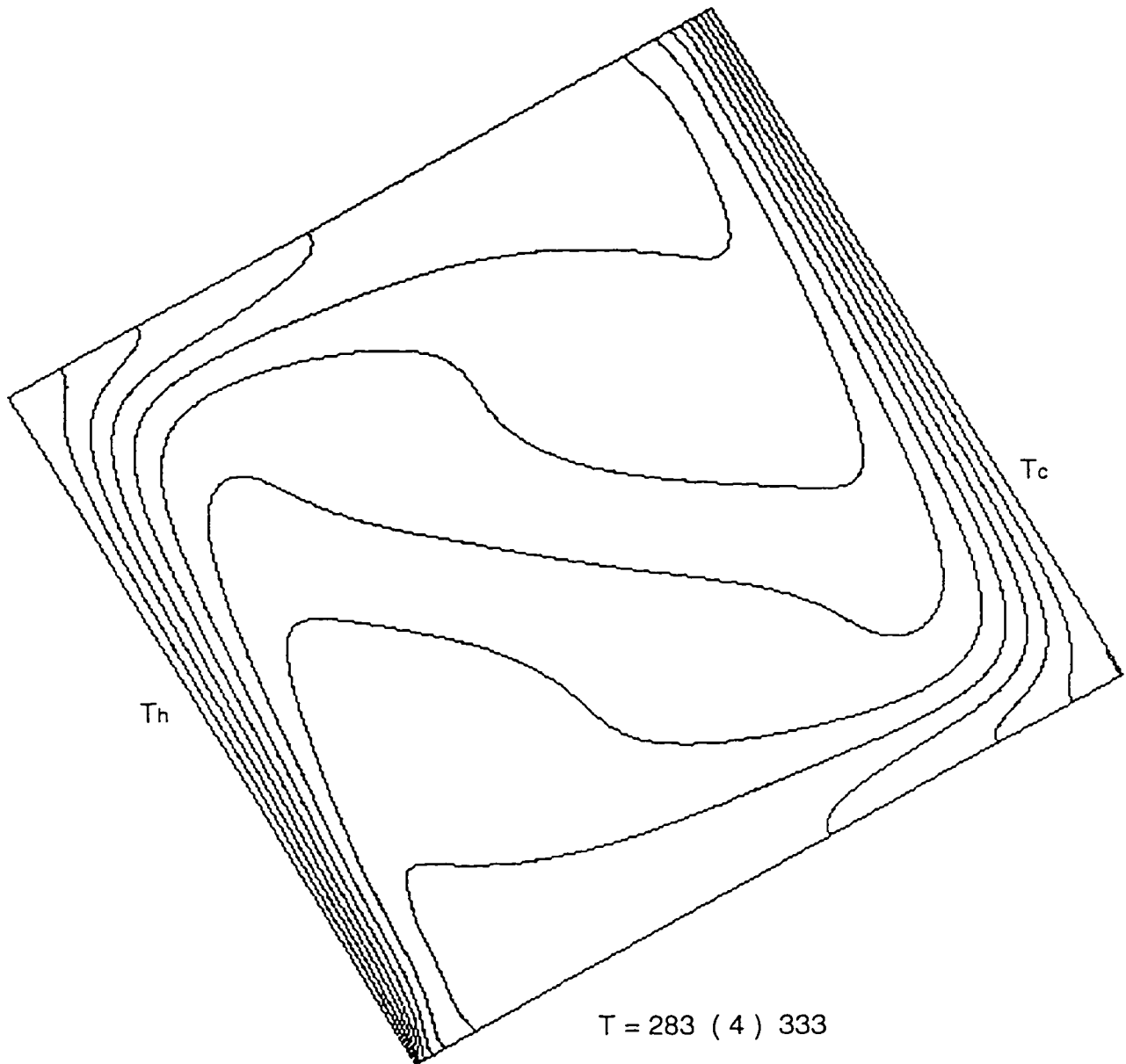


Figure 5.8: Isotherms for Laminar Natural Convection in an Enclosure without partition:  $Ra = 1 \times 10^6$ ,  $A=1.0$ ,  $Pr = 0.71$ ,  $\Phi = 60^\circ$



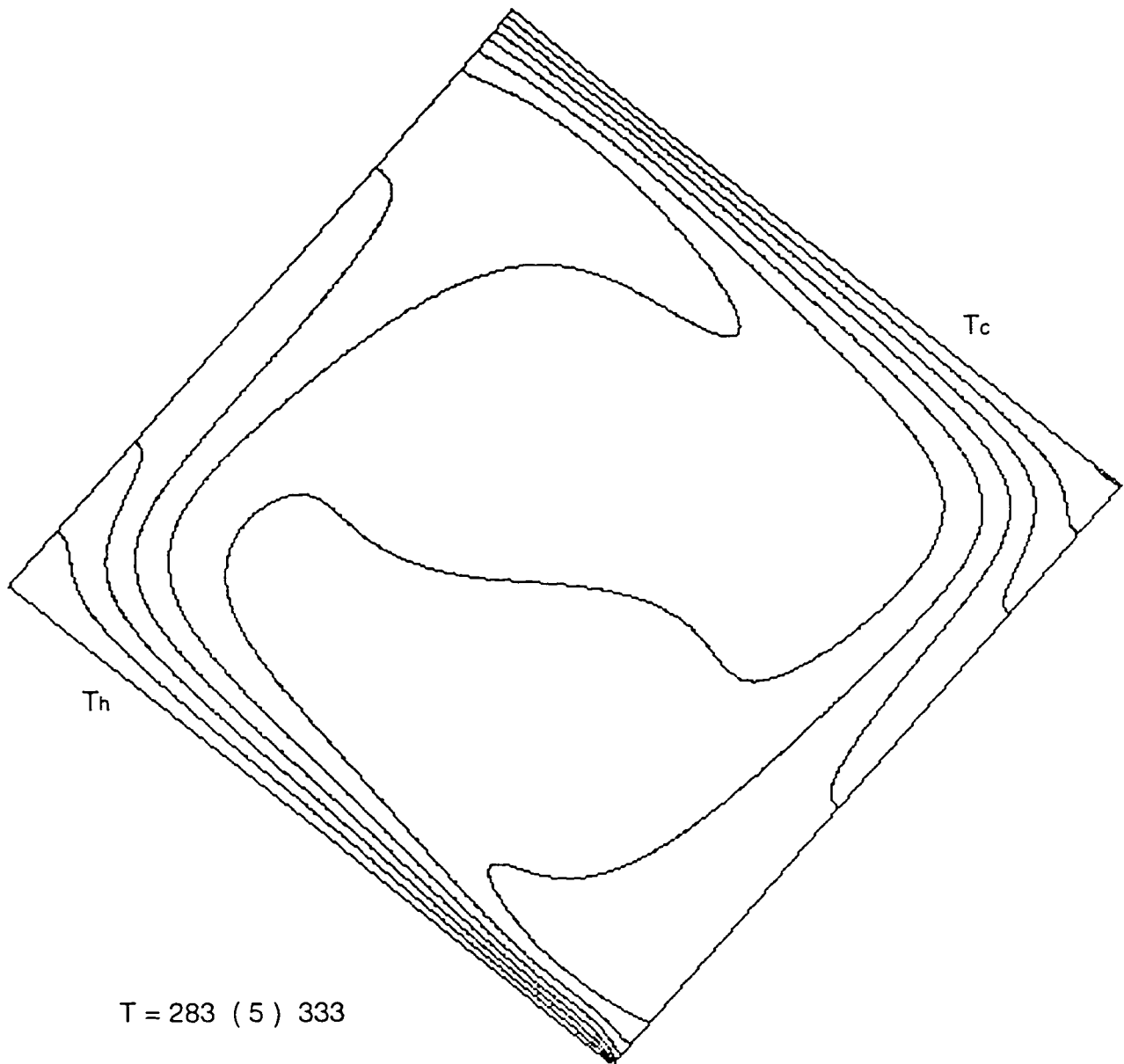


Figure 5.9: Isotherms for Laminar Natural Convection in an Enclosure without partition;  $Ra = 1 \times 10^6$ ,  $A=1.0$ ,  $Pr = 0.71$ ,  $\Phi = 40^\circ$

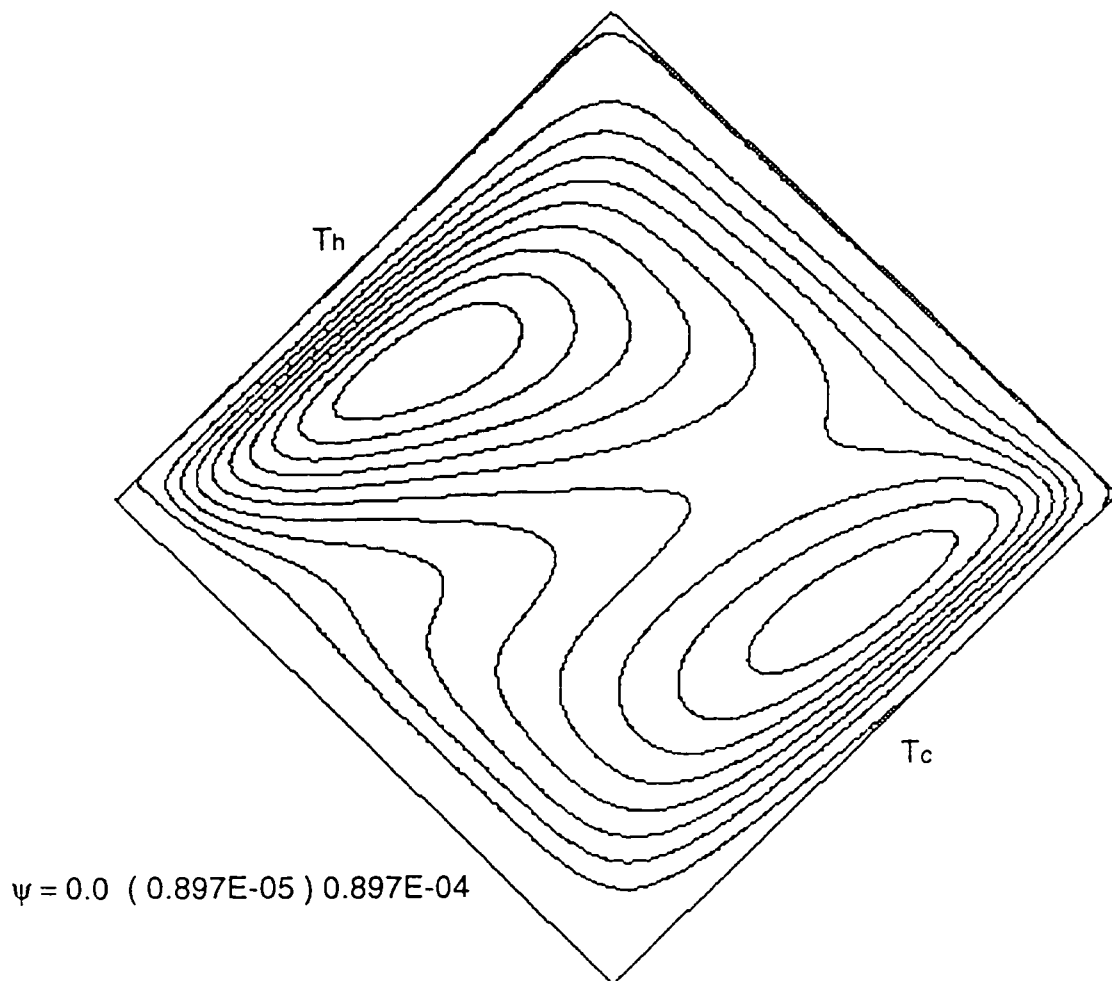


Figure 5.10: Streamlines for Laminar Natural Convection in an Enclosure without partition:  $Ra = 1 \times 10^6$ ,  $A=1.0$ ,  $Pr = 0.71$ ,  $\Phi = 135^\circ$

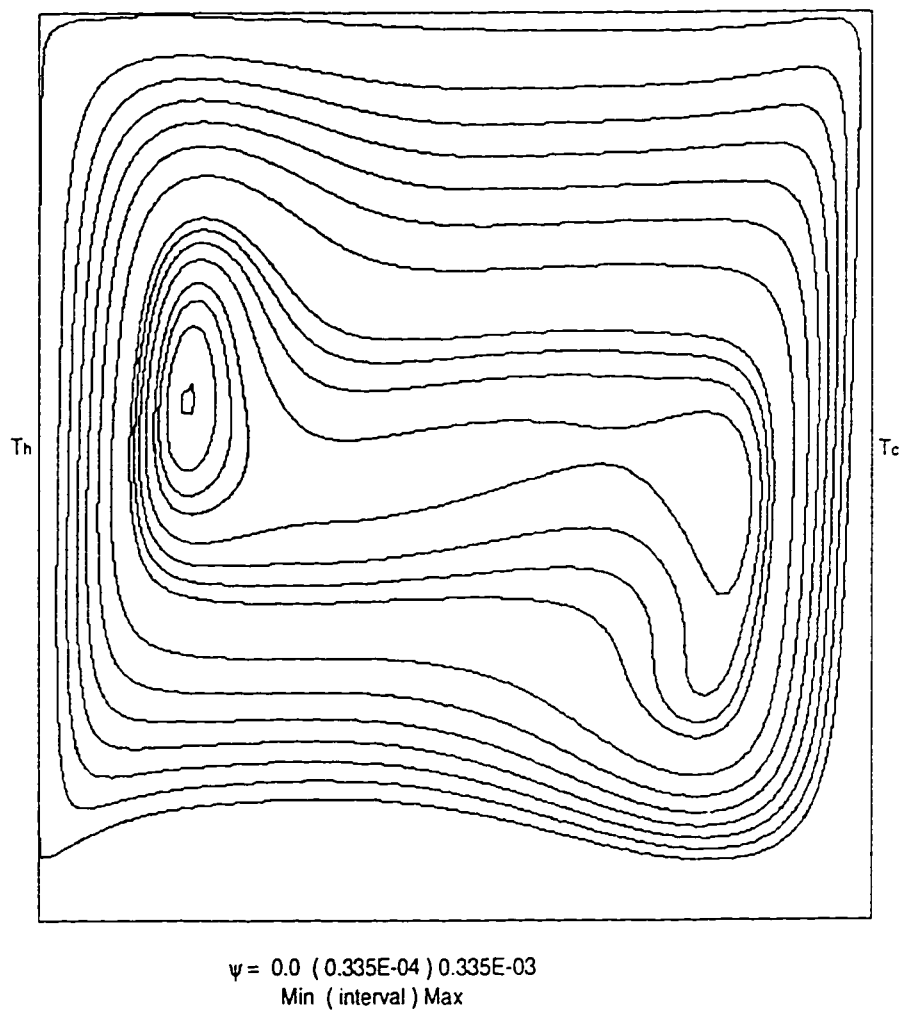


Figure 5.11: Streamlines for Laminar Natural Convection in an Enclosure without partition;  $Ra = 1 \times 10^6$ ,  $A=1.0$ ,  $Pr = 0.71$ ,  $\Phi = 90^\circ$

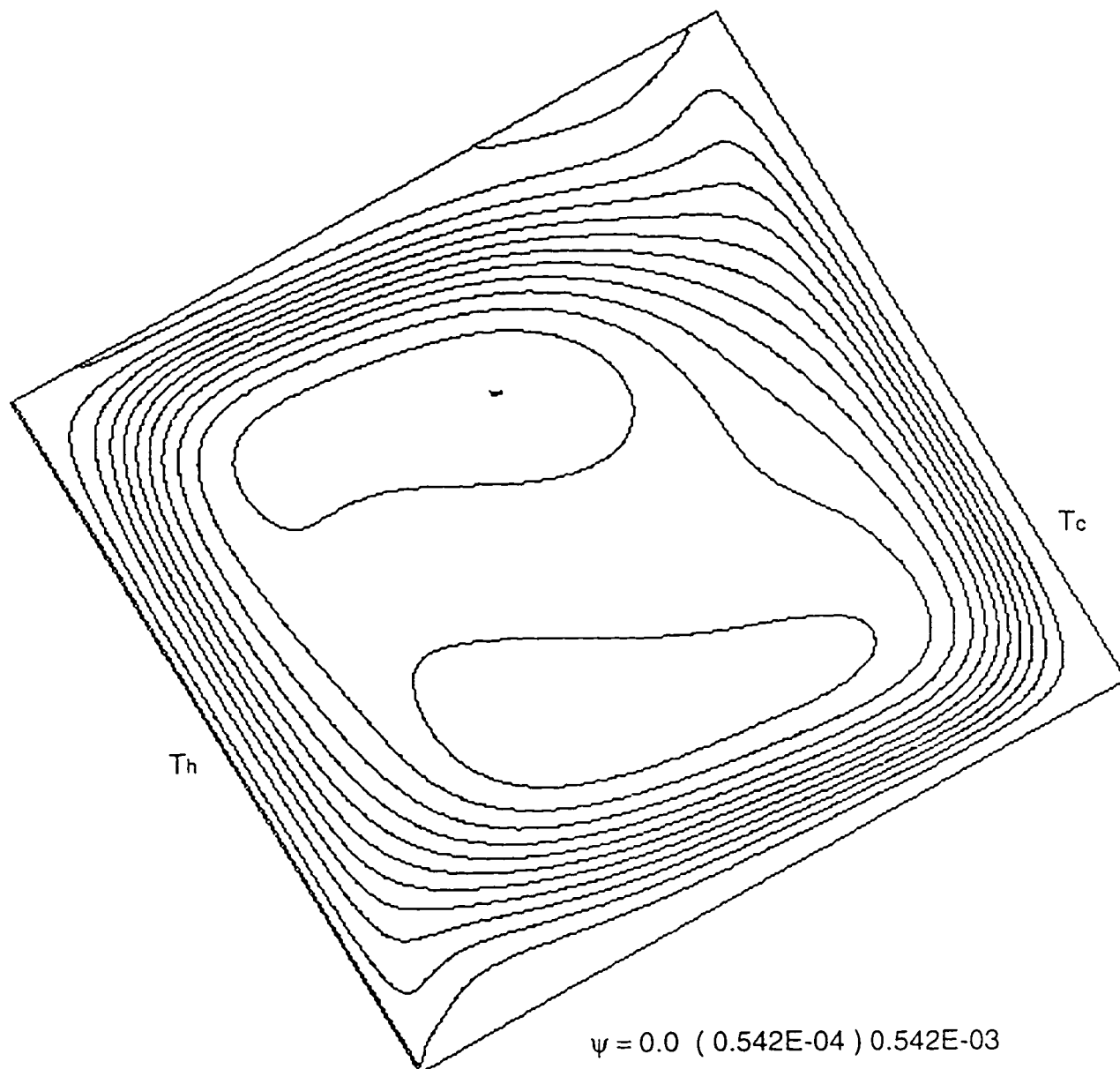


Figure 5.12: Streamlines for Laminar Natural Convection in an Enclosure without partition;  $Ra = 1 \times 10^6$ ,  $A=1.0$ ,  $Pr = 0.71$ ,  $\Phi = 60^\circ$

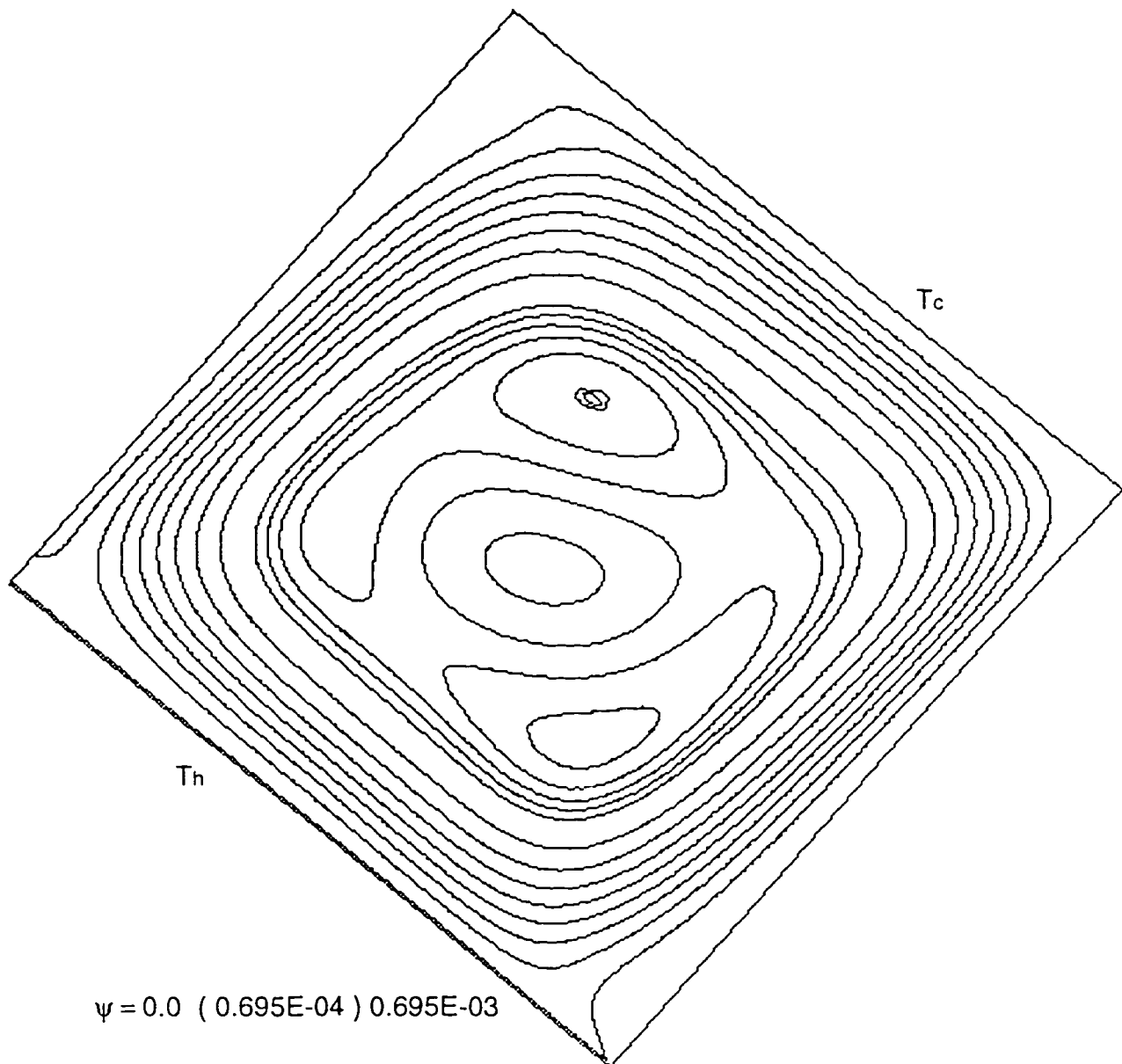


Figure 5.13: Streamlines for Laminar Natural Convection in an Enclosure without partition;  $Ra = 1 \times 10^6$ ,  $A=1.0$ ,  $Pr = 0.71$ ,  $\Phi = 40^\circ$

### 5.4.2 Effect of Angle of Inclination in Turbulent Flow

Figures 5.14 - 5.19 show the isotherms and streamlines at 90, 60 and 30 deg inclination angles for the case of turbulent natural convection in an enclosure without partition. Figures 5.14 and 5.17 show the isotherms and streamlines for an angle of inclination of  $\Phi = 90^0$ . As can be seen from the figures the flow is dominated by a thin boundary layer along the hot and the cold walls. The velocity and temperature distribution in a large part of the enclosure are very well stratified. Figures 5.15 and 5.18 show the isotherms and streamlines at  $\Phi = 60^0$ . As can be seen from figure 5.15 temperature gradient along the heated walls increases as the flow accelerates along the adiabatic walls. Figure 5.18 shows the formation of the secondary vortices along the top of the hot wall and along the bottom of the cold wall. These recirculating vortices diminishes as the angle of inclination is further reduced to 30 degrees. As can be seen from figure 5.19 that the flow along the adiabatic walls increases, squeezing the two vortices into the center of the cavity to form a unicellular structure. Figure 5.16 show steep temperature gradients along the walls indicating a rise in the heat transfer coefficient.

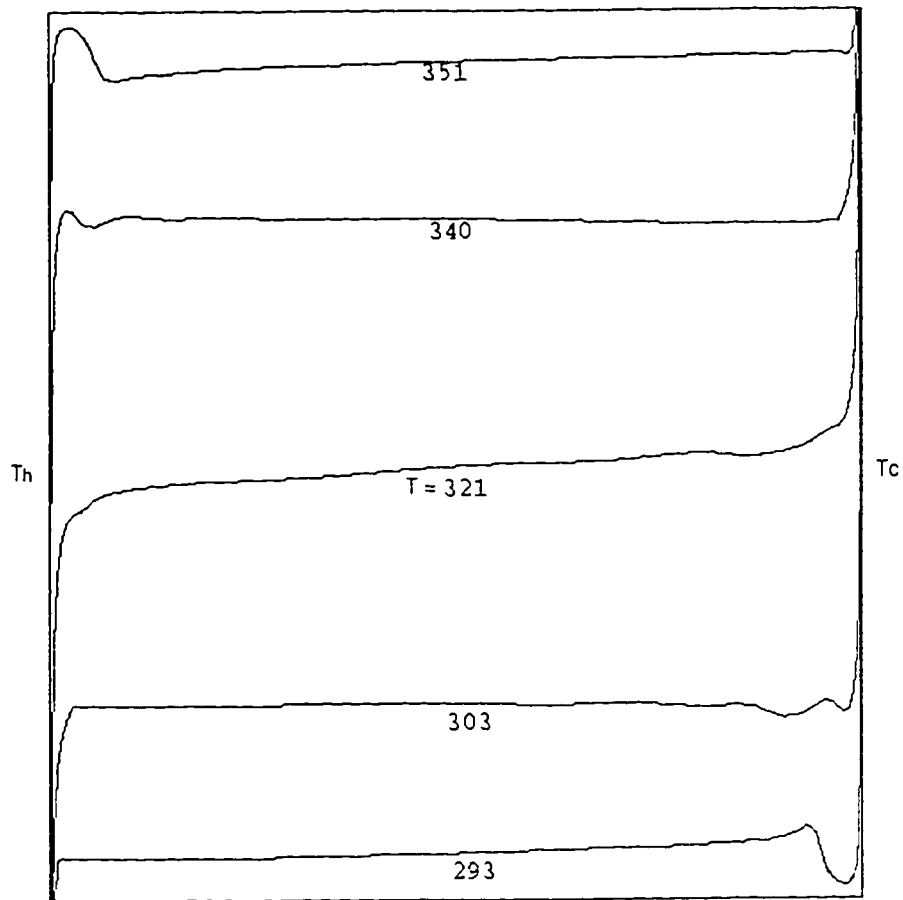


Figure 5.14: Isotherms for Turbulent Natural Convection in an Enclosure without partition;  $Ra = 1 \times 10^{10}$ ,  $A=1.0$ ,  $Pr = 0.71$ ,  $\Phi = 90^\circ$

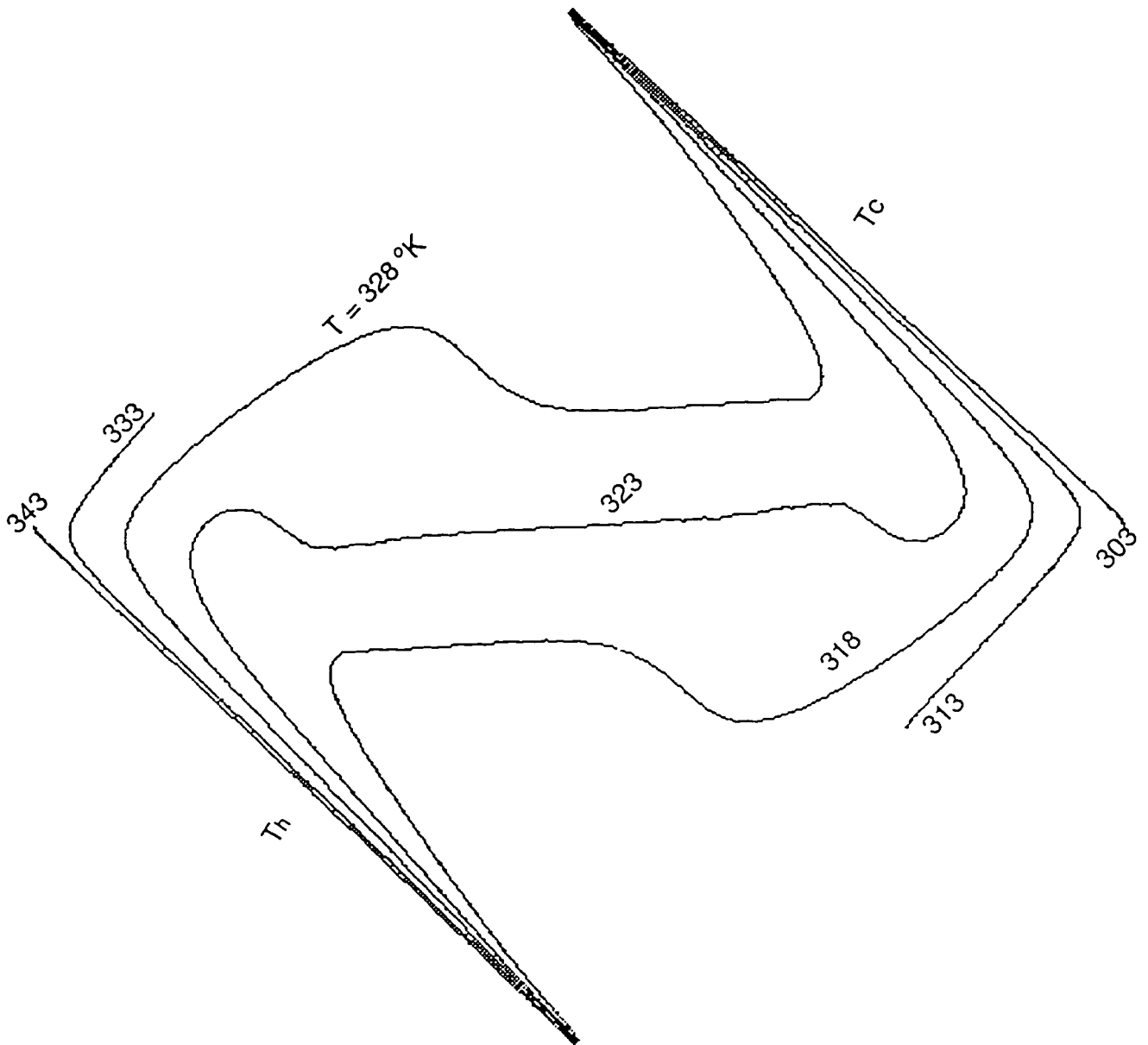


Figure 5.15: Isotherms for Turbulent Natural Convection in an Enclosure without partition:  $Ra = 1 \times 10^{10}$ ,  $A=1.0$ ,  $Pr = 0.71$ .  $\Phi = 60^\circ$



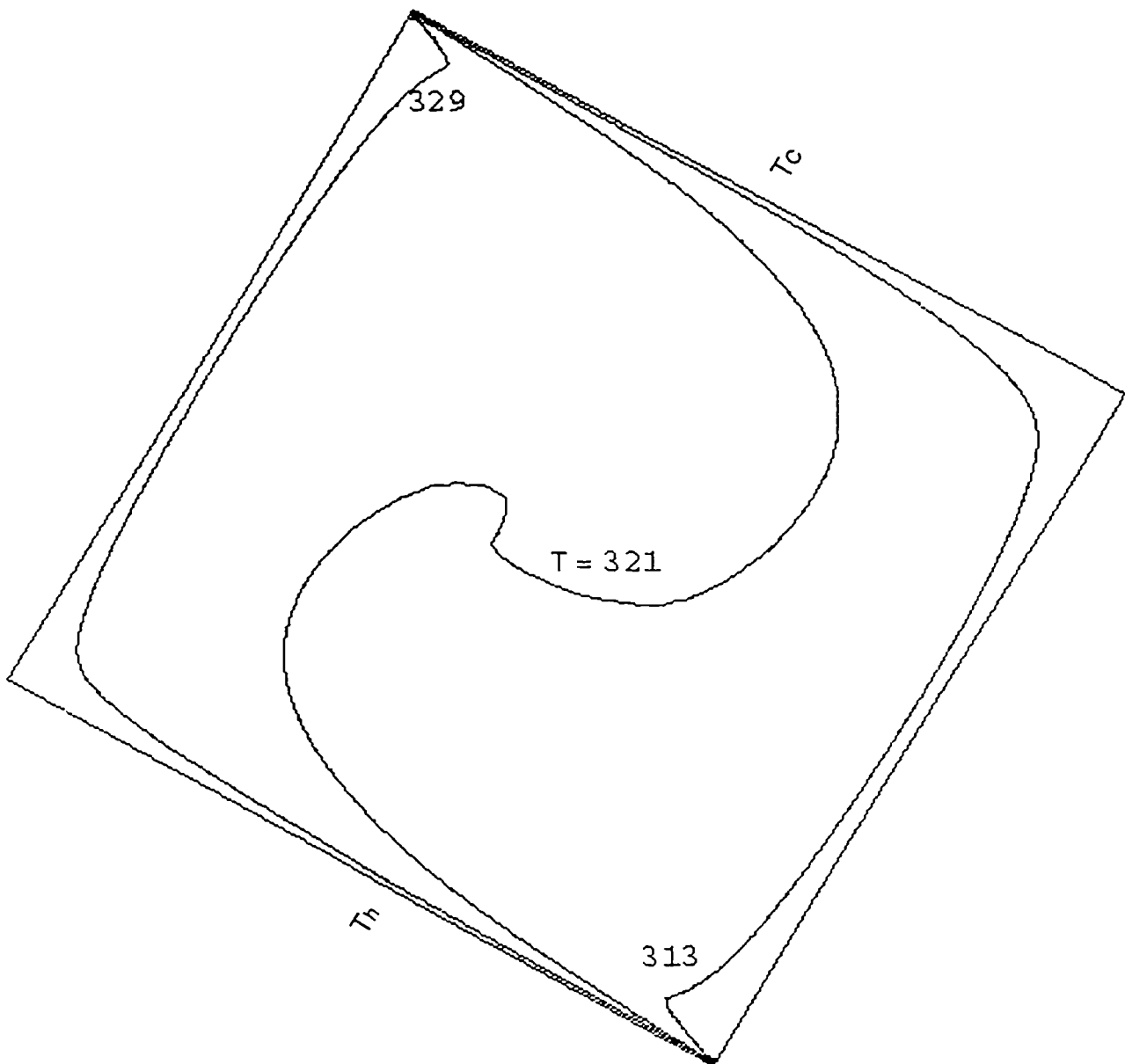


Figure 5.16: Isotherms for Turbulent Natural Convection in an Enclosure without partition;  $Ra = 1 \times 10^{10}$ ,  $A=1.0$ ,  $Pr = 0.71$ ,  $\Phi = 30^\circ$

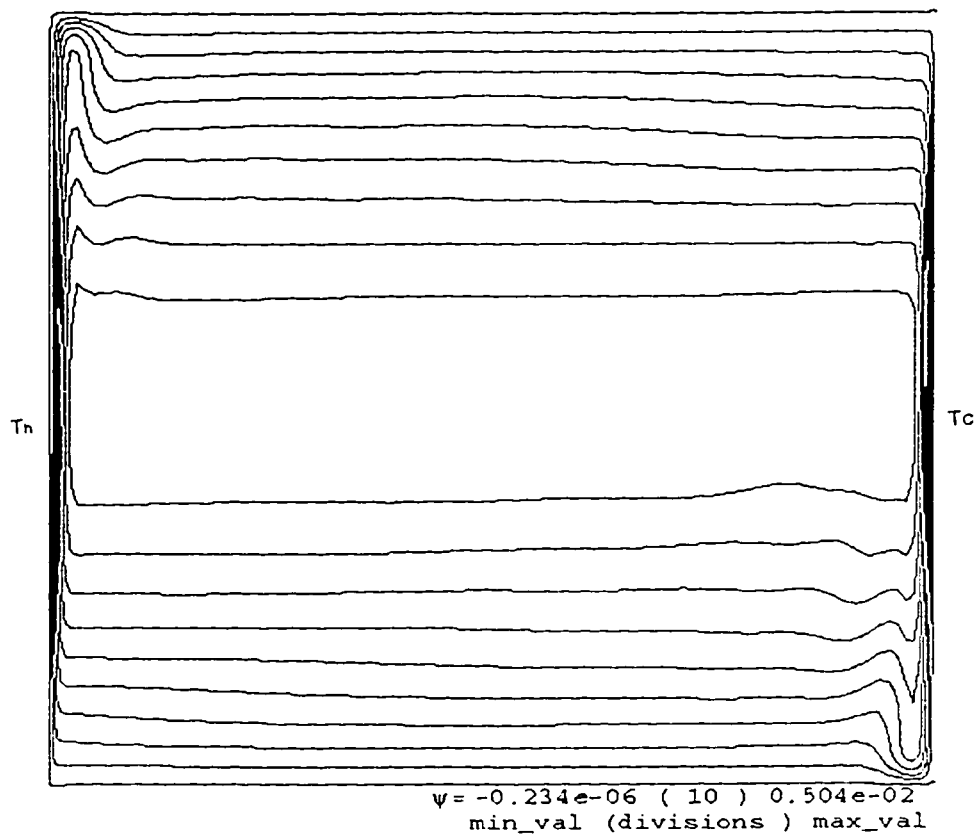


Figure 5.17: Streamlines for Turbulent Natural Convection in an Enclosure without partition;  $Ra = 1 \times 10^{10}$ ,  $A=1.0$ ,  $P_r = 0.71$ ,  $\Phi = 90^\circ$

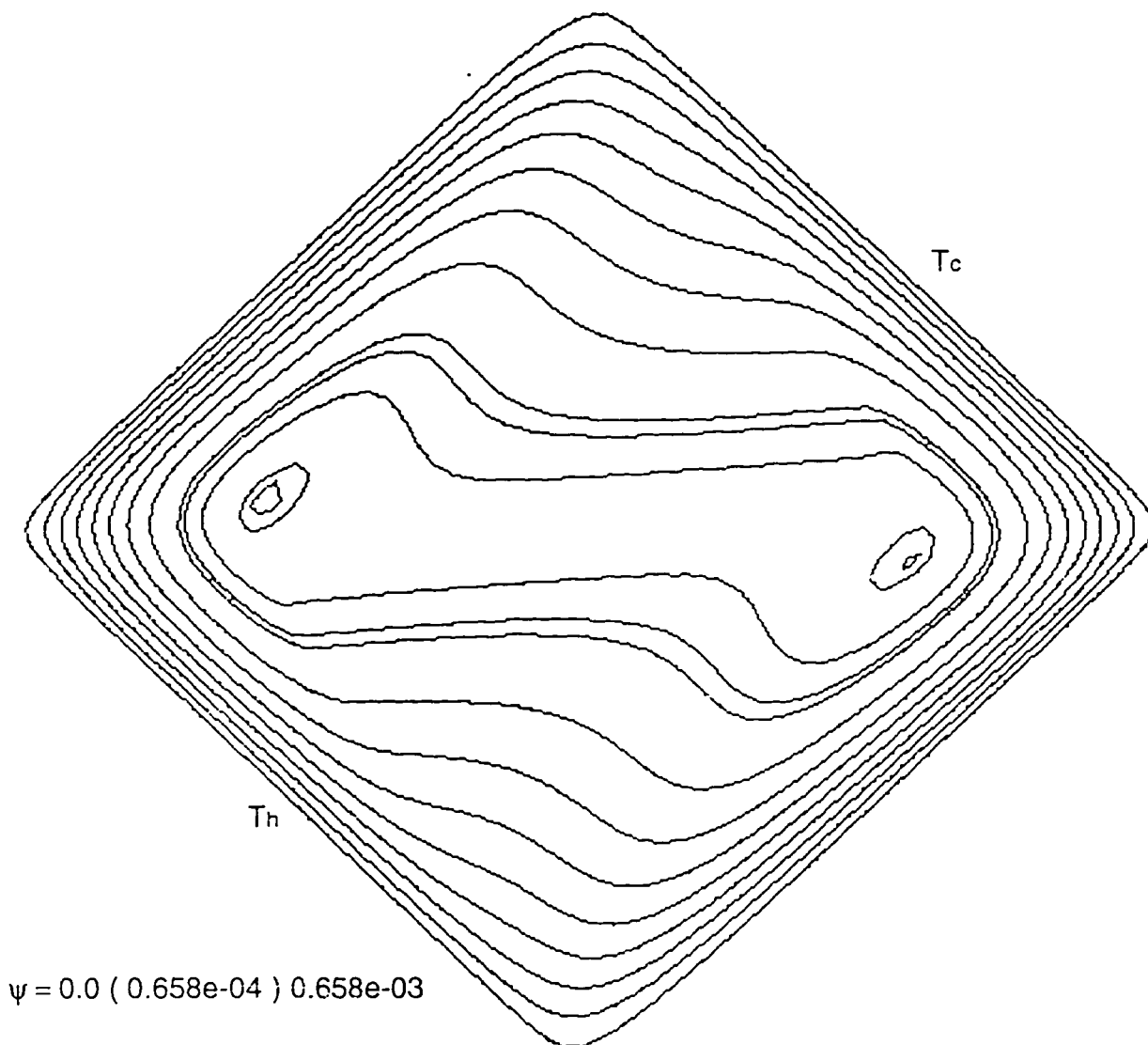
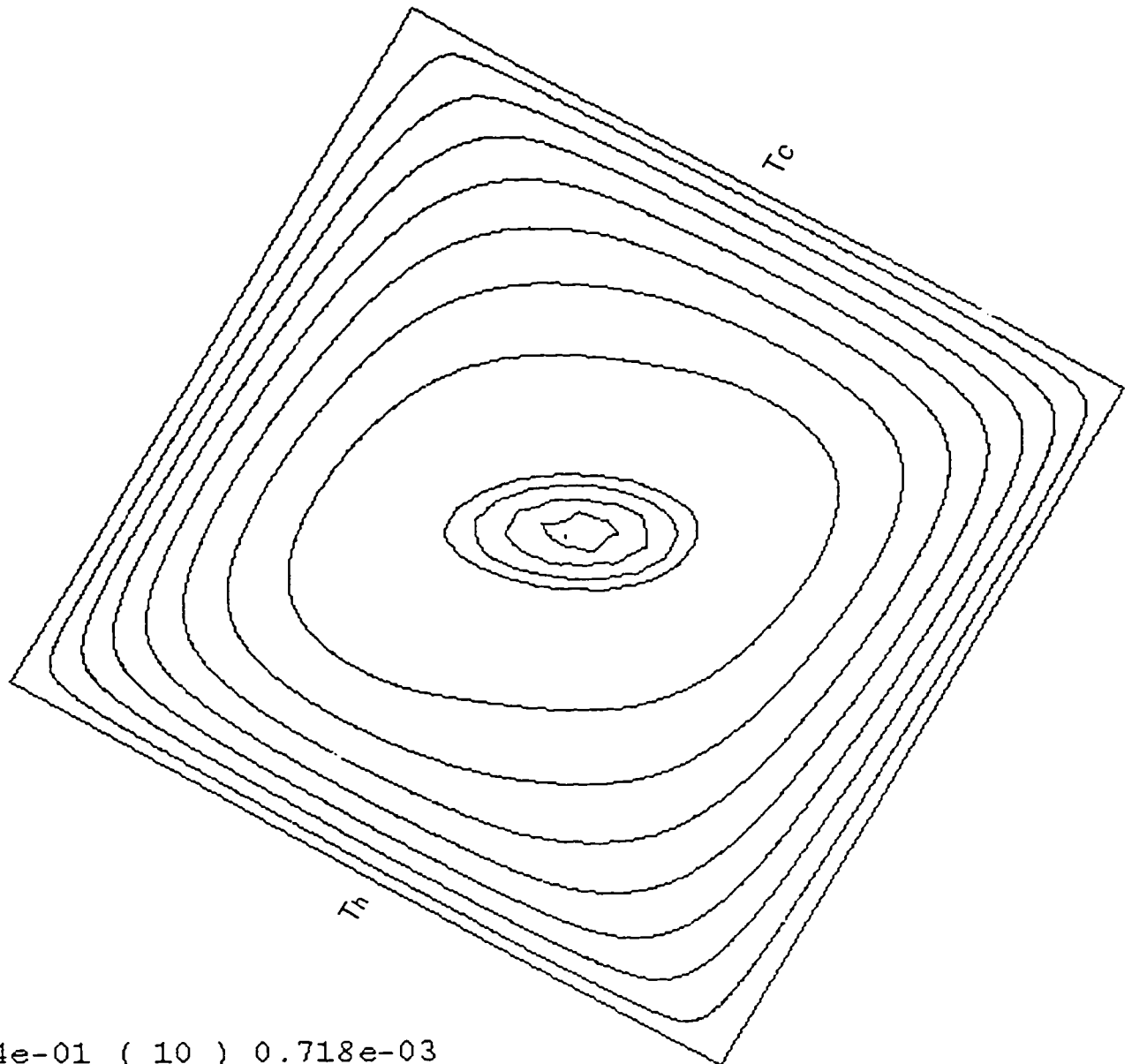


Figure 5.18: Streamlines for Turbulent Natural Convection in an Enclosure without partition:  $Ra = 1 \times 10^{10}$ ,  $A=1.0$ ,  $Pr = 0.71$ ,  $\Phi = 60^\circ$



$\psi = -0.224e-01$  ( 10 )  $0.718e-03$   
 max value ( divisions ) min value

Figure 5.19: Streamlines for Turbulent Natural Convection in an Enclosure without partition;  $Ra = 1 \times 10^{10}$ ,  $A=1.0$ ,  $P_r = 0.71$ ,  $\Phi = 30^\circ$

## 5.5 Natural Convection in Partitioned Enclosure

In an enclosure fully filled with air or any other fluid medium, convective currents are created due to the influence of the gravitational field and enhances the heat transfer. In order to reduce the heat transfer it is common to entirely fill the enclosure with a porous material as in the case of thermal insulation of building envelopes. It was pointed out by Tong and Gerner [30] that the same percent reduction in heat transfer is obtained when the enclosure is fully filled with a porous medium or it is bisected by a partition. Tong and Gerner [30] reported about 50% reduction in heat transfer in partitioned enclosure. Bisecting the enclosure with a solid partition was found to be economical way of reducing the heat transfer. The study was carried out for laminar flow and for different Rayleigh numbers with the highest being  $10^5$ .

The present study deals with the turbulent natural convection in partitioned enclosure. Influence of various parameters like number of partitions, Rayleigh number, Aspect ratio and the angle of inclination on the heat transfer and fluid flow characteristics will be discussed.

### 5.5.1 Effect of number of Partitions

The effect of partitions on the heat transfer characteristics of a vertical partitioned enclosure has been studied. Computations are carried out for different values of partitions ranging from 0 - 4 at  $Ra = 8 \times 10^{10}$ ,  $A=10:1$ ,  $Pr = 0.71$ ,  $K_r = 1.0$ ,  $t=0.1$

and  $\Phi = 90^\circ$ . The results are shown in terms of partition efficiency, which represents the reduction in heat transfer due to the introduction of partitions. The partition efficiency is defined as

$$\eta = 1 - \frac{Nu_{(N=1..N)}}{Nu_{(N=0)}} \quad (5.1)$$

Where  $Nu_{(N=0)}$  is the Nusselt number calculated when there is no partition and  $Nu_{(N=1..N)}$  is the number of partitions. Figure 5.20 shows the plot of partition efficiency versus the number of partitions. As can be seen the introduction of a single partition increases the partition efficiency significantly. In other words the introduction of a single partition results in a significant reduction in the enclosure heat transfer rate. The partition efficiency increases with the increase in number of partitions. Figures 5.21 to 5.26 show the isotherms and streamlines for the enclosure without and with multiple partitions. Figure 5.21 shows the isotherms for the enclosure without partition ( $N=0$ ), while figures 5.22 and 5.23 show the isotherms for a single and multiple partitioned enclosure.

As can be seen for the non partitioned case ( $N=0$ ) the boundary layer regime is clearly visible and as the number of partitions is increased the boundary layer regime gets distorted and conduction starts to dominate the flow. At  $N=4$  in figure 5.23 the temperature gradient is almost linear and therefore most of the heat transferred is through conduction. Figure 5.24 shows the streamlines for enclosure without partition ( $N=0$ ) while 5.25 and 5.26 show the streamlines for a single and multiple

partitioned enclosure. As can be seen from figure 5.24( $N=0$ ) most of the streamlines are concentrated near the walls indicating a steep rise in the velocity gradients near the walls.

Figure 5.27 shows the plot of the dimensionless temperature at the mid-height of the enclosure at various values of  $N$ . The temperature profile at  $N=0$  is of the boundary layer type with steep gradients near the walls and zero gradient in the core region indicating the presence of convective currents near the walls. At  $N=1$  the gradient near the wall is reduced to a great extent and at  $N=4$  the temperature profile is almost linear indicating conduction as the main mechanism of heat transfer.

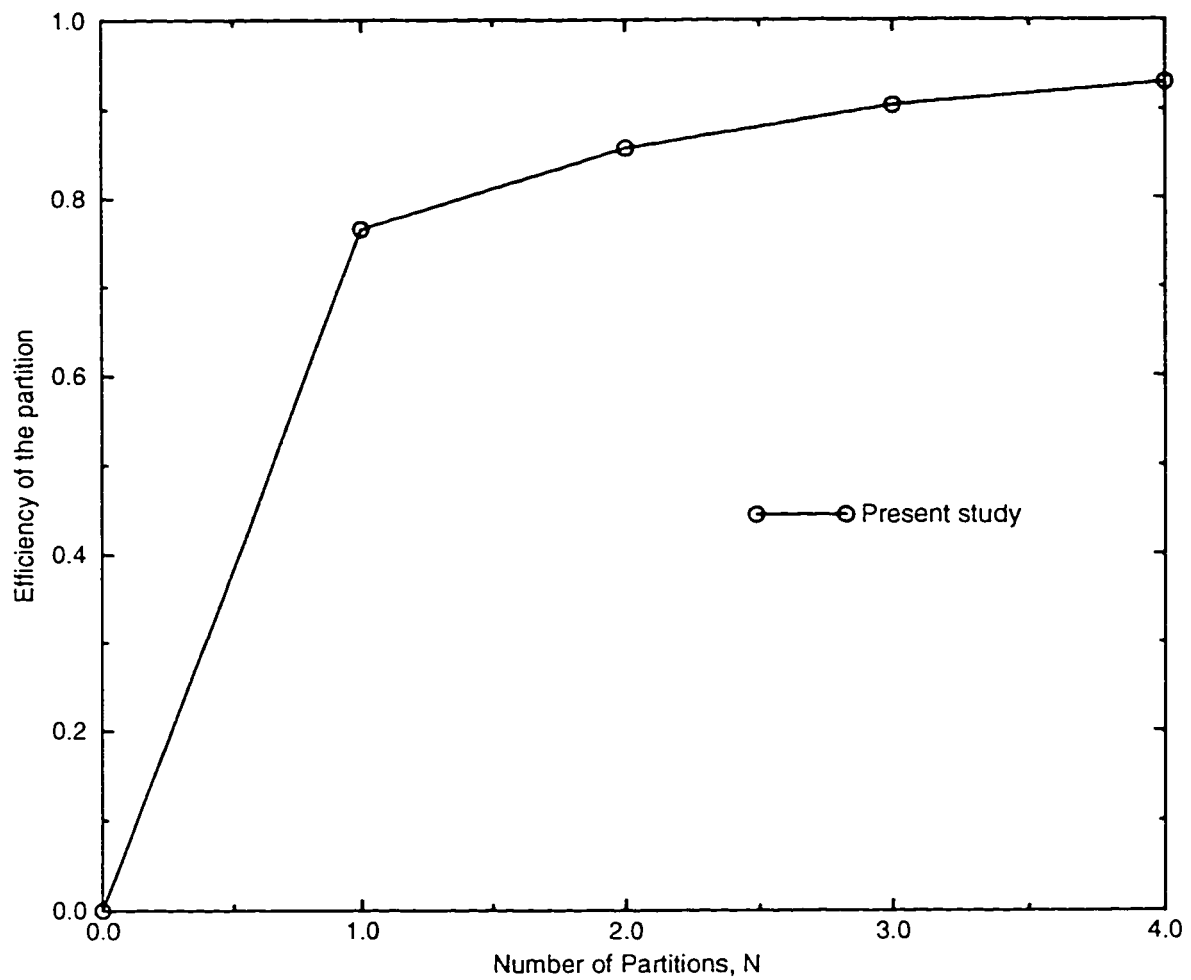


Figure 5.20: Effect of number of partitions on the Efficiency of the partition for Turbulent Natural convection in an enclosure with partition:  $Ra = 8 \times 10^{10}$ ,  $A=10.0$ ,  $\Phi = 90^\circ$



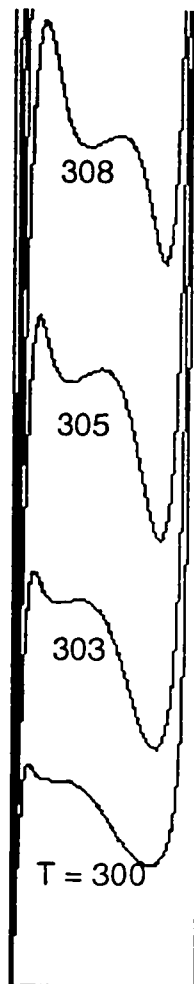
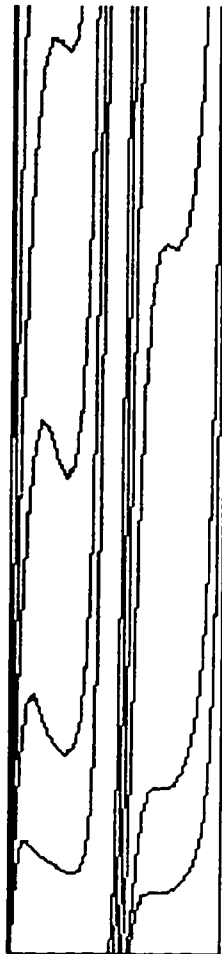
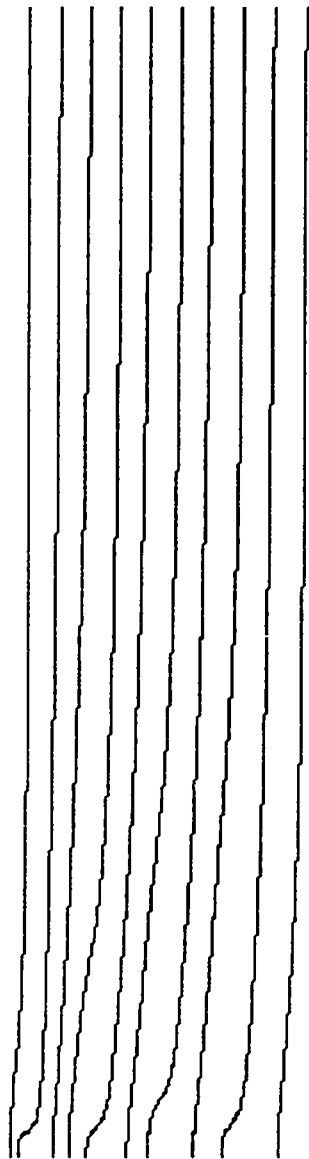


Figure 5.21: Isotherms for turbulent natural convection in an enclosure without Partition;  $Ra = 8 \times 10^{10}$ ,  $A=10.0$ ,  $\Phi = 90^\circ$



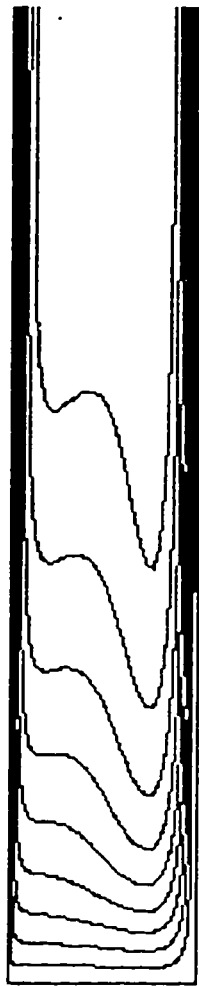
T = 294 ( 2 ) 322

Figure 5.22: Isotherms for turbulent natural convection in a single partition enclosure with  $Ra = 8 \times 10^{10}$ ,  $A=10.0$ ,  $N=1.0$ ,  $K_r = 1.0$ ,  $\Phi = 90^\circ$ ,  $t=0.1$



$$T = 294 ( 4 ) 322$$

Figure 5.23: Isotherms for turbulent natural convection in a multiple partitioned enclosure with  $Ra = 8.0 \times 10^{10}$ ,  $A=10.0$ ,  $N=4.0$ ,  $K_r = 1.0$ ,  $t=0.1$ ,  $\Phi = 90^\circ$



$\psi = 0.0 \quad (0.00047) \quad 0.0047$

Figure 5.24: Streamlines for turbulent natural convection in an enclosure without Partition;  $Ra = 8 \times 10^{10}$ ,  $A=10.0$ ,  $\Phi = 90^\circ$

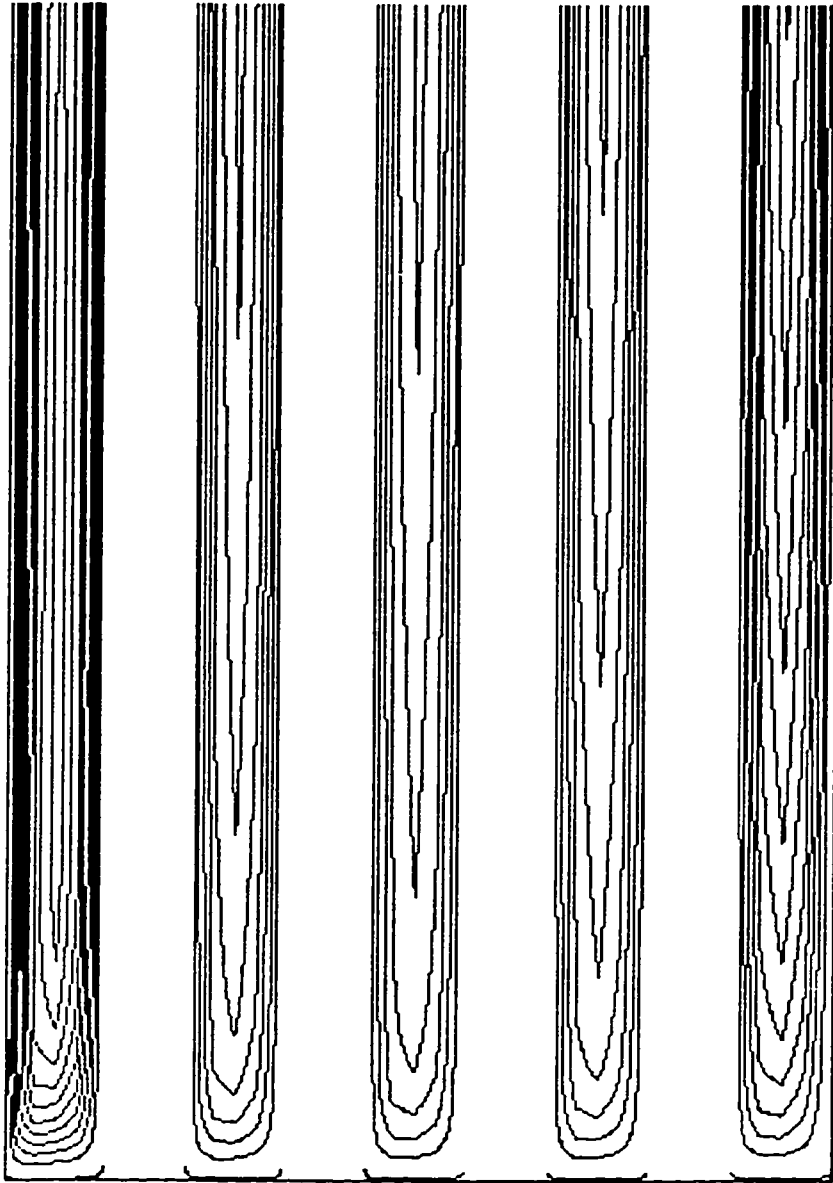
## NOTE TO USERS

THE ORIGINAL DOCUMENT RECEIVED BY UMI  
CONTAINED PAGES  
WITH POOR PRINT. PAGES WERE FILMED AS  
RECEIVED.

100

THIS REPRODUCTION IS THE BEST COPY AVAILABLE.

UMI



$$\psi = 0.00 ( 0.0000188 ) 0.000188$$

Figure 5.26: Streamlines for turbulent natural convection in a multiple partitioned enclosure with  $Ra = 8.0 \times 10^{10}$ ,  $A=10.0$ ,  $N=4.0$ ,  $K_r = 1.0$ ,  $t=0.1$ .  $\Phi = 90^\circ$

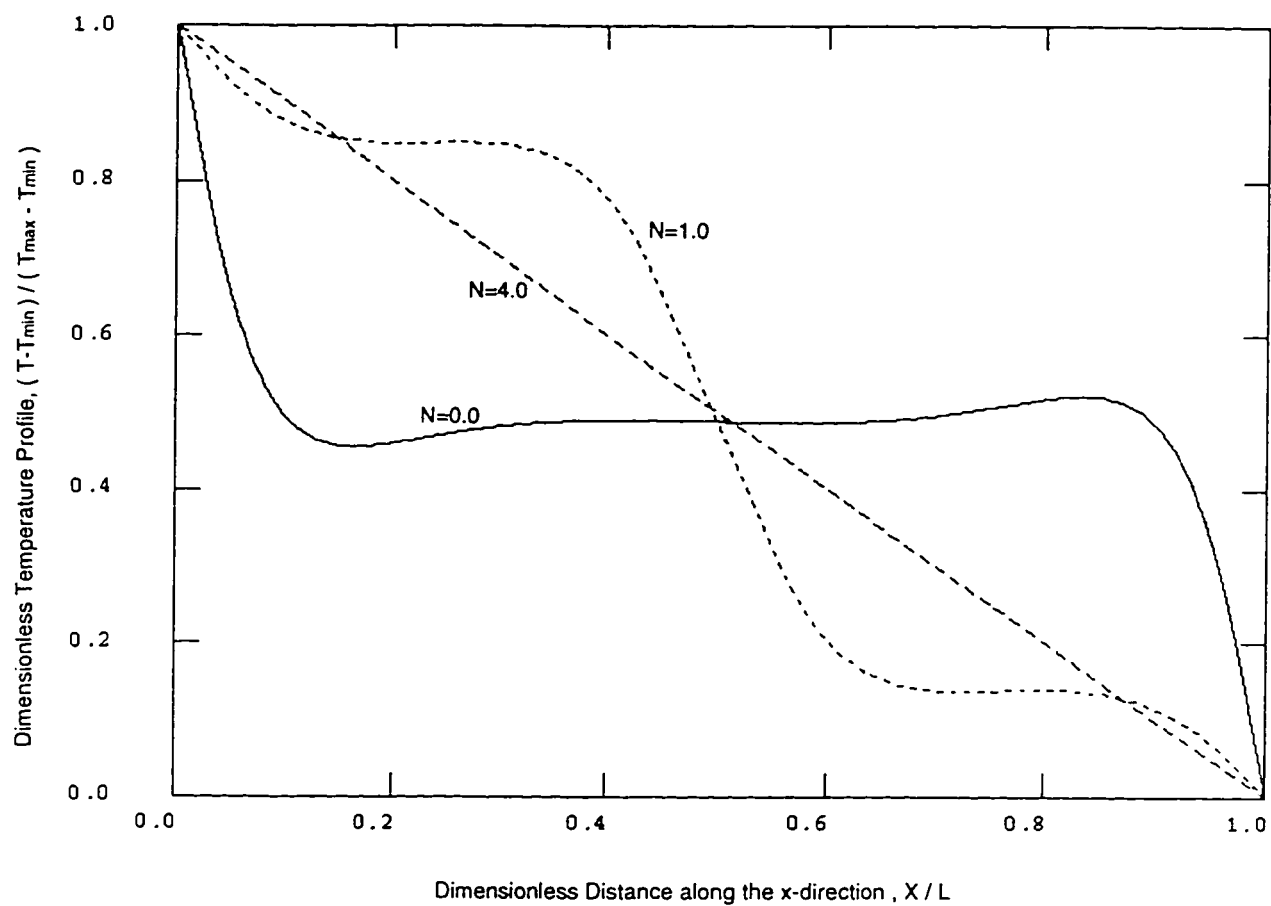


Figure 5.27: Dimensionless Temperature at the mid-height of the enclosure at different number of partitions.

### 5.5.2 Effect of Rayleigh number

The effect of the Rayleigh number on the heat transfer characteristics of a vertical partitioned enclosure has been studied for the Rayleigh number range of  $10^9$  to  $10^{13}$ . The Rayleigh number can be varied by either varying the temperature difference or varying the height of the enclosure as the Rayleigh number is a function of these two parameters. The enclosure height is being varied keeping the aspect ratio constant at 10:1.

The plots of the isotherms and streamlines are shown in figures 5.28 to 5.31. as can be seen from the figures 5.28 and 5.29 as  $Ra$  increases the temperature gradient near the walls also increases. Figure 5.30 shows the primary flow rotation from the hot wall to the cold wall with a curvature near the adiabatic walls. As the Rayleigh number increases ( $Ra = 10^{13}$ ) the rotating cells are stretched back to the upper side of the hot wall and to the lower side of the cold wall as shown in figure 5.31. This behavior is clearly visible in the plot of velocity vectors shown in figure (5.32). The velocity vectors moving away from the top of the hot wall and the bottom of the cold wall are dragged back towards the vertical walls forming a narrow cell. This is due to the increase in the buoyancy forces, forming a secondary flow region as described by Elder [7] and [8].

The effect of Rayleigh number on the Nusselt number for a vertical enclosure ( $\Phi = 90^\circ$ ) with a single centrally placed partition is shown in figure 5.33. As can be



seen from the figure as the Rayleigh number increases the Nusselt number increases. This is expected since an increase in the Rayleigh number is associated with increase in the temperature gradients.

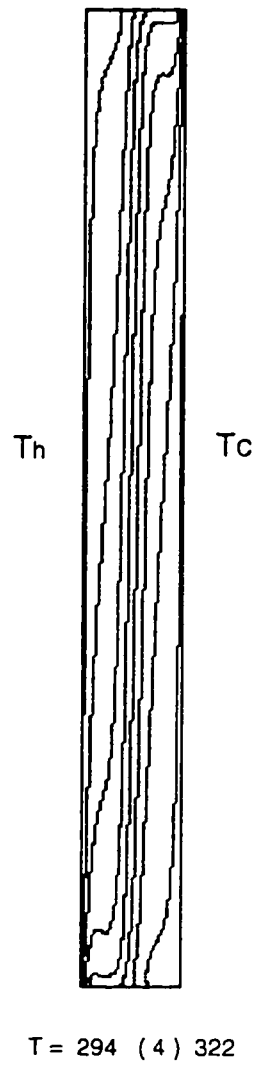


Figure 5.28: Isotherms for Turbulent Natural convection in an enclosure with partition;  $Ra = 1 \times 10^9$ ,  $A=10.0$ ,  $N=1$ ,  $K_r = 1.0$ ,  $t=0.1$ ,  $\phi = 90^\circ$

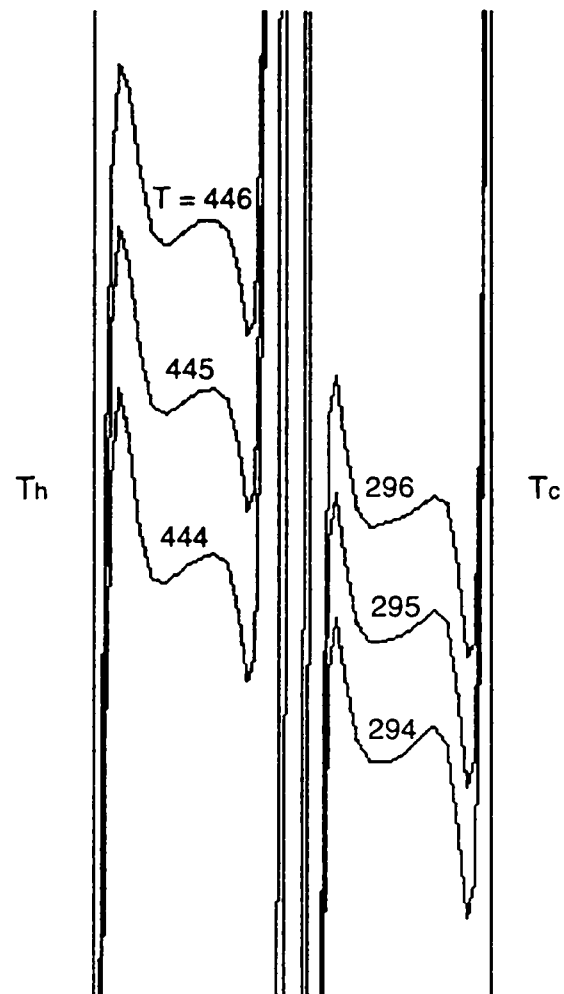
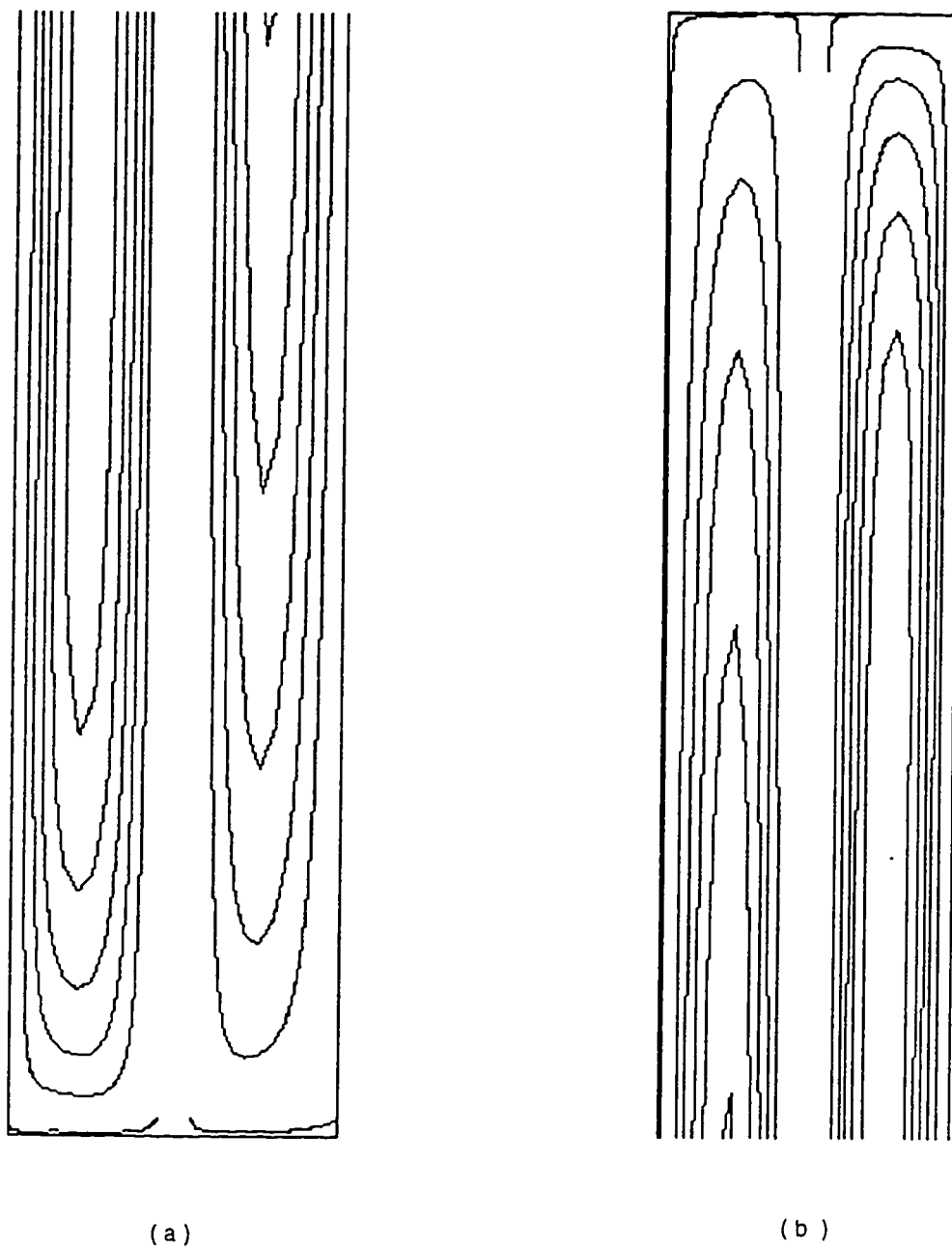


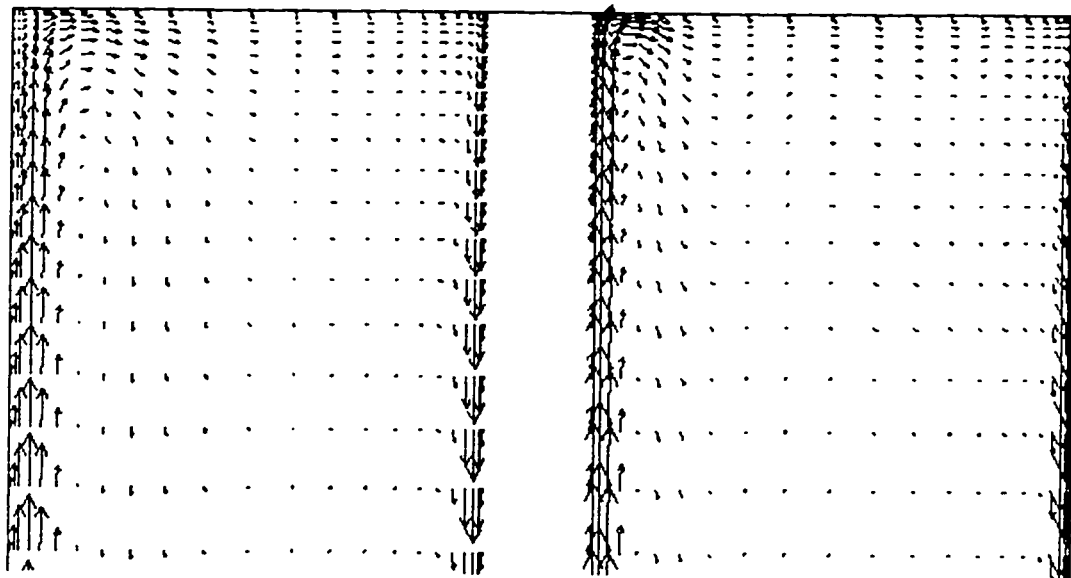
Figure 5.29: Isotherms for Turbulent Natural convection in an enclosure with partition:  $Ra = 1 \times 10^{13}$ ,  $A=10.0$ ,  $N=1$ ,  $K_r = 1.0$ ,  $t=0.1$ ,  $\Phi = 90^\circ$



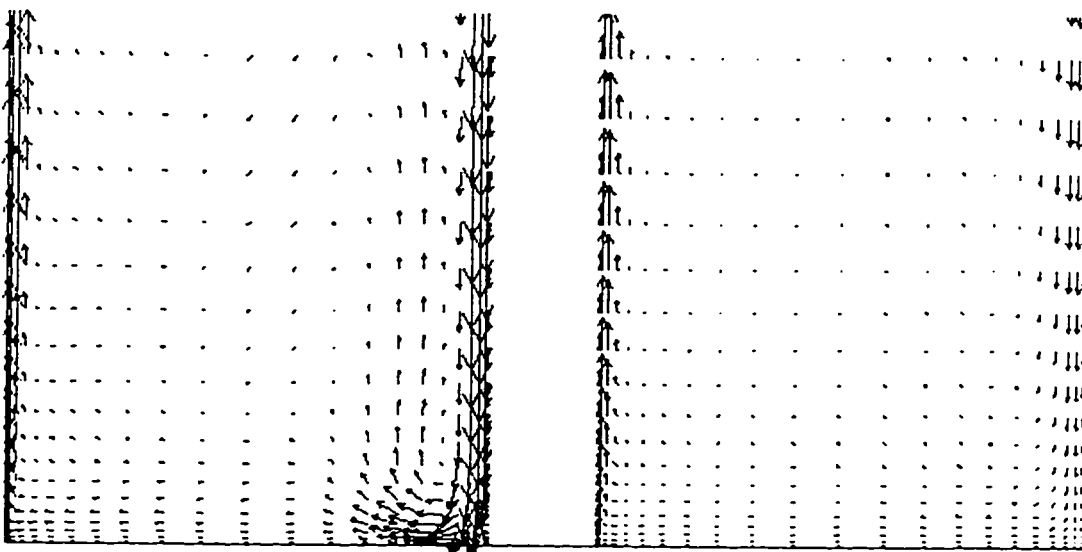
$$\psi = 0.00 ( 0.000614 ) 0.00614$$

Figure 5.30: Streamlines for Turbulent Natural convection in an enclosure with partition:  $Ra = 1 \times 10^9$ ,  $A=10.0$ ,  $N=1$ ,  $K_r = 1.0$ ,  $t=0.1$ ,  $\Phi = 90^\circ$ : (a) Magnified view of the bottom (b) Magnified view of the top





(b)



(a)

Figure 5.32: velocity vectors for Turbulent Natural convection in an enclosure with partition;  $Ra = 1 \times 10^{13}$ ,  $A=10.0$ ,  $N=1$ ,  $K_r = 1.0$ ,  $t=0.1$ ,  $\Phi = 90^\circ$ : (a) Magnified view of the bottom (b) Magnified view of the top

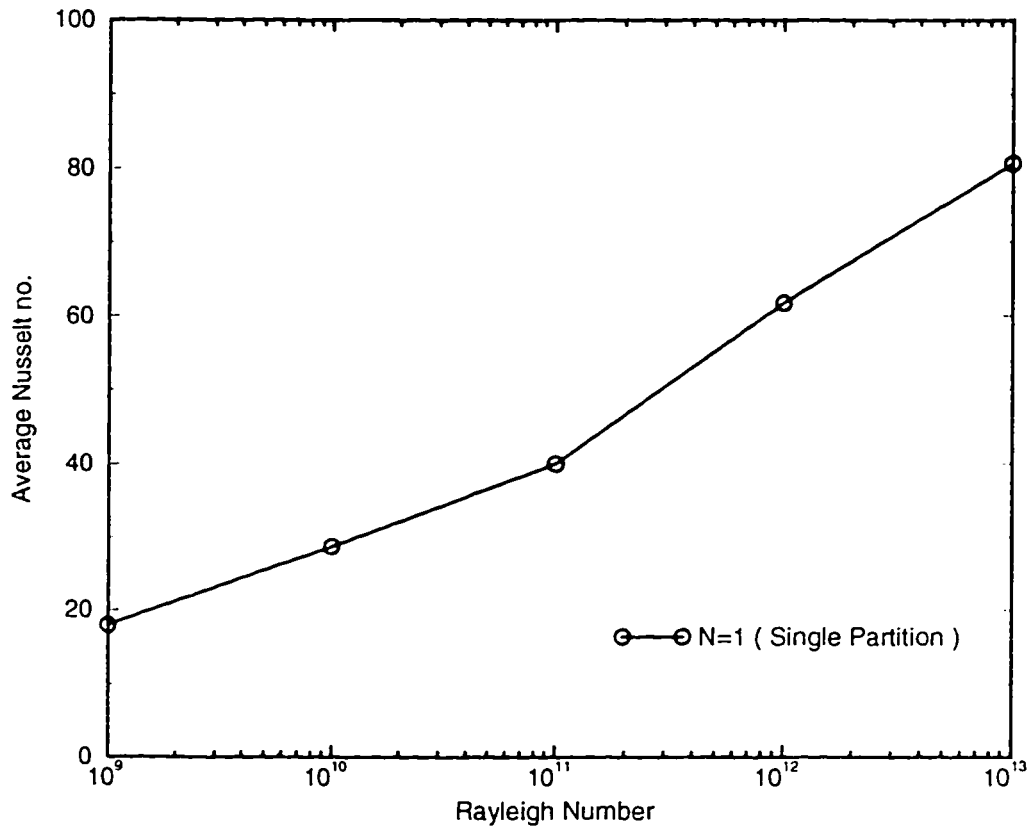


Figure 5.33: Effect of Rayleigh number on the Average Nusselt no. for Turbulent Natural convection in an enclosure with partition;  $\Phi = 90^\circ$ ,  $A=10$ ,  $N=1$ ,  $t=0.1$ ,  $K_r = 1.0$ ,  $P_r = 0.71$

### 5.5.3 Effect of Aspect ratio

The early studies of laminar natural convection in enclosures resulted in different opinions regarding the effect of aspect ratio. Eckert and Carlson [6] obtained a correlation for the Nusselt number as  $Nu = C \times Ra^{0.3}/A^{0.1}$  indicating significant effect of aspect ratio on the average Nusselt number. Varying the enclosure height 'H', will vary the Rayleigh number as well as the aspect ratio. It is this dependence of  $Ra$  on aspect ratio(A) that has made it difficult to clearly indicate the separate effects of  $Ra$  and aspect ratio(A) on  $Nu$ . In case of turbulent flow the literature indicates that the effect of aspect ratio on the Nusselt number is small and negligible.

In the present Study the effect of aspect ratio on Nusselt number has been studied for the case of  $Ra = 8 \times 10^{10}$ ,  $Pr = 0.71$ ,  $K_r = 1.0$ ,  $t=0.1$  and  $\Phi = 90^\circ$ . The aspect ratio, defined as the ratio of the height to the width, ranged from 2 to 15. Figure 5.34 shows the plot of aspect ratio versus the Nusselt number for  $N=0$  and  $N=1$ . As can be seen in both cases, the Nusselt number is found to be an increasing function of the aspect ratio. This can be explained by the observation that as aspect ratio increases the fluid velocity increases and fluid along the hot and cold walls remain in contact with them for a longer distance. This reduces the temperature difference near the walls, but consequently due to the decrease in the distance between the isothermal walls the distance near the wall  $dx$  decreases considerably which leads to an increase in the temperature gradient near the walls, thereby increasing the



average Nusselt number.

Figures 5.35-5.38 show the plots of isotherms and streamlines for  $A=2$  and  $A=15$  respectively.

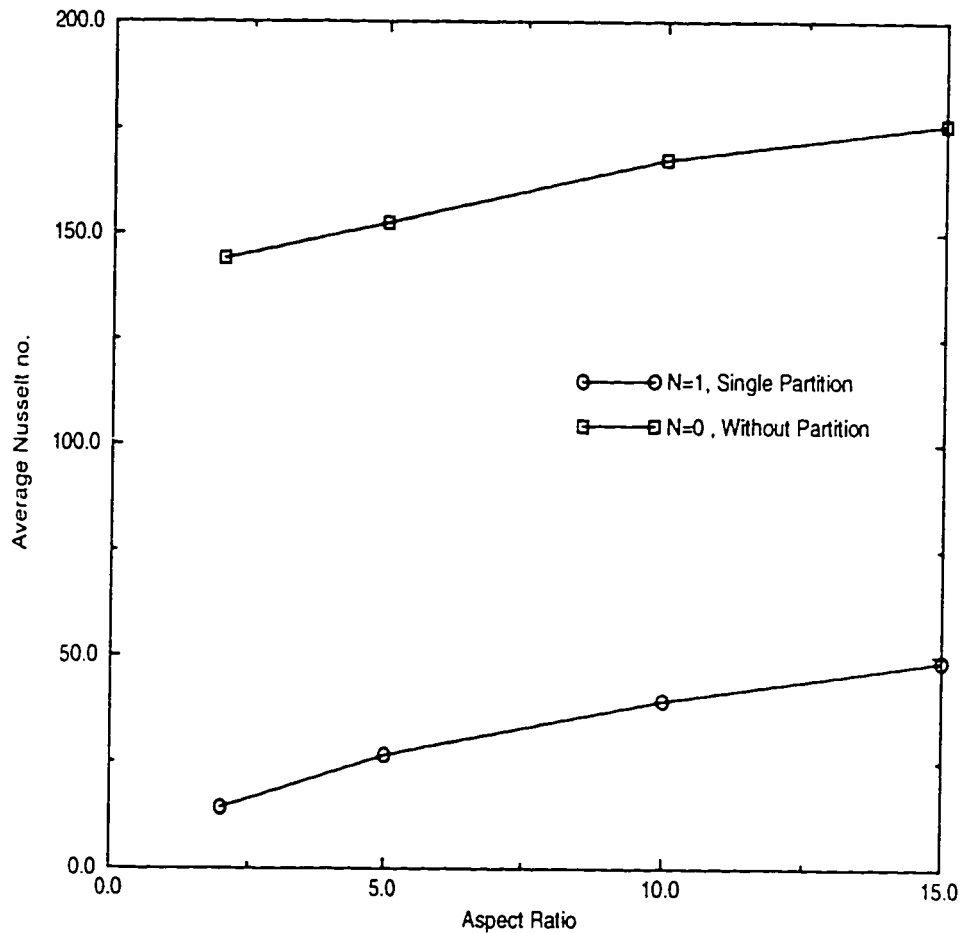


Figure 5.34: Effect of Aspect ratio on the Average Nusselt no. for Turbulent Natural convection in an enclosure with and without partition;  $Ra = 8.0 \times 10^{10}$ ,  $K_r = 1.0$ ,  $t=0.1$ ,  $\Phi = 90^\circ$

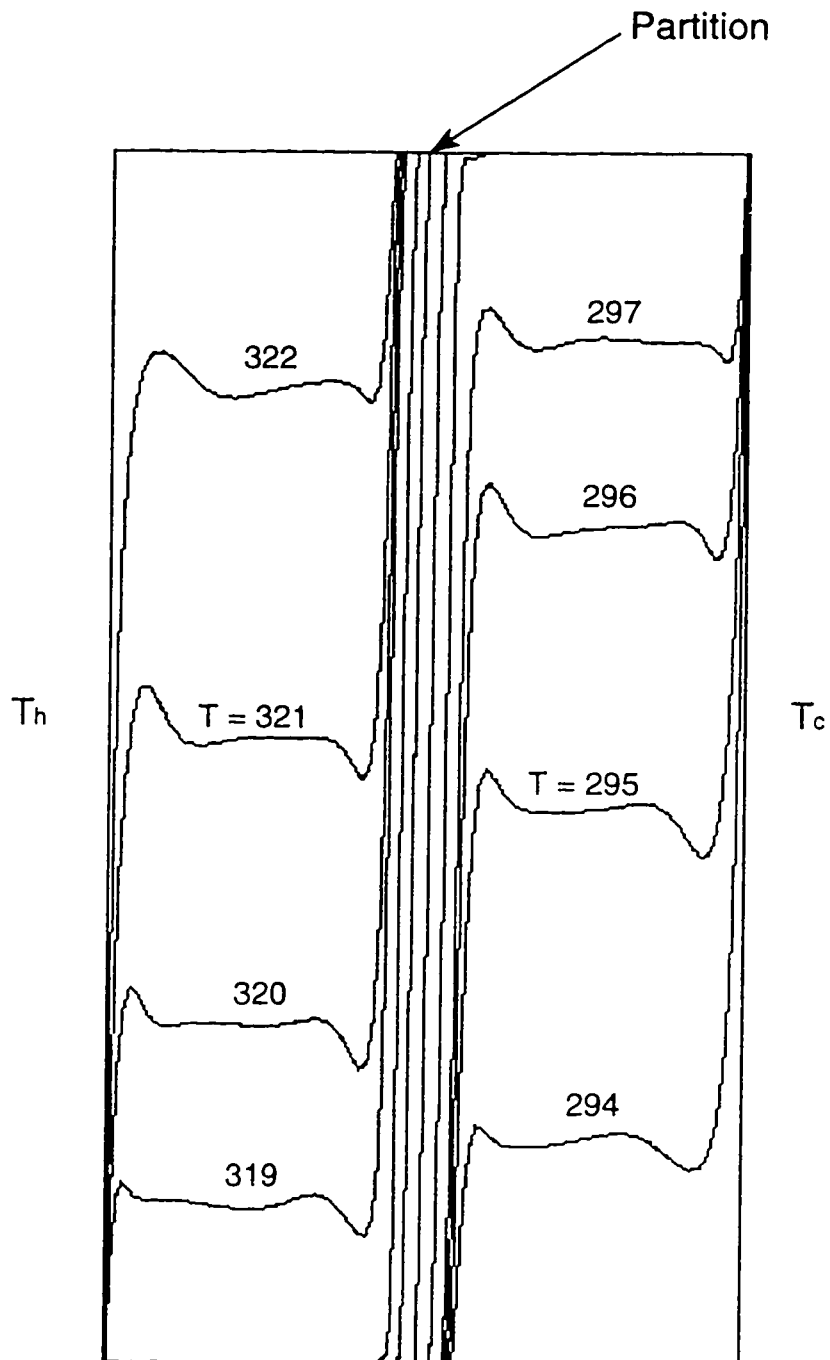
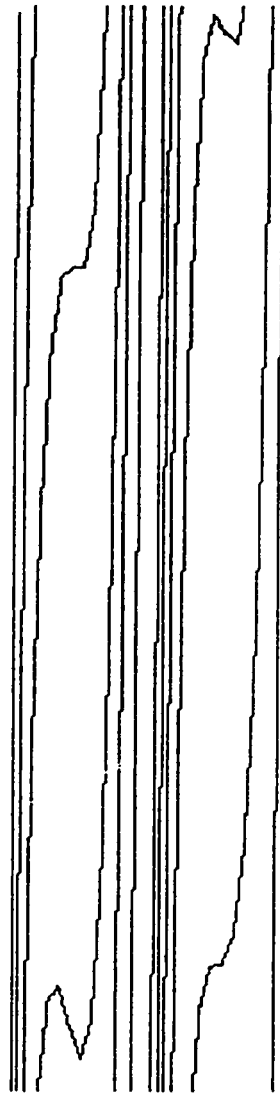
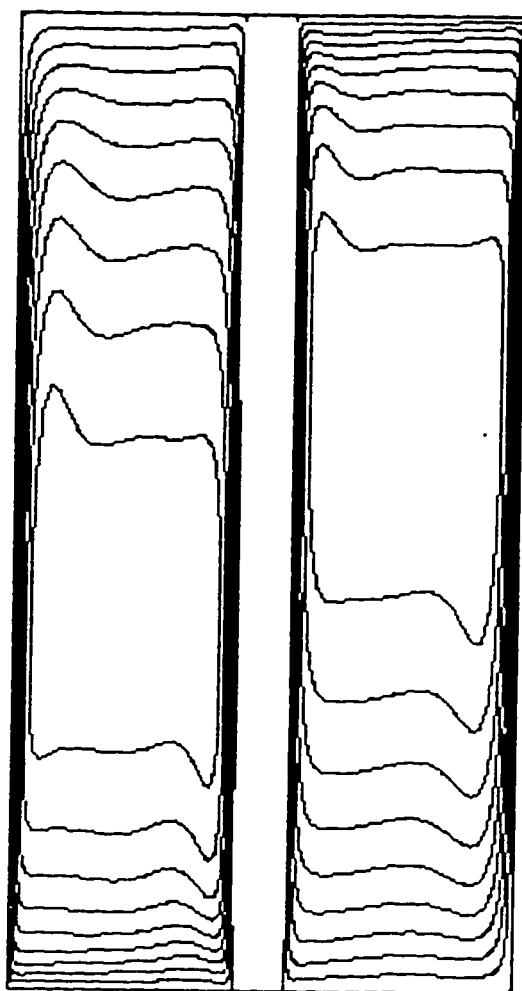


Figure 5.35: Isotherms for turbulent natural convection in a single partition enclosure with  $Ra = 8.0 \times 10^{10}$ ,  $A=2.0$ ,  $N=1.0$ ,  $K_r = 1.0$ ,  $t=0.1$ ,  $\Phi = 90^\circ$



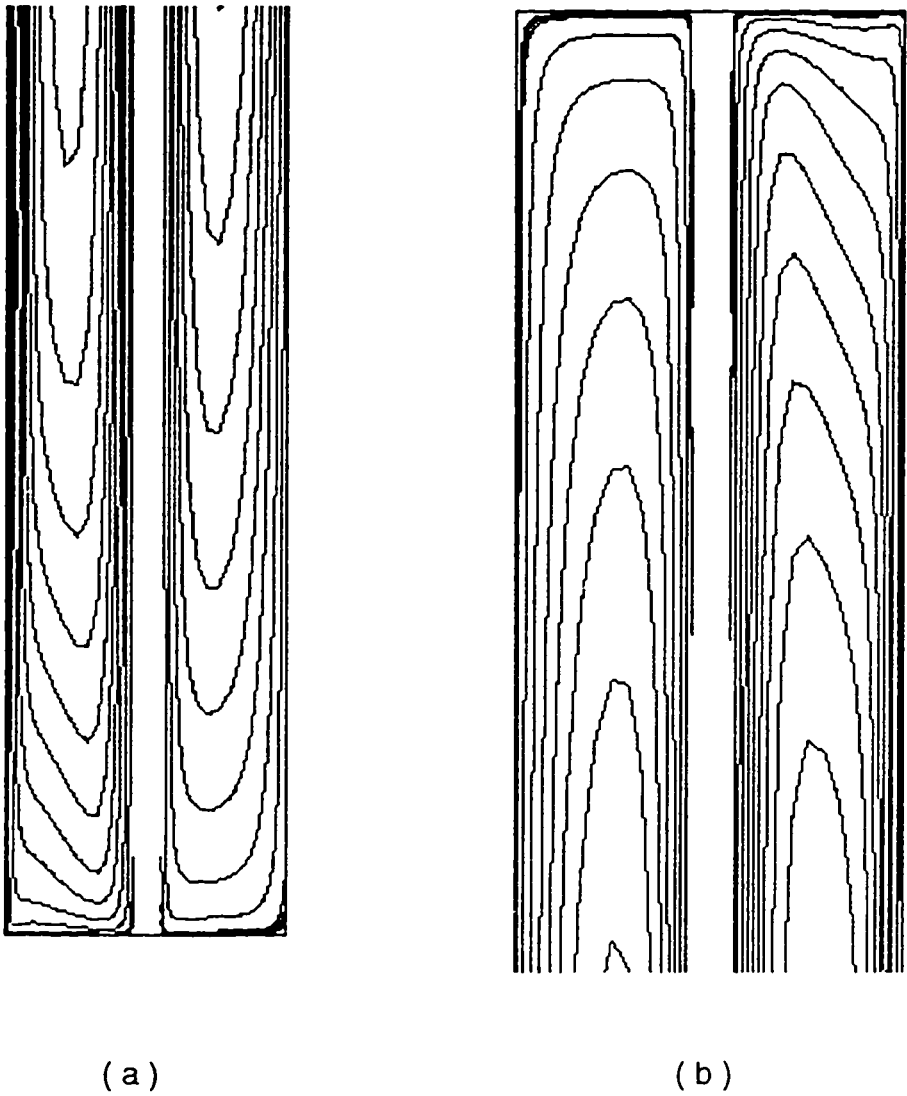
T = 294 ( 2 ) 322

Figure 5.36: Isotherms for turbulent natural convection in a single partition enclosure with  $Ra = 8.0 \times 10^{10}$ ,  $A=15.0$ ,  $N=1.0$ ,  $K_r = 1.0$ ,  $t=0.1$ ,  $\Phi = 90^\circ$



$$\psi = 0.0 (0.000214) 0.00214$$

Figure 5.37: Streamlines for turbulent natural convection in a single partition enclosure with  $Ra = 8.0 \times 10^{10}$ ,  $A=2.0$ ,  $N=1.0$ ,  $K_r = 1.0$ ,  $t=0.1$ ,  $\Phi = 90^\circ$



$$\psi = 0.00 ( 0.000306 ) 0.00306$$

Figure 5.38: Streamlines for turbulent natural convection in a single partition enclosure with  $Ra = 8.0 \times 10^{10}$ ,  $A=15.0$ ,  $N=1.0$ ,  $K_r = 1.0$ ,  $t=0.1$ ,  $\Phi = 90^\circ$

#### 5.5.4 Effect of Angle of Inclination

The effect of inclination angle  $\Phi$  on the heat transfer characteristics of an enclosure with a single partition of thickness  $t=0.1$  and conductivity ratio  $K_r = 1.0$  has been studied for  $Ra = 8 \times 10^{10}$  and  $A=10$ . The plot of the average Nusselt number versus the angle of inclination is shown in figure 5.39. As can be seen from the figure that as the inclination angle  $\Phi$  decreases, convection becomes more significant, and the heat transfer increases, passes through a peak and then begins to decrease again. The peak in Nusselt number occurs at an angle of inclination around 60 degrees for  $N = 1$ ,  $t=0.1$ ,  $K_r = 1$ . This result agrees with the one of an isothermally heated inclined cavity with a single diathermal partition that has been studied numerically by Acharya and Tsang [45]. According to Acharya and Tsang the maximum average Nusselt number was observed to occur at about 60 degrees for  $N = 1$ ,  $t=0.05$ ,  $K_r = 10$ .

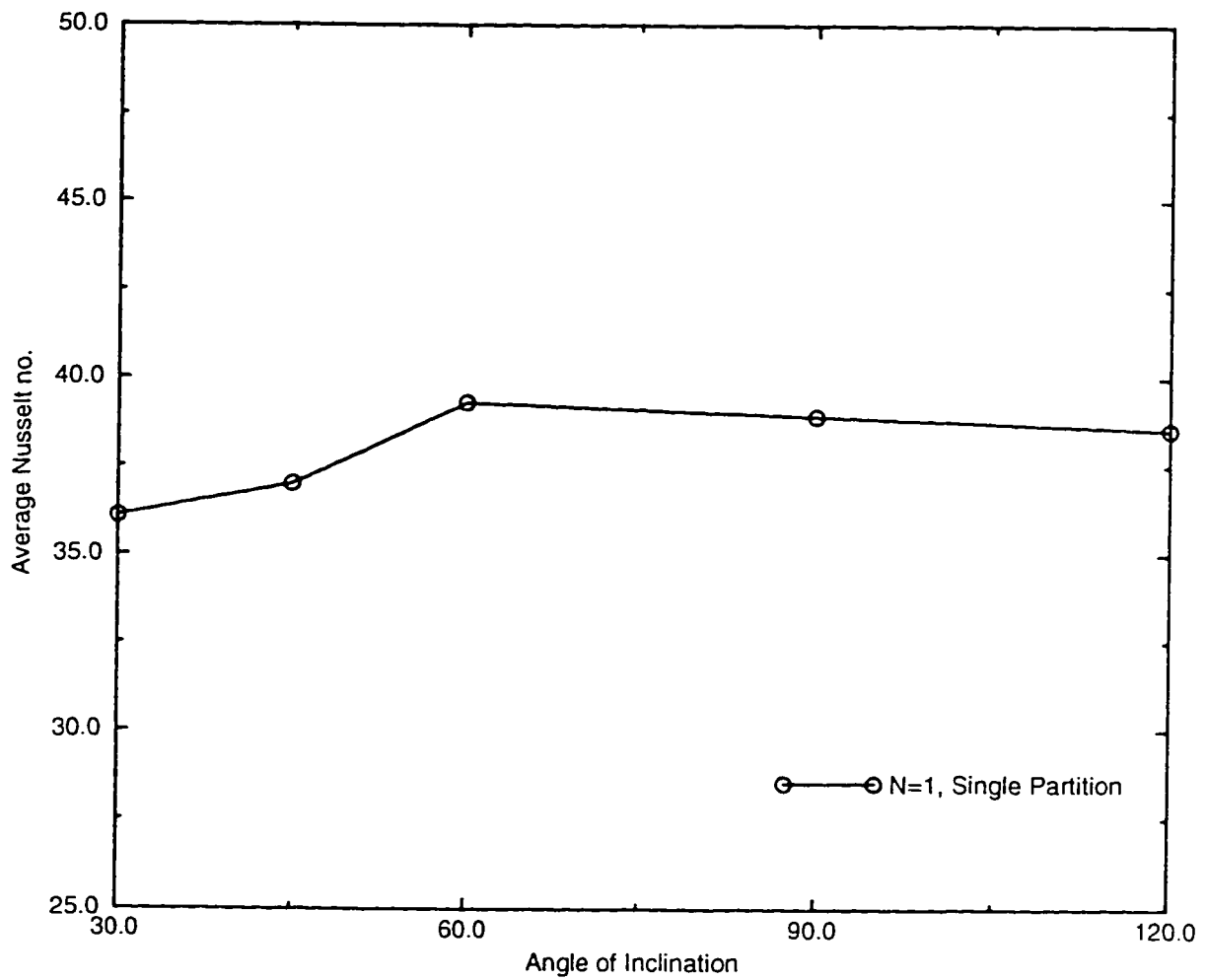


Figure 5.39: Effect of Angle of inclination on the Average Nusselt no. for Turbulent Natural convection in an enclosure with a partition;  $Ra = 8.0 \times 10^{10}$ ,  $A=10$ ,  $N=1$ ,  $K_r = 1.0$



# Chapter 6

## Conclusions and Recommendations

### 6.1 Conclusions

This study represents the results of a comprehensive numerical investigation of the turbulent heat transfer and fluid flow characteristics of natural convection in rectangular partitioned enclosures. A general purpose computer code called PHOENICS is used to perform the numerical computations. The numerical procedure has been validated by comparing the present results for both laminar and turbulent natural convection with those of Kuper et. al. [28], Hamady et. al. [44] and Giel et. al's [10] results. During the course of the investigation, the effect of various parameters such as the Rayleigh number, the aspect ratio, the number of partitions and the

angle of inclination were investigated.

The conclusions derived from the present study can be summarized as

- The present study results for laminar natural convection in an enclosure are in a good agreement with the experimental results of Hamady et. al [44]. This validates the numerical procedure used in this study.
- The standard  $K - \varepsilon$  model with wall functions gives a higher prediction for the heat transfer coefficient for natural convection in enclosures, whereas the low Reynold's extension of the  $K - \varepsilon$  model results are in a good agreement with the experimental results of Giel et. al. [44]
- Partitions do reduce the heat transfer by natural convection in enclosures. The use of 1 partition reduces the average  $\overline{Nu}$  significantly. The rate of reduction decreases as more partitions are added.
- For an enclosure divided by a partition with finite thickness and conductivity the  $\overline{Nu}$  is found to be an increasing function of the Rayleigh number. Upto a  $Ra$  of  $10^{11}$  the rate of increase is slow but as  $Ra$  further increases a steep rise in the  $\overline{Nu}$  is observed.
- For a partitioned enclosure the  $\overline{Nu}$  is found to be an increasing function of the aspect ratio at a constant Rayleigh number. This is true provided that the aspect ratio, the Rayleigh number and the Nusselt number are defined in

terms of the height of a rectangular enclosure.

## 6.2 Recommendations

- The scope of this study is limited by the assumption of two dimensional steady turbulent natural convection flow. Further studies are required to extend the results of the present investigation to the unsteady and/or three dimensional turbulent flow.
- The effect of thickness, conductivity and the position of the partition on the heat transfer rate need to be investigated.
- Second order turbulence models like the algebraic flux model can also be applied in the further studies.

# Bibliography

- [1] Krieth F and M. S. Bohn. "*Principles of Heat Transfer*". West Publishing Company, 1993.
- [2] Adrian Bejan. "*Convective Heat Transfer*". Jhon Wiley & Sons, 1984.
- [3] Jaluria Y. "*Natural Convection Heat and Mass Transfer*". Pergamon Press, 1980.
- [4] Ostrach S. "Natural Convection in Enclosures". *Journal of Heat Transfer*, 110:1175-1189, 1988.
- [5] Batchelor G. W. ". *Quarterly Applied Mathematics*, 12:209, 1954.
- [6] Eckert E. R. G and W.O. Carlson. "Natural Convection in an Air Layer Enclosed Between Two Vertical Plates with Different Temperatures". *Int. Journal of Heat and Mass Transfer*, 2:106-120, 1961.
- [7] Elder J. W. "Laminar Free Convection in Vertical Slot". *Journal of Fluid Mechanics*, 23(Part I):77-98, 1965.

- [8] Elder J. W. "Turbulent Free Convection in Vertical Slot". *Journal of Fluid Mechanics*, 23(Part II):99-111, 1965.
- [9] Schmidt F. W, P. W. Giel, R. E. Philips, and D. F Wang. "A Comparision of Experimental and Predicted Results for Laminar Natural Convection in an Enclosure". *Int. J. Heat and Fluid Flow*, 7(3):183-190, 1986.
- [10] Giel P. W, F. W. Schmidt. R. E. Philips, and D. F Wang. "A Comparision of Experimental and Predicted Results for Laminar Natural Convection in an Enclosure". *Int. J. Heat and Fluid Flow*, 215:229-335, 1986.
- [11] Emery A and N. C. Chu. "Heat Transfer across Vertical Layers". *Journal of Heat Transfer*, 87:110-116, 1965.
- [12] MacGregor R. K and A. F. Emery. "Free Convection Through Vertical Plane Layers- Moderate and High Prandlt Number Fluids". *Journal of Heat Transfer*. 91:391-403, 1969.
- [13] Nobuhiro Seki, Shoichiro Fukusaka, and Hideo Inaba. "Heat Transfer of Natural Convection in a Rectangular Cavity with Vertical Walls of Different Temperatures". *Bulletin of the JSME*, 21(152):246-253. 1978.
- [14] Markatos N. C and C. A. Pericleous. "Laminar and Turbulent Natural Convection in Enclosed Cavity". *21st National Heat Transfer Conference*, HTD-26:59-68, 1983.

- [15] De Vahl Davis G. "Natural Convection of Air in a Square Cavity: a Benchmark Numerical Solution". Technical report. 1982/FMT/2, School of Mech. and Ind. Engg., University of new south wales., 1982.
- [16] Ozoe H, A. Mouri, M. hiramitsu, S.W. Churchill, and N. Lior. "numerical calculations of three dimensional turbulent natural convection in a cubical enclosure". *Journal of Heat Transfer*, 108:806–813, 1986.
- [17] Ince N. Z and B. E. Launder. "On the Computation of Bouyancy Driven Turbulent Flows in Rectangular Enclosure". *International Journal of Heat and Fluid Flow*, 10(2):59–68, 1989.
- [18] Henkes R. A. W. M, F. F. Van der Vlut, and C. J. Hoogendoorn. "Natural Convection Flow in a Square Cavity Calculated with Low Reynolds Number Turbulence Models". *International Journal of Heat and Mass Transfer*, 34(2):377–388, 1991.
- [19] Hanjalic K and S. Vasic. "Computation of Turbulent Natural Convection in Rectangular Enclosure with an Algebraic Flux Model". *International Journal of Heat and Mass Transfer*, 36(14):3603–3624, 1993.
- [20] Heindel T. J, S. Ramadhyani, and F. P. Incropera. "Assesment of Turbulent Models for Natural Convection in an Enclosure". *Numerical Heat Transfer*, 26(Part B):147–172, 1994.

- [21] Henkes R. A. W. M and C. J. Hoogendoorn. "Scaling of the Turbulent Natural Convection Flow in a Heated Square Cavity". *Journal of Heat Transfer*, 116:400–408, 1994.
- [22] Betts P. L and A. A. Dfa'alla. "Turbulent Buoyant Air Flow in a Tall Rectangular Enclosure". In *Significant Questions in Buoyancy Affected Enclosure or Cavity Flows*, pages 377–388. ASME Winter Annual Meeting, Anaheim, 1986.
- [23] Sun Y. S and A. F. Emery. "Multigrid Computation of Natural Convection with a Conductive Baffle". *Numerical Heat Transfer*, 25(Part A):593–603. 1994.
- [24] Arnold J. N, I. Cotton, and D. K. Edwards. "Experimental Investigation of Natural Convection in Inclined Rectangular Regions of Differing Aspect Ratios". *Journal of Heat Transfer*, 98:67–71, 1976.
- [25] Hollands K. G. T, T. E. Unny, G. D. Raithby, and L. Konieck. "Free Convection Heat Transfer Across Inclined Air Layers". *Journal of Heat Transfer*, 98:189–193, 1976.
- [26] El-Sherbiny S. M, G. D. Raithby, and K. G. T. Hollands. "Heat Transfer by Natural Convection Across Vertical and Inclined Air Layers". *Journal of Heat Transfer*, 104:96–102, 1982.

- [27] Badr H. M and M. S. Siddiqui. "Coupled Convective Heat Transfer from an Inclined Flat Plate Enclosure". *Arabian Journal for Science and Engineering*, 15(3):437–451, 1990.
- [28] Kuyper R. A, T. H. Van Der Meer, Henkes R. A. W. M, and C. J. Hoogendoorn. "Numerical Study of Laminar and Turbulent Natural Convection in an Inclined Square Cavity". *International Journal of Heat and Mass Transfer*, 36(11):2899–2911, 1993.
- [29] Ben Yedder R and E. Bilgen. "Turbulent Natural Convection and Conduction in Enclosures Bounded by a Massive wall". *International Journal of Heat and Mass Transfer*, 38(10):1879–1891, 1995.
- [30] Tong T. W and F. M. Gerner. "Natural Convection in Partitioned Air Filled Rectangular Enclosure". *International Communications in Heat and Mass Transfer*, 13:99–108, 1986.
- [31] Ben Anderson and Adrain Bejan. "Heat Transfer Through Single and Double Vertical Walls in Natural Convection : Theory and Experiment". *International Journal of Heat and Mass Transfer*, 24(10):1611–1620, 1981.
- [32] Nishimura T, M. Shiraishi, and Y. Kawamura. "Natural Convection Heat Transfer in Enclosures with an off-center Partition". *International Journal of Heat and Mass Transfer*, 30(8):1758–1762, 1987.



- [33] Nishimura T, F. Nagasawa, and Y. Kawamura. "Natural Convection in Horizontal Enclosure with Multiple Partition". *International Journal of Heat and Mass Transfer*, 32(9):1641-1647, 1989.
- [34] Kangni A, R. B. Yedder, and E. Bilgen. "Natural Convection and Conduction in Enclosure with Multiple Vertical Partition". *International Journal of Heat and Mass Transfer*, 34(11):2819-2825, 1991.
- [35] Mamou M, M. Hasnaoui, and P. Vasseur E. Bilgen. "Natural Convection Heat Transfer in Inclined Enclosures with Multiple Conducting Solid Partitions". *Numerical Heat Transfer*, 25(Part A):295-315, 1994.
- [36] Vasseur P, M. Hasnaoui, and E. Bilgen. "Analytical and Numerical Study of Natural Convection Heat Transfer in an Inclined Composite Enclosure". *Applied Scientific Research*, 52:187-207, 1994.
- [37] Hermann Schlichting. "*Boundary Layer Theory*". Mc.Graw Hill Book Company, England, 1987.
- [38] Wolfgang Rodi. "Turbulence Models and Their Applications in Hydraulics". Technical report, International Association of Hydraulic Research, University of Karlsruhe, Karlsruhe, FRG, 1984.
- [39] Launder B. E and D. B. Spalding. "*Lectures in Mathematical Models of Turbulence*". Academic Press Inc., London, 1972.

- [40] Patankar S. V. "*Numerical Heat Transfer and Fluid Flow*". Hemisphere Publishing Corporation, McGraw Hill Book Company NY, 1980.
- [41] Hoffman J. D. "*Numerical Methods for Engineers and Scientists*". McGraw Hill Book Company, NY, 1992.
- [42] "*The PHOENICS Reference Manual*". TR 200 a, CHAM, 1991.
- [43] "*The PHOENICS Reference Manual*". TR 200 b, CHAM, 1991.
- [44] Hamady F. J, J. R. Lloyd, H. Q. Yang, and K. T. Yang. "Study of Local Natural Convection Heat Transfer in an Inclined Enclosure.". *International Journal of Heat and Mass Transfer*, 32:1697-1708, 1989.
- [45] Acharya S and C. H. Tsang. "Natural Convection in a Fully Partitioned Inclined Enclosure ". *Numerical Heat Transfer*, 8:407-428, 1985.

## Vita

- M. A. RAZZAQ KHAN
- Born in India.
- Permanent Address :  
H.No. 16-10-123/13, Old Malakpet,  
Hyderabad 500036, A. P., INDIA, Ph.0091-40-548903.
- Received Bachelor of Engineering (B.E.) degree in Mechanical Engineering from Osmania University, Hyderabad, India in August 1992.
- Joined KFUPM in September 1993. Received Master of Science (M.S.) degree in Mechanical Engineering with specialization in Thermal Sciences from KFUPM, in June 1996.